

# **Controls on Arsenic Mobility in Mine Waste from Gold Deposits**

**Heather Jamieson**

**Stephen R. Walker, Claudio Andrade, Skya Fawcett,  
Stephanie L. DeSisto, Jennifer Kavalench, Lori Wrye,  
Mackenzie Bromstad, Faith Opio, Cirisse Stephen**

*Geological Sciences and Geological Engineering, Queen's  
University, Canada*

**Michael B. Parsons,**

*Geological Survey of Canada (Atlantic), Canada*

# Risks to human and ecosystem health associated with arsenic-rich mine waste

Poor quality drainage



ingested or inhaled dust



These risks depend on:

1. Sulfide to carbonate ratio
2. Processing history
3. Oxidation products of arsenopyrite

Research approach: investigate the relationship between arsenic mineralogy and risk to human and ecosystem health

### Case Study #1

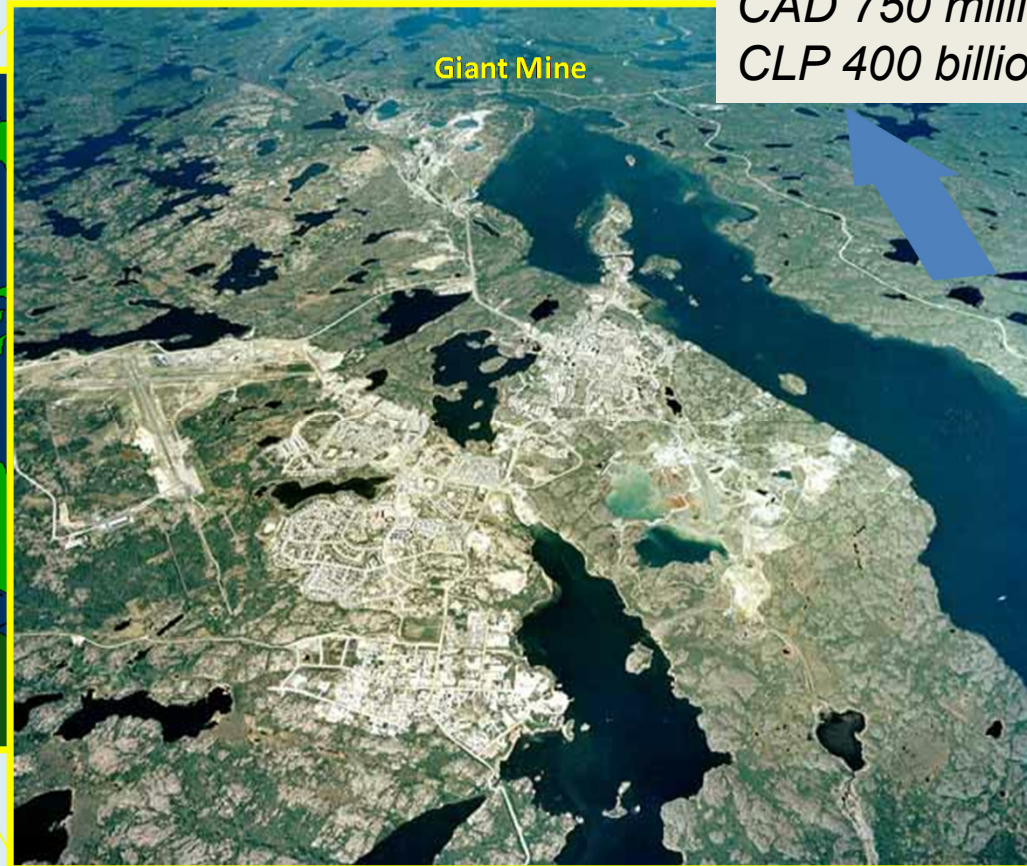
Giant Mine,  
Yellowknife, Canada

### Case Study #2

Historic Gold Mines,  
Nova Scotia, Canada

# Giant mine, Yellowknife

*Estimated cleanup cost  
CAD 750 million  
CLP 400 billion*



- Gold deposit containing arsenopyrite
- Mined and processed from 1949-1999
- Few emission controls during operation
- Complex legacy of arsenic contamination, expensive remediation

## Roaster ~1955



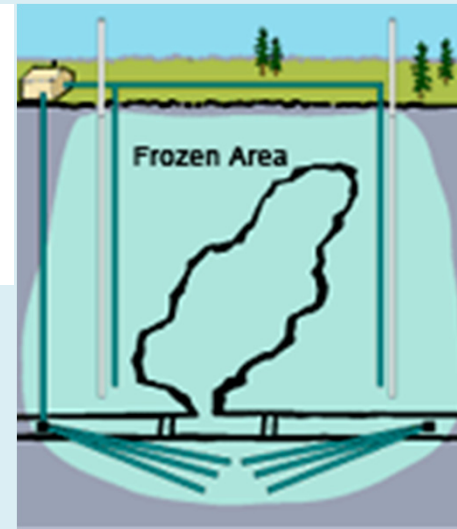
Ore was roasted to liberate gold, producing arsenic trioxide ( $\text{As}_2\text{O}_3$ ) originally released to the surrounding area from the stack.

1949-1951: 7400kg As/day

1958: 1500 kg/day

1999: <200 kg/day

20,000 tonnes in total



Remediation plan includes *in situ* freezing of roaster waste

Later, arsenic trioxide was captured and stored underground



237,000 tons underground



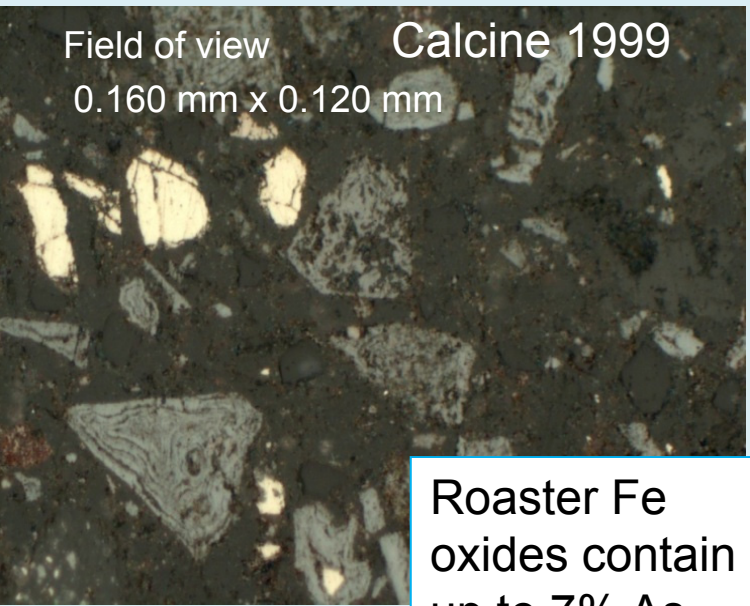
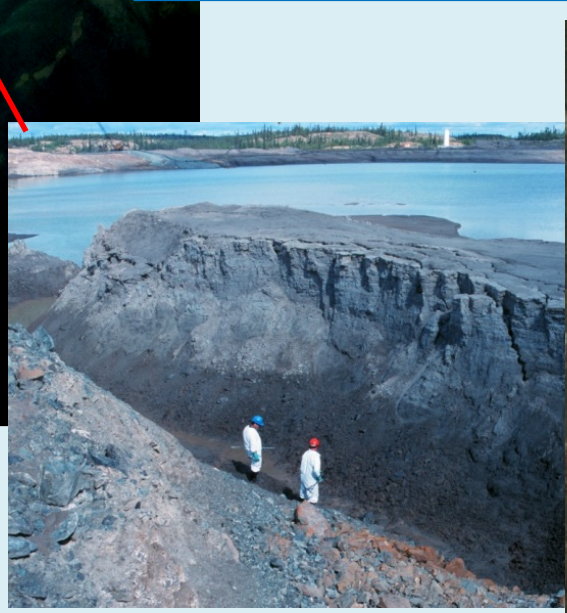
# Consequences of roasting gold ore: Water quality - neutral pH



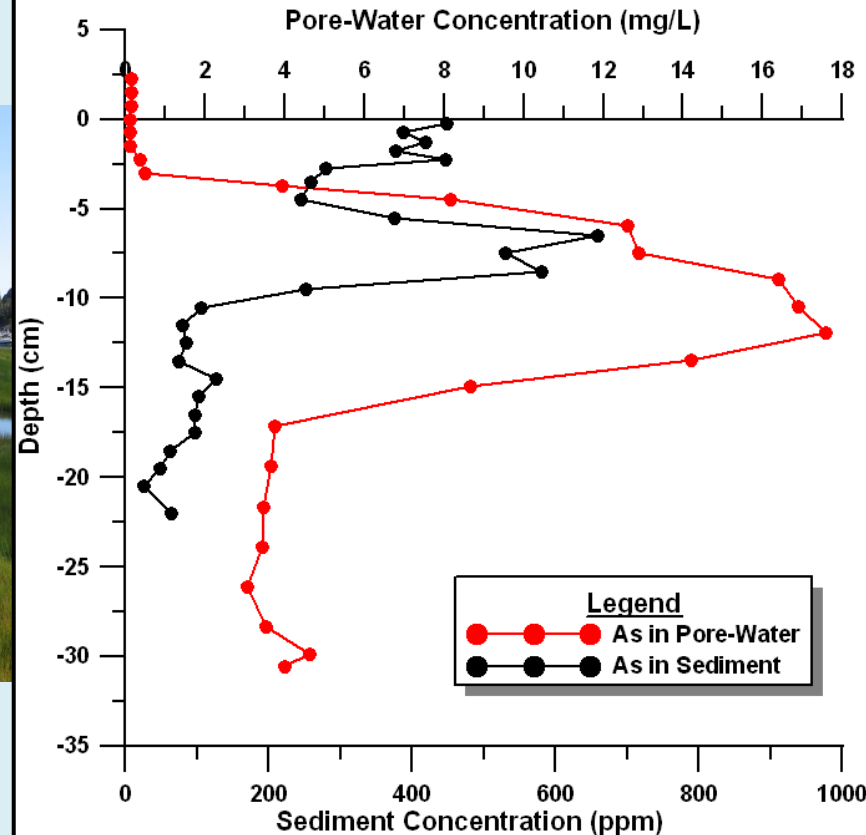
Tailings are mixture of carbonate-bearing flotation tailings and roaster waste (>75% of arsenic in tailings from roaster waste)

Roasting destroys arsenopyrite and forms arsenic trioxide and porous Fe oxides amenable to cyanidation

No acid rock drainage because (1) carbonate (dolomite) is present (2) sulfide content is initially low and partially removed by roasting



# Consequences of roasting gold ore: Water quality – high As



**Sediment Quality Guideline:**  
150 ppm arsenic  
**MMER** 0.5 mg/L  
**Drinking water guideline:**  
0.010 mg/L

Arsenic in sediments increases during time of active mining and emission controls. Similar pattern shown for Cu, Sb, Zn and Pb. Concentrations 4x higher in vegetated area due to trapped fines.

Some As released from sediments migrates up and is recaptured in surface Fe oxyhydroxides.

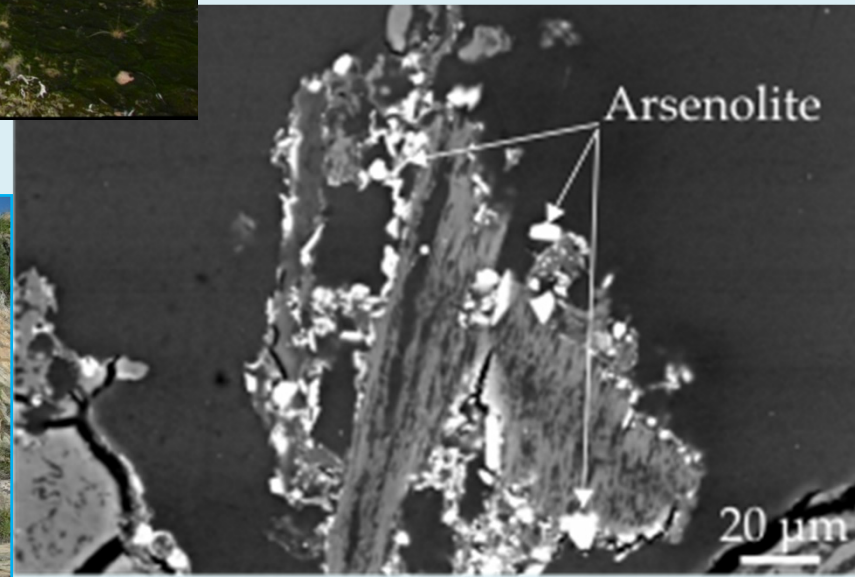
# Consequences of roasting gold ore: Arsenic trioxide in soil



Arsenic trioxide from early years of operation persists, especially in soil pockets on high outcrops

Total As 100s to 1000s mg/kg

**Soil Quality Guideline:**  
12 mg/kg As  
**Site specific industrial**  
340 mg/kg

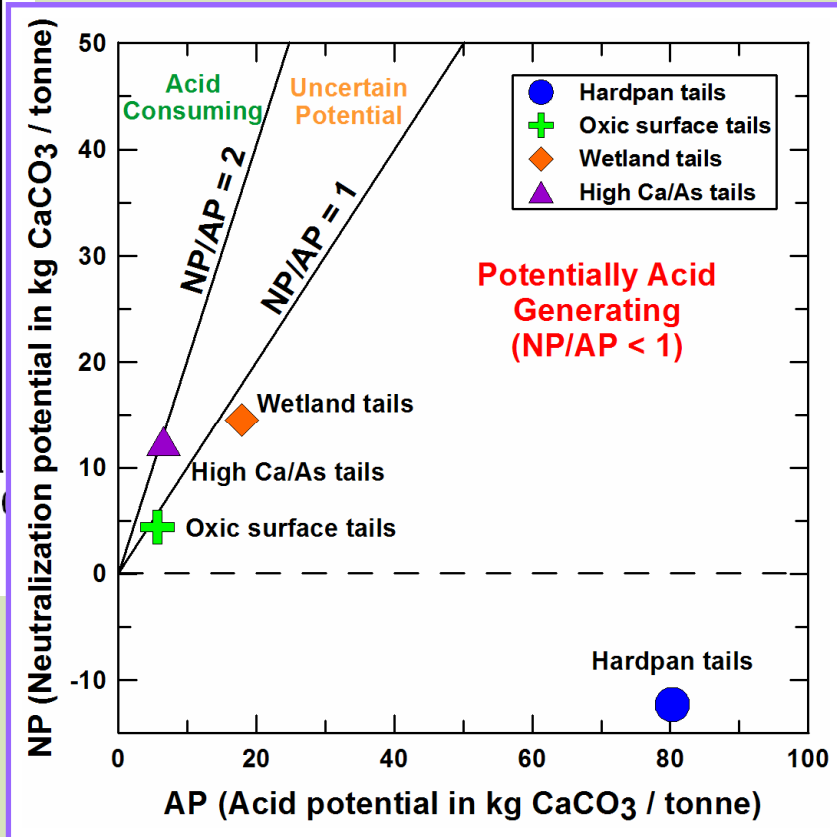
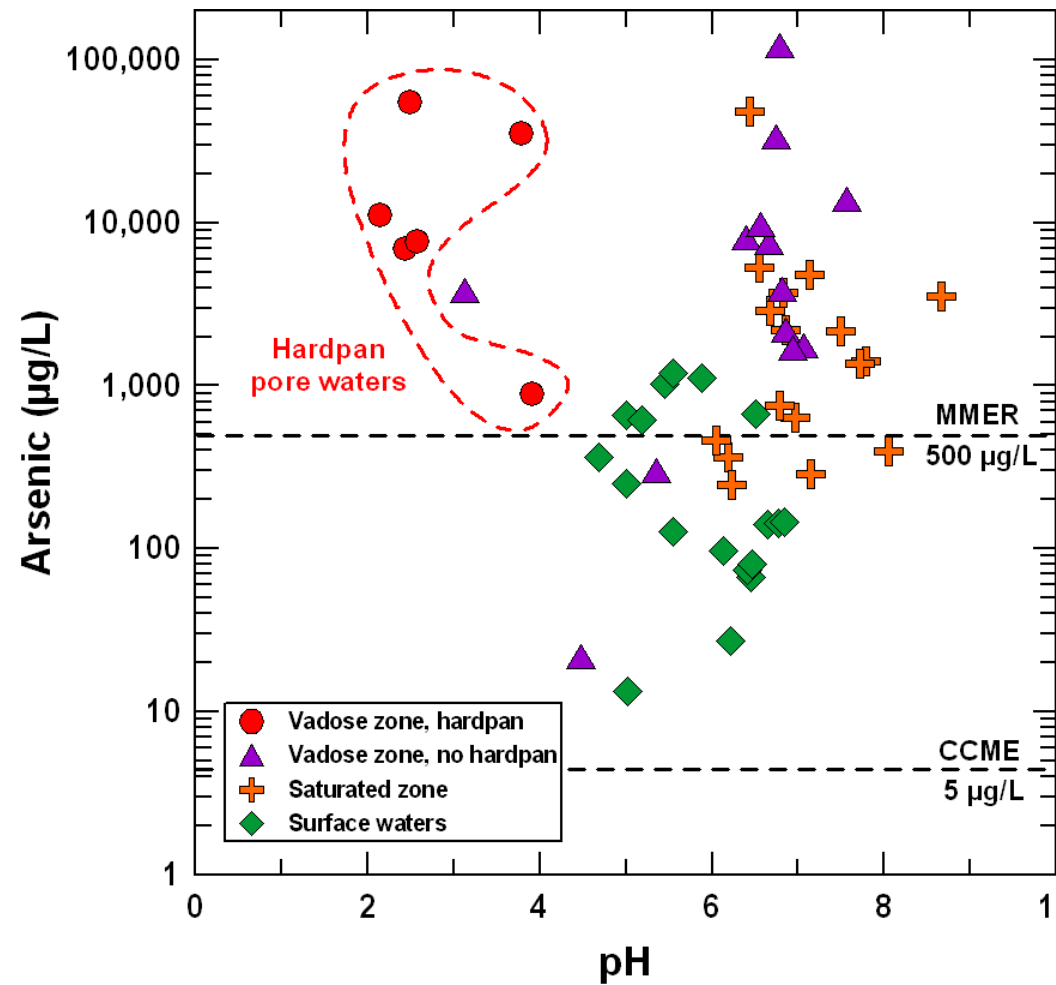


# Historic gold mines, Nova Scotia, Canada



- Gold deposits containing arsenopyrite
- Many small mines throughout the province, publicly accessible
- Few emission controls during operation (1860-1940)
- Complex legacy of arsenic contamination, no remediation plan yet

# Weathered As-rich tailings: Water quality – mostly pH neutral, high As



# Weathered As-rich tailings: Human exposure and total As concentration



Total As in near surface waste <math><150\ \mu\text{m}</math> fraction, mg/kg

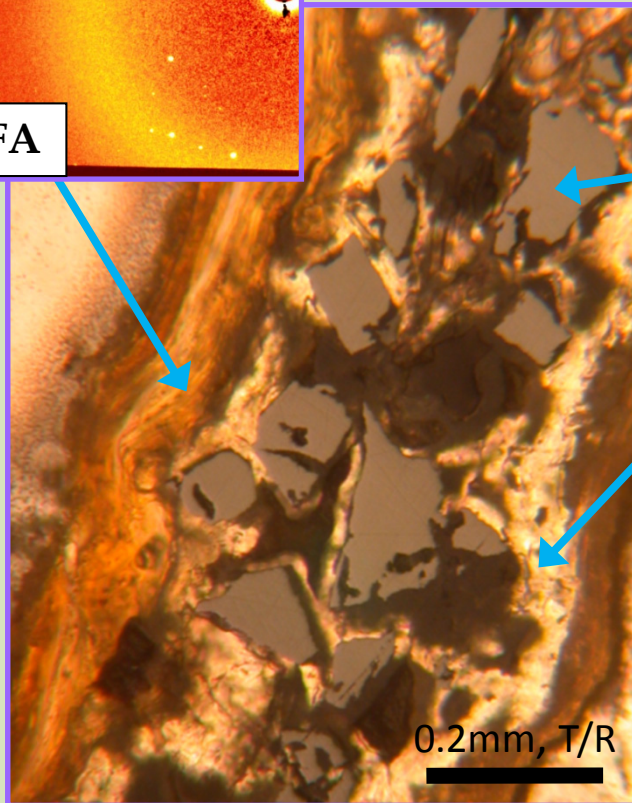
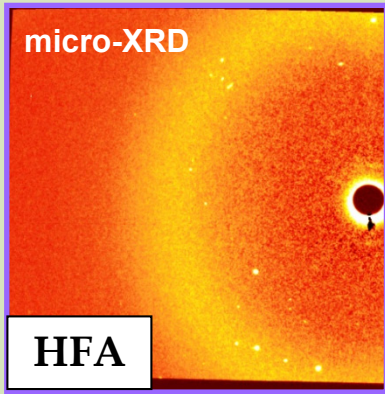
Site	Max	Median
Goldenville	210,000	38,900
Montague	62,100	10,600
Caribou	310,000	72,600



CCME soil quality guideline 12 mg/kg = 12 ppm

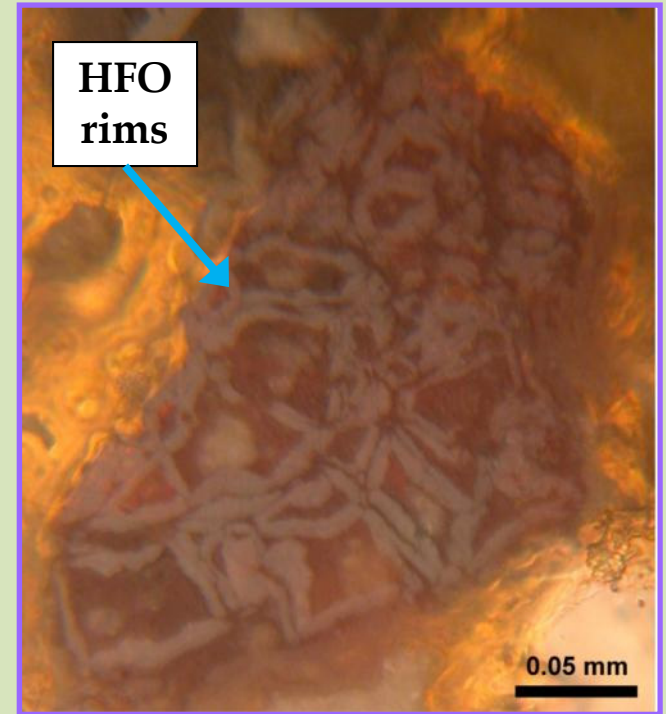
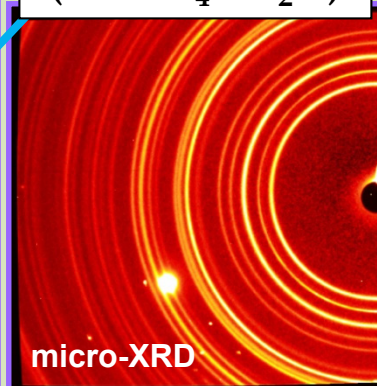
# Hardpan Mineralogy

Hardpan Phase	Avg. Mole % Fe/As
Scorodite (n=9)	0.95
HFA (hydrous iron arsenate) (n=45)	1.29
HFO (hydrous iron oxide) (n=8)	6.54



Arsenopyrite (FeAsS)

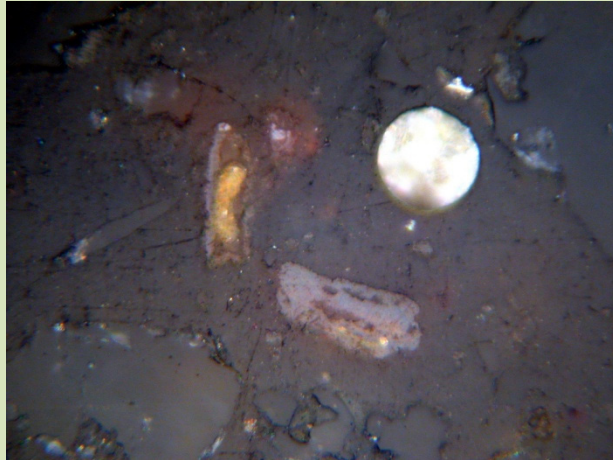
Scorodite (FeAsO<sub>4</sub>·2H<sub>2</sub>O)



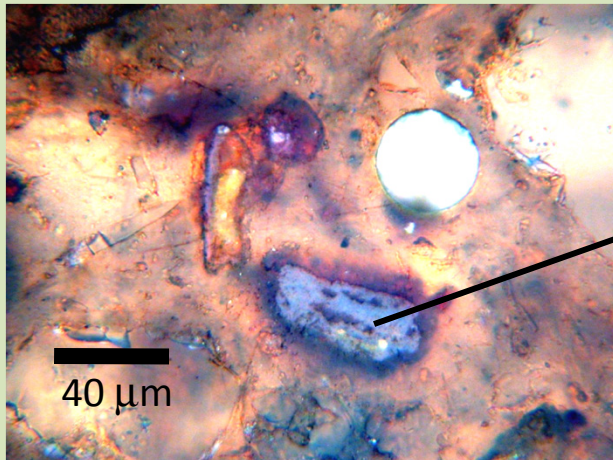
From DeSisto, S.L. 2008. Dynamic arsenic cycling in scorodite-bearing hardpan cements,

DeSisto et al. 2011 Montague Gold Mines, Nova Scotia. MSc, Queen's University, Kingston, ON.

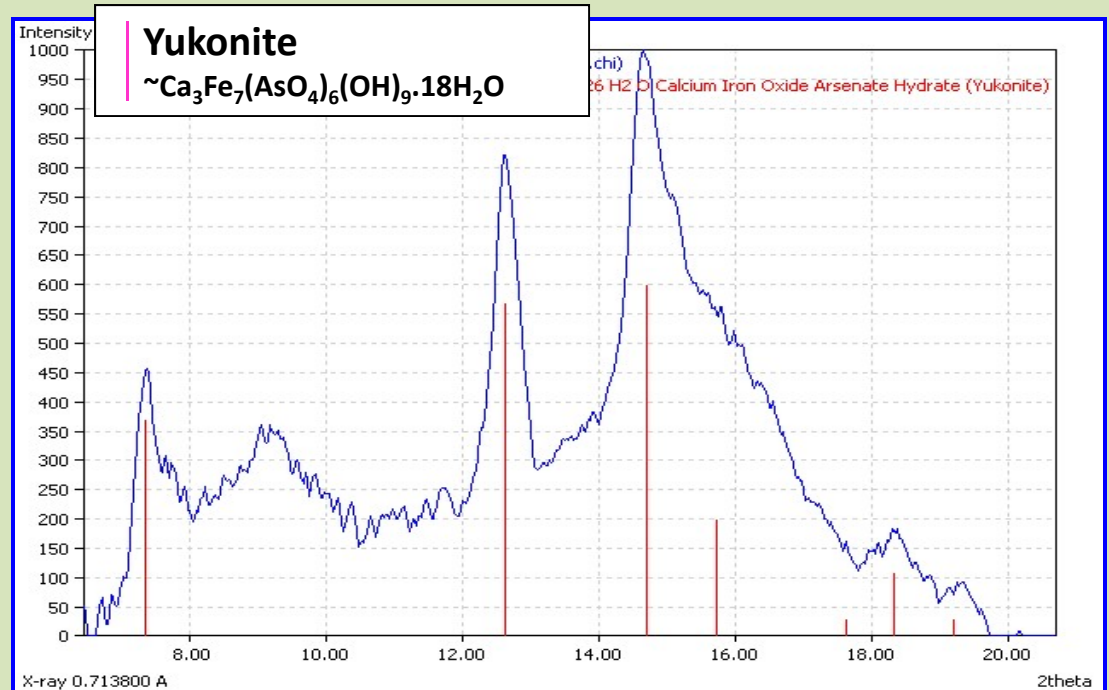
# Yukonite



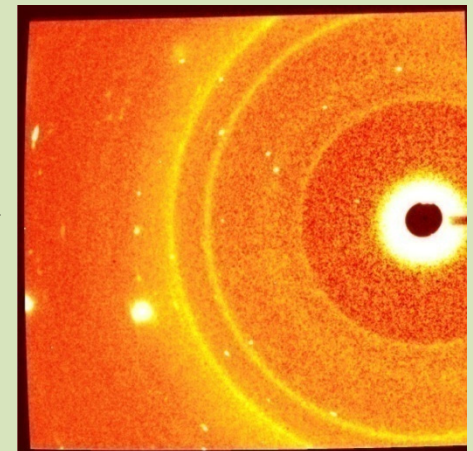
Reflected light



Transmitted and reflected light



$\text{Fe}_2\text{O}_3 = 32.7\%$   
 $\text{As}_2\text{O}_5 = 35.6\%$   
 $\text{SO}_4 = 0.3\%$   
 $\text{CaO} = 7.4\%$



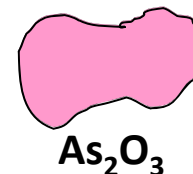
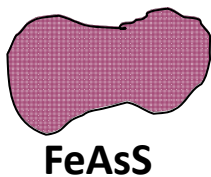
*Walker et al. 2009*

Risk of exposure through oral ingestion is limited by nature of As-hosting solid phase

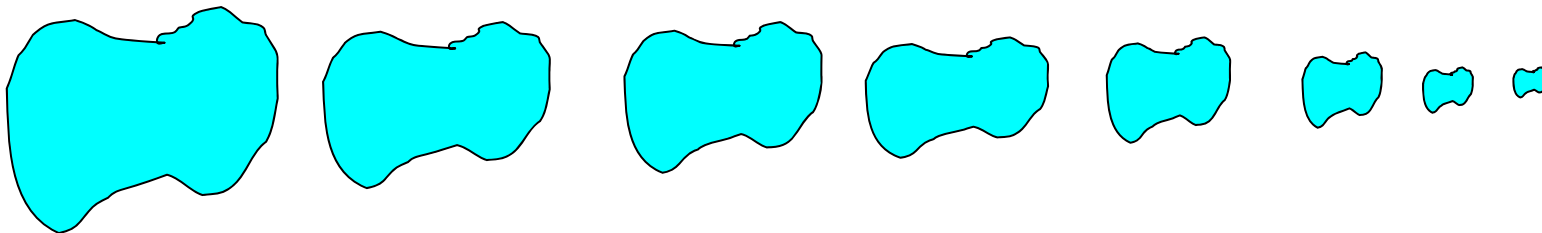
Modified from Ruby *et al.*, 1999



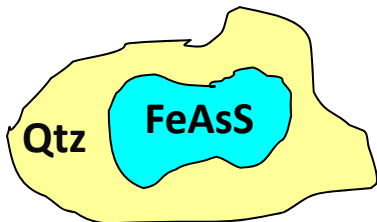
**Mineral Form**



**Grain Size**



**Encapsulation or Rimming of Grains**



# Weathered As-rich tailings: Mineralogy and Bioaccessibility

22 samples tested using simulated stomach and intestine fluids  
and detailed mineralogy

- **Primary Sulfides** (arsenopyrite and pyrite [with <1% As])
- **Fe arsenates** (scorodite, kankite, amorphous)
- **As-bearing iron oxyhydroxides**  
(goethite, akaganeite, lepidocrocite, amorphous)
  
- **Ca-Fe arsenates** (yukonite, amorphous)  
in Ca-rich, carbonate-bearing tailings
- **Pharmacosiderite** (potassium iron arsenate)
- **Tooeleite** (ferric arsenite-sulfate)
- **Realgar** (secondary arsenic sulfide)

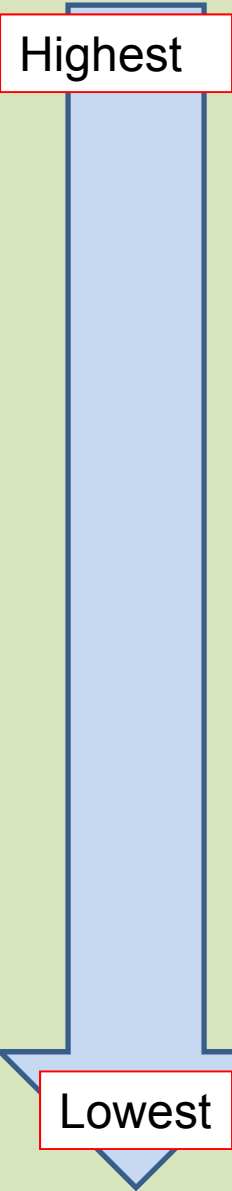
Samples from acid  
tailings showed  
**LOW**  
**BIOACCESSIBILITY**

Samples from  
neutral tailings  
showed **HIGH**  
**BIOACCESSIBILITY**

*Details in Walker et al. (2009), Muenier et al. (2010)*

# Explanation of variable arsenic bioaccessibility

*Ranking from Plumlee and Morman 2011*



Arsenic trioxide - ***Highly soluble in wide range of conditions – field evidence suggests kinetic control***

Calcium iron arsenate – ***Field evidence indicates these minerals co-exist with calcite, thus likely to dissolve in acid gastric fluids***

Amorphous iron arsenate (HFA)

Arsenic-bearing iron-oxyhydroxides (HFO)

Arsenic-rich pyrite, realgar

Arsenopyrite - ***Tends to be present as coarse primary sulfide in mine waste, unlikely to dissolve rapidly***

Scorodite – ***Known to be stable at low pH, unlikely to dissolve in gastric fluid***

# Practical Conclusions

1. Arsenic in water may be high even with no acid mine drainage
2. Some arsenic minerals present more risk to human health than others (arsenic trioxide, yukonite)
3. Processing and emission control history may control As mobility
4. Depositional environment controls long-term stability
5. Identifying As minerals is important in understanding risk – some are easy, others not

# Acknowledgements

- NSERC (Natural Sciences and Engineering Research Council of Canada)
- Aboriginal Affairs and Northern Development Canada
- Environment and Health Program, Earth Sciences Sector, Natural Resources Canada
- NSERC MITHE (Metals in the Human Environment) Strategic Network
- Beamline X26A, National Synchrotron Light Source (NSLS), Brookhaven National Laboratory, funded by US DOE

# Arsenic bioaccessibility via digestion (in vitro)

Highest

Arsenic trioxide  $\text{As}_2\text{O}_3$

Calcium iron arsenate

Yukonite  $\text{Ca}_7\text{Fe}_{12}(\text{AsO}_4)_{10}(\text{OH})_{20} \cdot 15\text{H}_2\text{O}$

Pharmacosiderite  $\text{KFe}_4(\text{AsO}_4)_3(\text{OH})_4 \cdot 6-7\text{H}_2\text{O}$

Amorphous iron arsenate (HFA)  $\text{Fe}/\text{As} = 1 \text{ to } 3$

Arsenic-bearing iron-oxyhydroxides (HFO)  $\text{Fe}/\text{As} > 3$

Arsenic-rich pyrite  $\text{FeS}_2$ , Realgar  $\text{As}_4\text{S}_4$

Arsenopyrite  $\text{FeAsS}$

Lowest

Scorodite  $\text{FeAsO}_4 \cdot 2\text{H}_2\text{O}$



# The distinction between ore processing and post-depositional transformation on the speciation of arsenic and antimony in mine waste and sediment

Skya E. Fawcett\*, Heather E. Jamieson

Department of Geological Sciences and Geological Engineering, Queen's University, Kingston, Ontario, Canada K7L 3N6

## ARTICLE INFO

### Article history:

Received 7 October 2009  
Received in revised form 14 February 2010  
Accepted 15 February 2010  
Available online 21 February 2010

Editor: J. Fein

### Keywords:

Antimony  
Arsenic  
XANES  
Roaster oxide  
Speciation

## ABSTRACT

Roasting of As and Sb-associated gold ore at the Giant mine, Yellowknife, Canada, resulted in complex solid–gas phase reactions between As, Sb, and roaster-derived Fe-oxides. Antimony, As, and their respective hosting in two roaster waste streams and mine-impacted sediment were characterized using EPMA,  $\mu$ XRD,  $\mu$ XRF, bulk and  $\mu$ XANES. The roaster oxides in mine waste and sediment host As and Sb in multiple oxidation states. In the cyanided roaster dust (ESP residue – composed of fine-grained particles mobilized during roasting, and sublimated phases),  $3^+$  is the dominant As and Sb oxidation state in the bulk sample and in the roaster-generated iron oxides that host these elements. Conversely,  $5^+$  is the dominant As and Sb oxidation state in the bulk calcine (oxidized and cyanided material collected from the roaster bed), and in the roaster Fe-oxide grains therein. These results have important implications for predicting the fate of As and Sb in the environment, and for distinguishing between anthropogenically-influenced speciation and speciation resulting from post-depositional transformations. Arsenic and Sb-bearing roaster iron oxides and other As and Sb-bearing phases in mine-impacted sediment collected from the surficial zone (0 to  $-1$  cm) and relatively reducing zone ( $-16$  cm) are also described. Arsenic and Sb associated with roaster oxides in the relatively reducing sediment have undergone post-depositional transformation and 10–20% of As and Sb are attenuated via precipitation as sulfide or sorption to sulfide surfaces. The attenuation of Sb is more efficient than As, and Sb is only mobile at the micron scale. In the relatively reducing sediment, where most of the As is reduced to  $As^{3+}$ , a  $Sb^{5+}$  bound to oxygen phase persists and represents 58% of the total Sb.

© 2010 Elsevier B.V. All rights reserved.

## 1. Introduction

Understanding the solid-state speciation of elements is essential to predict their stability in the environment and is especially pertinent to the design of effective remediation strategies of industrial sites (Foster et al., 1998; O'Day et al., 1998; Morin et al., 1999; Savage et al., 2000; Kneebone et al., 2002; Walker et al., 2005; Beauchemin and Kwong, 2006). Arsenic and Sb are two elements commonly associated in ore bodies that can have negative impacts on human and ecosystem health if released to the aqueous environment (Filella et al., 2002a and references therein; WHO, 1993). Their mobility, toxicity, and potential bioavailability are dependent upon their oxidation states (Filella et al., 2002a; Smedley and Kinniburgh, 2002). Arsenic and Sb are in the same group in the periodic table, have similar electronic structures, exist primarily in the  $3^+$  and  $5^+$  oxidation states in biological and environmental samples, and form oxyanions in water. The oxidation state of As and Sb is controlled primarily by Eh and pH and, in the

aqueous state, comparable As and Sb oxyanions occupy similar regions in pH–Eh diagrams (Vink, 1996; Filella et al., 2002b; Smedley and Kinniburgh, 2002). Because of their many similarities As and Sb are often assumed to exhibit similar geochemical behaviour.

In many ways As and Sb occur as similar mineralogical forms. For example, the crystal structure of  $As_2O_3$  is analogous to  $Sb_2O_3$  (Wedepohl, 1974). However, in many cases the manner in which these elements are incorporated in mineral structures does differ. For example, stibnite ( $Sb_2S_3$ ), the primary Sb-sulfide, and orpiment ( $As_2S_3$ ) have the same lattice constants but unrelated crystal structures (Wedepohl, 1974). Moreover, pyrochlore crystal structures (Fd-3m), mixed-oxidation state, and oxysulfide minerals common to the Sb-system are absent from the As-system, or not found in nature. Both As and Sb are hosted in sulfosalt minerals. However, Sb, not As, commonly occupies multiple crystallographic sites within this group. In the sulfosalt minerals As always bonds in trigonal coordination with sulfur whereas around Sb additional bonds must be considered (Wedepohl, 1974). When Sb bonds to more than three sulfur atoms in sulfosalts, departures from the galena-type array occur and complex distribution patterns of short and long Sb–S bonds are observed (Makovicky, 1989).

The Giant gold mine site near Yellowknife, Canada provides an opportunity to compare the behaviour of As and Sb because they are both present in the ore, mine waste, and the downstream aquatic

\* Corresponding author. Currently at Lorax Environmental Services Inc., 2289 Burrard St, Vancouver, British Columbia, Canada V6J 3H9. Tel.: +1 604 688 7173; fax: +1 604 688 7175.

E-mail addresses: [sfawcett@lorax.ca](mailto:sfawcett@lorax.ca) (S.E. Fawcett), [jamieson@geol.queensu.ca](mailto:jamieson@geol.queensu.ca) (H.E. Jamieson).

environment. The Giant mine was in operation between 1948 and 1999. Samples used in this study include the processed materials calcine and Electrostatic Precipitator (ESP) residue, and sediment samples from Baker Pond. Baker Pond lies immediately downstream of the settling pond and polishing ponds and was impacted by significant tailings deposition following dam breaches during turbulent spring flow events (Berube et al., 1974). Included for analysis in this study were materials derived from roasting processes utilized to liberate gold in the ore, namely the calcine and ESP residue. In the Giant ore As is present as arsenopyrite and arsenical pyrite. Antimony is present as stibnite ( $\text{Sb}_2\text{S}_3$ ) and a number of sulfosalts including: boulangerite ( $\text{Pb}_5\text{Sb}_4\text{S}_{11}$ ), berthierite ( $\text{FeSb}_2\text{S}_4$ ), chalcocite ( $\text{Cu}_2\text{S}$ ), jamesonite ( $\text{PbFeSb}_6\text{S}_{14}$ ) and tetrahedrite ( $(\text{Cu,Fe})_{12}(\text{Sb,As})_4\text{S}_{13}$ ). To liberate the gold, the ore at Giant was roasted which produced volatile As and Sb phases which can react with Fe-oxides formed during the decomposition of arsenopyrite and pyrite. The calcine is the oxidized material that remains in the roaster bed following roasting while the ESP residue is composed of fine-grained particles that were mobilized during roasting, and phases that sublimated in the ESP following volatilization in the roaster. Within roaster waste streams As has been found to be associated with hematite and maghemite, the decomposition products of sulfides in roasters (McCreadie and Blowes, 2000; Walker et al., 2005). In fact, the As content in roaster-derived maghemite is documented to be as high as 18.6% (Paktunc et al., 2006). Furthermore, Walker et al. (2005) found that As associated with maghemite and hematite in the Giant mine waste is hosted in the  $3^+$  and  $5^+$  oxidation states, evidence that the solid–gas phase reactions that occurred in the roaster were complex.

The decomposition and transformation of Sb minerals in the roaster are not well understood. Metallurgical reports from the Giant mine suggest that Sb was volatile in the roaster (Berube et al., 1974). Antimony content in the roaster feed was closely monitored because Sb concentrations exceeding 0.75% caused clinkering (formation of glassy phases not amenable to cyanidation) of the roaster bed, reportedly due to the formation of an Sb-sulfate mineral (Marsden and House, 2006). One study on the decomposition of jamesonite ( $\text{PbFeSb}_6\text{S}_{14}$ ) at higher roasting temperatures (750 °C) demonstrated that the final products depended on the amount of oxygen and steam present (Zhu et al., 2006). In the presence of steam, Sb was preferentially vaporized and no Sb products were found in the calcine (Sb was completely volatilized). In the presence of air and the absence of steam, jamesonite transformed into a stable  $\text{Pb}_4\text{Sb}_3\text{FeO}_{13}$  phase, hindering the volatilization of Sb. Steam would have been present in the roaster at Giant mine since the roaster feed was in the form of a slurry. However the roasting temperatures (500 °C) are lower than in the study on jamesonite by Zhu et al. (2006). The decomposition of sulfosalts in the Giant roaster may have been complex and their resulting products at 500 °C are unknown.

Most of the As and Sb in the ore went to the roaster (Fawcett et al., 2006), and was then discharged to the environment. The reductive dissolution of roaster-derived maghemite and hematite has been observed (McCreadie and Blowes, 2000) and has resulted in a release of As and Fe to pore-water (Martin and Pedersen, 2002). Also, Fe-oxides may undergo other transformations in response to the onset of more reducing conditions (Froelich et al., 1979; Cornell and Schwertmann, 1996). For example, maghemite and hematite are expected to recrystallize to form magnetite (Cornell and Schwertmann, 1996) and the fate of the adsorbed ions during these transformations is not clearly understood. For example, the transformation of an amorphous Fe-(oxyhydr)oxide to a crystalline Fe-(oxyhydr)oxide will result in a decrease in the amount of sorption sites, and hence decrease the amount of an ion that can be adsorbed (Tufano and Fendorf, 2008). However, it has recently been observed that the reduction of an Fe-(oxyhydr)oxide can actually increase retention of As owing to an increase in the binding strength of the newly-formed Fe-oxide (Herbel and Fendorf, 2006; Kocar et al., 2006; Pedersen et al., 2006; Tufano and Fendorf, 2008).

The rate of transformation or dissolution is dependant on a number of kinetic and thermodynamic considerations, including the presence of adsorbed ions and structurally incorporated elements (Cornell and Schwertmann, 1996). The size of the crystallites can also affect the rate of transformation and dissolution. Micro- and nano-crystalline minerals often exhibit adapted phase stability and reaction kinetics when compared to the equivalent macro-crystalline minerals (Banfield and Zhang, 2001; Navrotsky, 2001). Based on the nature of the  $\mu\text{XRD}$  pattern (smooth rings rather than spotty rings), Walker et al. (2005) identified the maghemite grains in Giant tailings as “polycrystalline nanoparticulate composite grains”.

Using bulk and micro-XANES,  $\mu\text{XRD}$ , petrography, and conventional and synchrotron-based microprobe we have characterized the roaster products (calcine and Electrostatic Precipitator (ESP) residue) in order to understand the reactivity of As and Sb in the roaster, and evaluate their potential stability in the environment. To investigate their post-depositional transformations, we studied As and Sb associated with maghemite and other phases in the submerged Baker Pond sediment at two different depths below the sediment–water interface. The distinct geochemical behaviour of As and Sb under reducing conditions is documented.

## 2. Background

Giant is a gold mine located 5 km north of Yellowknife, Canada, on the northern arm of Great Slave Lake. Giant produced gold for fifty years, between 1948 and 1999, and is expected to undergo major remediation. The ore deposits are located in the Archean Yellowknife Bay supergroup greenstone belt, and hosted in deformation and alteration zones that crosscut the Kam Group mafic volcanics (Canam, 2006). The ore zones contain 5–15% sulfides, which include pyrite, arsenopyrite, sphalerite, chalcocite, stibnite, and Sb-bearing sulfosalts (Coleman, 1957). The Au is refractory and hosted primarily in arsenopyrite, and to a lesser extent in pyrite and quartz (Coleman, 1957). To extract gold, the ore was crushed, subject to froth floatation, roasting, and cyanidation.

Roasting was conducted at 500 °C over two stages. The first stage of roasting was oxygen-restricted with the purpose of volatilizing As and S. The second stage of roasting was oxidizing and transforming the arsenopyrite and pyrite into porous Fe-oxides (maghemite and hematite). Porous and fractured hematite and maghemite are the desired end-products of roasting because they are amenable to cyanidation and hence, gold extraction. Specific details of the roasting process are discussed in detail by More and Pawson (1978) and Walker et al. (2005). Roasting produced three separate streams, the calcine, which is what remains in the roaster bed, the ESP residue which is composed of the fine-grained particles collected from the off-gases, and the sublimated gaseous phase is collected in the baghouse. In this study we focus on As and Sb in the calcine and ESP residue, but it should be noted that a significant amount of As and Sb was collected in the baghouse.

Arsenic trioxide is the volatile phase produced in the roasting of arsenopyrite (Marsden and House, 2006). Hot gases and dust were passed through the electrostatic precipitator where dust was removed. The gases were then cooled and desublimated producing arsenic trioxide which was collected in the baghouse and is currently being stored in the underground stopes (SRK Consulting and SENES Consultants Ltd., 2007). The Sb gaseous phase was likely  $\text{Sb}_2\text{O}_3$ , the predicted decomposition phase of stibnite (the primary Sb-bearing ore mineral) in roasters, and a phase that exhibits high vapour pressure even at low roasting temperatures (Marsden and House, 2006). The mixed-oxidation state Sb mineral,  $\text{Sb}_2\text{O}_4$ , is also predicted to be thermodynamically stable under the roasting conditions (Asryan et al., 2004). There is evidence that Sb was completely volatilized in the roaster at Giant (discussed later), but the reaction products have never been characterized.

Following cyanidation, the calcine and ESP residue are mixed, along with the finest fraction of floatation tailings (which contain low amounts of As and Sb) and discharged to the tailings ponds. Baker Pond is a natural pond that lies downstream from the current water treatment plant. Prior to the operation of the water treatment plant in 1981 and the implementation of better sedimentation controls, significant amounts of tailings flowed over the ice-covered dams in the spring and were deposited in the northernmost section of Baker Pond (Berube et al., 1974). Additional work at Baker Pond documents a redox profile that is moderately oxidizing in the surficial sediment and moderately reducing 16 cm below the sediment–water interface (Fawcett, 2009).

### 3. Methods

#### 3.1. Sample collection and preparation

Baker Pond sediment cores were extracted using a gravity corer and clear core tubes 60 cm in length and 7.5 cm in diameter. At the time of sampling, August 2005, the pond surface was approximately 1.5 m above the sediment–water interface (SWI). The entire core is massive in appearance, light grey in colour, and composed of very fine-grained sediment. Cores were immediately covered to avoid photo-oxidation reactions during transport. The core was extruded immediately following collection in a laboratory at centimeter intervals in a nitrogen-purged glovebag. The extruded core samples were immediately frozen for transport. Two samples were chosen from a larger suite of samples for analyses: BP01 (sediment from the 0 to –1 cm interval) and BP15 (sediment from the –16 cm interval) and were dried under a N<sub>2</sub> atmosphere. Walker et al. (2005) describe the collection and treatment of the calcine and ESP residue samples provided by the staff at the Giant mine.

Detachable thin sections were prepared for the calcine, ESP residue, and the two sediment samples from Baker Pond using a method described by Walker et al. (2005). Thin sections were examined microscopically in both reflected and transmitted light. Roaster oxide grains were identified and targeted using petrography in all but the Baker Pond sections. Due to the very fine-grained nature of the Baker Pond sediment, targets for  $\mu$ XANES and  $\mu$ XRD analyses were chosen based on element associations evident in the  $\mu$ XRF maps, rather than petrography. Thin sections were detached from the glass slide, mounted on Kapton<sup>TM</sup>, and oriented 45° to the beam.

#### 3.2. Analyses

Micro-XANES,  $\mu$ XRD, and  $\mu$ XRF analyses are performed on thin sections using a monochromatic beam focused to  $5 \times 1.5 \mu\text{m}$ . Details regarding the experimental setup of the microprobe end station at the PNC-XOR beamline at the Advanced Photon Source (APS), including imaging, micro-XAS, and  $\mu$ XRD are outlined by Heald et al. (2007). Micro-XRD experiments are conducted in transmission mode by tuning the incident beam to 30,700 eV, and measured using a FujiBas2500 area detector. The d-spacings are determined by integrating the 2D pattern using Fit2D to produce a powder diffraction pattern (Hammersley, 1998). The pattern is processed, and the phases are identified using HIGHSCORE PLUS<sup>TM</sup> software.

Bulk XANES spectra were collected from all samples using an unfocused beam approximately 0.5 mm in diameter. The bulk samples were mounted in 3 mm-thick teflon holders and sealed with Kapton<sup>TM</sup> tape. All Sb XANES were collected at the Sb K-edge (30,491 eV), and As XANES at the As K-edge (11,868 eV), over two sessions at the PNC-XOR undulator beamline, 20-ID, at the APS in Chicago, U.S.A. A Si(311) double-crystal monochromator was used to control the X-ray energy and was calibrated with the Sb metal at the Sb K-edge, and Au foil near the As K-edge. The second crystal of the monochromator was detuned by 20% from the peak intensity (as measured by a pre-slit ion chamber upstream of the sample slits) at 200–250 eV above the K-edges of Sb or As, to

reduce the presence of higher harmonic energies from the monochromator. The KB mirrors at 2 mrad angle provided further harmonic rejection. Spectra were collected in fluorescence mode using a 7-element Canberra Ge(Li) detector. Three to five scans were collected for each sample. The individual scans were calibrated to a Sb<sub>2</sub>O<sub>3</sub> standard, and a Au standard in the case of As, that was run simultaneously. The first and last scans exhibited consistent features and position in the near edge, thereby confirming no beam damage had occurred.

Processing of XANES data and linear combination fitting analyses were carried out using ATHENA software (Ravel, 2007; ATHENA, 2007). Linear combination fitting was performed on the normalized As and Sb spectra. Different fitting approaches were employed on As and Sb K-edge XANES spectra because the energy-dependence of the near edge for the Sb materials is more readily apparent by examination of the derivatives of the spectra. Fawcett et al. (2009) discuss linear combination fitting of Sb K-edge XANES spectra in detail. The model compounds used in fitting Sb K-edge spectra include Sb<sub>2</sub>O<sub>5</sub> and Sb<sub>2</sub>O<sub>3</sub> obtained commercially (Fisher Scientific, 99.995%), and tetrahedrite ((Cu,Fe,Zn)<sub>12</sub>Sb<sub>4</sub>S<sub>13</sub>) was obtained from the Miller Museum (M361) at Queen's University, and were verified by X-ray diffraction. For a detailed analysis of twelve Sb reference spectra relevant to this study, and justification for choosing Sb<sub>2</sub>O<sub>5</sub>, Sb<sub>2</sub>O<sub>3</sub>, and tetrahedrite for fitting of the sample spectra, see Fawcett et al. (2009).

Scorodite (FeAsO<sub>4</sub>), arsenolite (As<sub>2</sub>O<sub>3</sub>), orpiment (As<sub>2</sub>S<sub>3</sub>), and arsenopyrite (FeAsS) were employed in fitting As K-edge spectra. Scorodite (M6303) and arsenopyrite (M5579) were acquired from the Miller museum at Queen's University, orpiment from Natural Resources Canada mineral library, and arsenolite is a J.T. Baker reagent. Justification for the use of these four standards in the analysis of As in the Giant Mine samples is described in detail in Walker et al. (2005). The percentages reported in the linear combination fitting analyses are normalized to 100%. Before correction Sb totals vary between 90% and 115%, but are generally greater than 98% and 108%. Arsenic totals vary from 90% to 100%.

Some grains in the calcine were analyzed using electron probe micro-analysis (EPMA) to quantify the amount of Sb associated with the maghemite grains previously analyzed for As by Walker et al. (2005). EPMA data were collected with an ARL-SEMQ electron microprobe at an accelerating voltage of 15 kV, a take-off angle of 52.5°, 100 mA emission current, and a 40 nA beam current. Matrix corrections of the intensity measurements were made using a ZAF correction program supplied by Tracor Northern. Analytical standards for EPMA included: Sb metal from Johnson Matthey and Co. Ltd., and tetrahedrite from Luce, Yale University, for Sb, and calcium phosphate from the University of Keppler, West Germany, for Ca. The tetrahedrite standard was analyzed six times over the course of the data collection. The average calculated apparent concentration is 20.48% which is close to the reference value of 20.3%. The relative standard deviation of the six analyses is 1.79% and all values are within 4% of the reference value. The calculated minimum detection limit based on three standard deviations of the distribution of (counts on the peak) – (counts on the background) (Fialin et al., 1999) is 0.6%. However, at a calculated apparent concentration of 0.3% the signal of the Sb peak is 30% above the background signal. Furthermore, precision (+/–2 $\sigma$ ) calculated based on the formula in Fialin et al. (1999) (includes statistical error on the k-ratios relating to low concentrations), using the counting statistics on 0.3% concentration sample points, is 28%. At 0.2% the precision increases to 65%. Therefore, the detection limit is determined to be 0.3% based on an acceptable precision value of <50% (Fialin et al., 1999).

## 4. Results

#### 4.1. Arsenic and Sb concentration

The grain shown in Fig. 1, a mixture of maghemite and hematite as confirmed by  $\mu$ XRD, is the same grain analyzed by Walker et al. (2005) using the same techniques as employed in this study. The As data

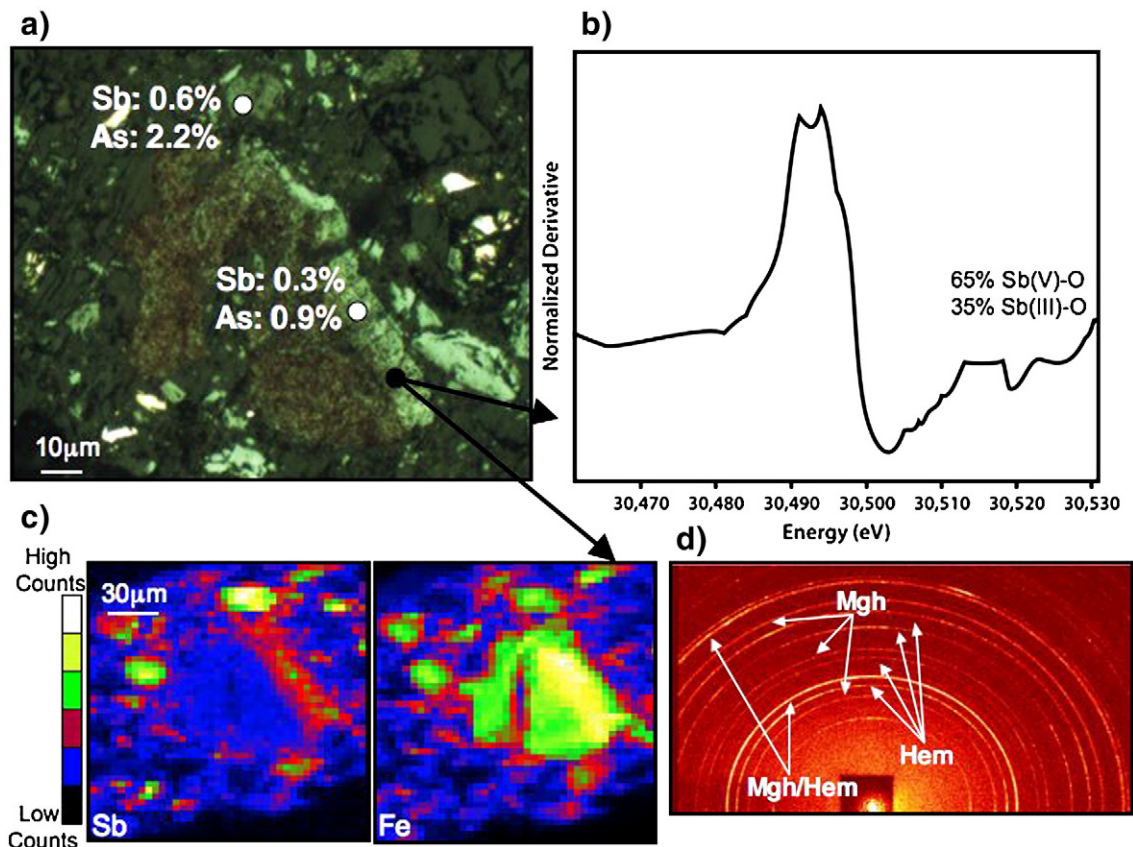


**Fig. 1.** EPMA,  $\mu$ XANES,  $\mu$ XRF, and  $\mu$ XRD results of a hematite-rich maghemite grain from the calcine (M2M Ca6). a) Petrographic image in transmitted and reflected light, EPMA analytical points are given by the white circles, the black circle corresponds to the location of  $\mu$ XANES (b) and  $\mu$ XRD (d) analyses. c)  $\mu$ XRF map showing Fe and Sb distributions, white corresponds to higher counts and black to lower counts (normalized to deadtime correction). d) Smooth-ringed  $\mu$ XRD pattern showing d-spacings 2.95, 2.71, 2.51, 2.21, 2.08, 1.85, 1.61, 1.49, and 1.47.

corresponding to this grain is described in detail by Walker et al. (2005) and will only be summarized here. Arsenic and Sb associated with the maghemite grain are elevated 0.9% and 0.3%, respectively. The  $\mu$ XRF images show that Sb is more concentrated in the maghemite-rich part of the grain, rather than the hematite-rich part of the grain. Walker et al. (2005) also found lower As concentrations in hematite compared to maghemite. In total, 27 maghemite grains in the calcine were analyzed for As resulting in an average concentration of 2.9% and a maximum of 7.6% (Walker et al., 2005). Seven maghemite and hematite grains in the calcine were analyzed for Sb resulting in an average concentration of 0.6% and a maximum concentration of 1.4%.

The varying degree of porosity in the maghemite and hematite grains may account for the variability in the EPMA-determined concentrations of As and Sb in the roaster oxides. The standards used to determine concentrations by EPMA are solid and homogeneous, while the roaster oxides exhibit different textures and different degrees of porosity. Therefore, the concentration is dependent on degree of porosity and even the position on the grain where the analysis is conducted. It would be expected that the real concentration is higher than the calculated apparent concentration. Still, it is obvious that the roaster oxides host significant amounts of As and Sb.

#### 4.2. Arsenic and antimony speciation in roaster oxides

In the calcine, As and Sb associated with maghemite are hosted in multiple oxidation states:  $\text{As}^{5+}$  bound to oxygen ( $\text{As}^{5+}\text{-O}$ ),  $\text{As}^{3+}$  bound to oxygen ( $\text{As}^{3+}\text{-O}$ ),  $\text{As}^{-1}$  bound to sulfur ( $\text{As}^{-1}\text{-S}$ ),  $\text{Sb}^{5+}\text{-O}$  and  $\text{Sb}^{3+}\text{-O}$ . In the XANES region the oxidation state and the next-nearest atom can be determined (based on shape and edge-position comparisons with model compounds), but the exact mineral phase

was not resolved in this study (i.e.  $\text{As}^{5+}\text{-O}$  bonding is present, which may be scorodite or another  $\text{As}^{5+}$  bound to oxygen phase). Because arsenopyrite is identified using petrography the  $\text{As}^{-1}\text{-S}$  component is attributed to relic arsenopyrite. An example of a maghemite grain in the calcine is shown in Fig. 1. The relative proportion of each oxidation state associated with maghemite in the calcine is variable (see Table 1). The error involved in linear combination fitting of Sb XANES spectra may account for some of the variability in percent composition, but cannot explain a range of 29%. More likely it reflects the stability of both oxidation states, in various relative amounts, under roasting conditions and subsequent cyanidation. In the ESP residue,  $3^+$  is consistently the dominant oxidation state of both As and Sb associated with maghemite (see Fig. 2 and Table 1). An example of a maghemite grain in the ESP residue is shown in Fig. 2.

Shown in Fig. 3 are the  $\mu$ XRD and  $\mu$ XANES spectra from roaster oxide grains located in the surficial layer (0 to  $-1$  cm depth), and from  $-16$  cm where conditions are relatively reducing. The grains presented in Fig. 3 were not visible under reflected or transmitted light microscopy, likely because they were buried in the section. Because the  $\mu$ XRD patterns of maghemite and magnetite are similar, an unambiguous distinction between these two minerals is difficult without petrographic information. Magnetite may have formed in the roaster, and may also be the product of maghemite reduction in the environment (Cornell and Schwertmann, 1996). The smooth  $\mu$ XRD rings shown in Fig. 3 are consistent with the  $\mu$ XRD patterns collected on maghemite grains in the roaster materials, which suggests that these grains are primary, or transformed, roaster oxides. In the following discussion these smooth-ringed maghemite or magnetite grains in Baker Pond are referred to simply as roaster oxides.

The dominant As and Sb species associated with roaster oxides in the surficial sediment is  $5^+$ , and  $3^+$  in the deeper sediment. In the

**Table 1**

Linear combination fitting (LCF) results and goodness of fit statistics (chi squared) of roaster oxide grains and bulk As and Sb XANES spectra. Arsenic spectra were only collected on a selected number of grains.

Sample	LCF of antimony				LCF of arsenic				Shown in Fig.	
	Sb <sup>5+</sup> -O	Sb <sup>3+</sup> -O	Sb <sup>3+</sup> -S	Chi Squared	As <sup>5+</sup> -O	As <sup>3+</sup> -O	As <sup>3+</sup> -S	As <sup>-1</sup> -S		Chi Squared
<i>Calcine</i>										
M2M CA6	65	35	0	0.00168	45	40	0	15	0.0454	1
M2M2_1	41	59	0	0.0159						
M2M2_2	61	39	0	0.0045						
M2M08_1	63	37	0	0.00752						
Bulk	60	40	0		48	39	0	13		
<i>ESP residue</i>										
M4MT2a	12	88	0	0.0012	24	76	0	0	0.139	2
M4MT2a_bk					24	76	0	0	0.0875	
M4MT2a_3	0	100	0	0.00295						
M4MT2c_1	16	84	0	0.00126						
M4MT2c_2	5	95	0	0.00132						
M4MT2c_4	16	84	0	0.00122						
M4MT2c_5	0	100	0	0.00245						
Bulk	11	89	0		22	88	0	0		
<i>Surficial Baker Pond</i>										
BP01_2b	74	26	0	0.00671	75	25	0	0	0.0636	3
BP01_3	52	48	0	0.00065						
BP01_5	45	55	0	0.00299	78	22	0	0	0.149	
BP01_6b	61	39	0	0.00274						
Bulk	70	30	0		62	21	0	17		5
<i>Deeper Baker Pond</i>										
BP15_1b	18	19	63	0.00179	15	85	0	0	0.193	3
BP15_201b	20	20	60	0.0582						
BP15_202b	19	19	62	0.0115	15	85	0	0	0.0851	

roaster oxides from the deeper sediment, both the associated As and Sb appear to have undergone transformation. The proportion of As<sup>3+</sup>-O associated with maghemite grains from deeper samples is

higher than is observed in any of the grains discussed thus far. Antimony shows a transformation of Sb bound to O to Sb<sup>3+</sup>-S suggesting a destabilization of Sb bound to the roaster oxide and a

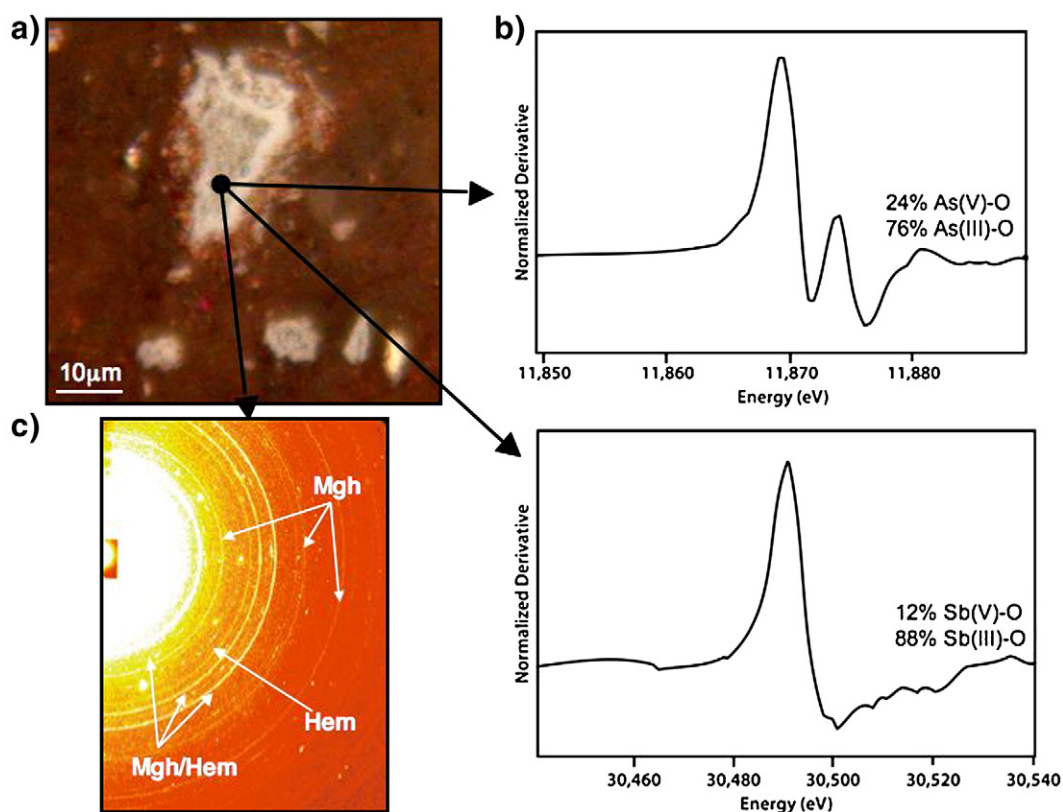


**Fig. 2.** μXANES and μXRD results of a hematite-rich maghemite grain from the ESP residue (M4M-T2a). a) Petrographic image in transmitted and reflected light, the black circle corresponds to the location of μXANES (b) and μXRD (c) analyses. d) Smooth-ringed μXRD pattern showing d-spacings 2.95, 2.71, 2.51, 2.21, 2.08, 1.61, and 1.47.

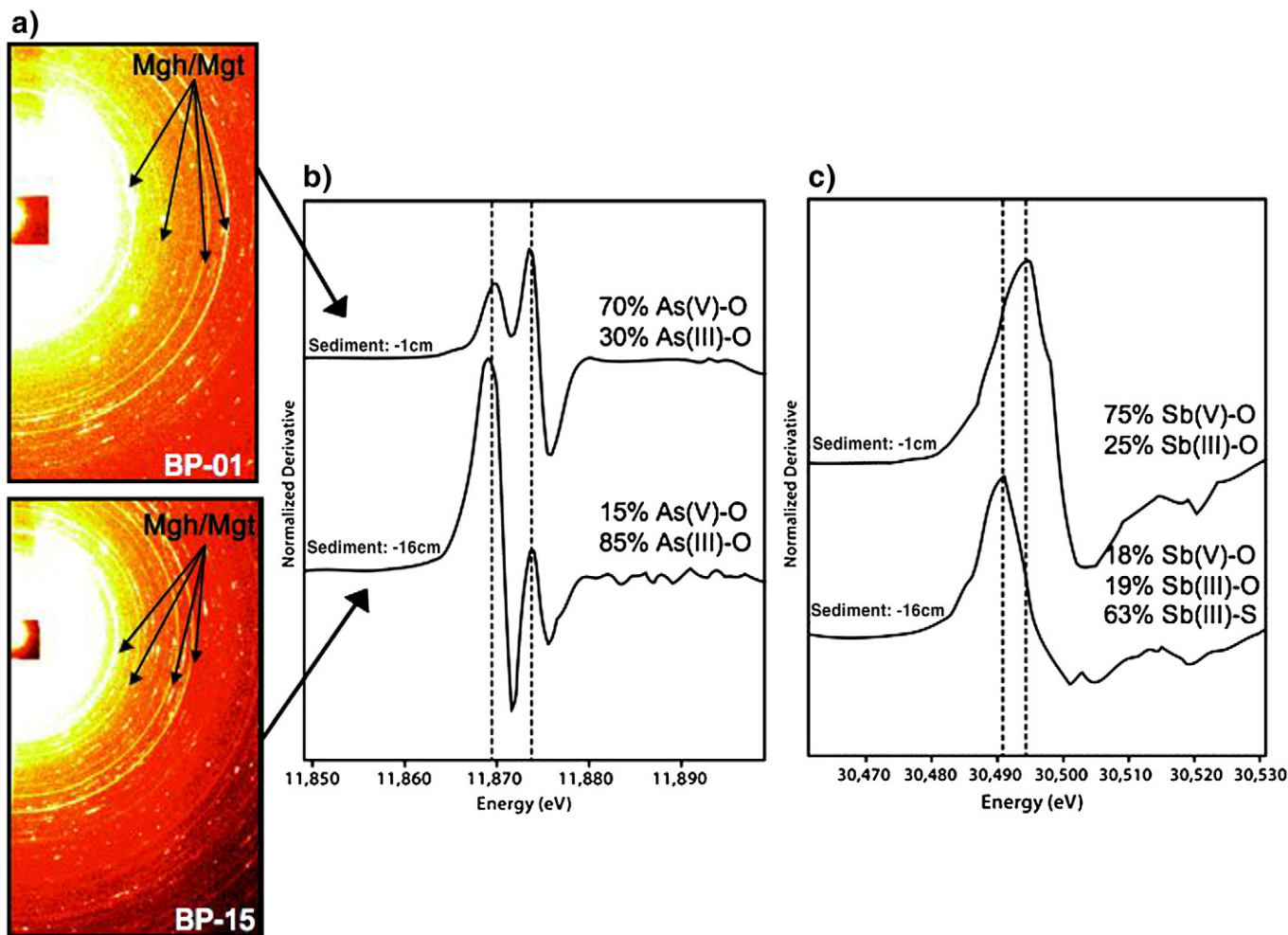


Fig. 3.  $\mu$ XRD and  $\mu$ XANES results of two maghemite grains: the topmost  $\mu$ XRD pattern (including d-spacings 2.95, 2.51, 1.61 and 1.47) and  $\mu$ XANES scans were acquired from a maghemite/magnetite grain located in the surficial layer (BP01\_2b, 0 to  $-1$  cm), and the underlying  $\mu$ XRD pattern (including d-spacings 2.95, 2.51, 1.61 and 1.47) and  $\mu$ XANES scans were acquired from a maghemite/magnetite grain located at  $-16$  cm (BP15\_1b). The linear combination fitted spectra are shown in Figs. 6 and 7.

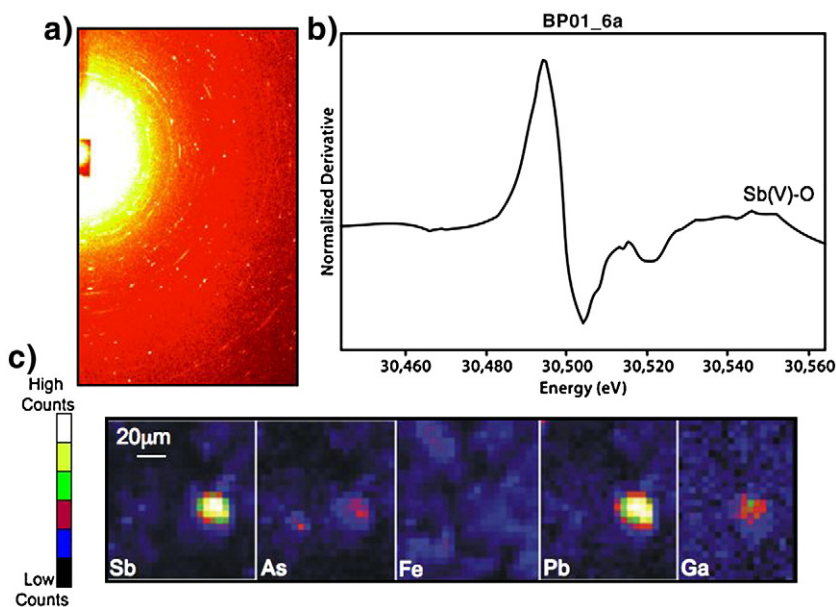


Fig. 4.  $\mu$ XRD (a), Sb  $\mu$ XANES (b), and Sb, As, Fe, Pb, and Ga  $\mu$ XRF maps (c) of an Sb-rich grain from the surficial (0 to  $-1$  cm) Baker Pond sediment (BP01\_6a). The absence of smooth rings suggests that the phase is not nanocrystalline in nature and therefore could not be fit using the methods described in this study. The linear combination fitted spectra are shown in Fig. 6.

reprecipitation or sorption of  $\text{Sb}^{3+}$  onto secondary sulfides (visible in thin section).

#### 4.3. Additional arsenic and antimony-bearing phases identified

In addition to roaster oxides, other As and Sb-bearing phases are identified in the Baker Pond sediment and are illustrated in Figs. 4 and 5. The surficial grain shown in Fig. 4 is an  $\text{Sb}^{5+}$ -O phase that is also rich in Pb and contains some Ga and As. The Fe content is relatively low, which precludes an Fe-(oxyhydr)oxide and  $\text{FePb}_4\text{Sb}_3\text{O}_{13}$  (a decomposition product of jamesonite (Zhu et al., 2006)). Diffraction of the BP01\_6a grain is minimal and so is likely amorphous, and not roaster-derived. Water treatment processes or weathering processes may be forming these Sb-Pb-oxide particles, or Sb and Pb may be surface-sorbed to metal-(oxyhydr)oxides, clays, or oxysulfates. Similar grains were not observed in the calcine or ESP residue.

In the deeper (–16 cm) zone  $\text{As}^{3+}$ -S and  $\text{Sb}^{3+}$ -S phases are encountered, as shown in Fig. 5. These are phases that formed post-depositionally as there was no  $\text{As}^{3+}$ -S present in the ore or produced in the roaster. Antimony<sup>3+</sup>-S was present in the ore (stibnite and sulfosalts host Sb in the 3<sup>+</sup> oxidation state and bound to sulfur). However, more than 99.7% of the Sb in the ore went to the roaster, and in the roaster it was completely reacted, and no  $\text{Sb}^{3+}$ -S phases remained after roasting (see bulk fits of calcine and ESP residue in Table 1). Also, this  $\text{Sb}^{3+}$ -S phase is only observed at depth where conditions are relatively reducing which implies its formation occurred post-deposition. The grain is very small, and may even be smaller than the beam (5  $\mu\text{m}$ ) such that the spotty  $\mu\text{XRD}$  pattern could originate from the As and Sb-bearing grain, or surrounding and underlying grains. An unambiguous interpretation of the  $\mu\text{XRD}$  pattern at this grain scale is not possible.

Adsorption of Sb and As onto mackinawite and pyrite has been reported (Farquhar et al., 2002; Gallegos et al., 2007; Wolthers et al., 2007; Kirsch et al., 2008). However, the Fe content appears to be low, as shown in the  $\mu\text{XRF}$  maps. The precipitation of an amorphous  $\text{As}^{3+}$  and  $\text{Sb}^{3+}$  sulfide phase from solution is also possible and in the case of As, has been suggested as an important attenuation mechanism by other researchers (Moore et al., 1988; Newman et al., 1997; La Force et al., 2000; McCreadie and Blowes, 2000; Farquhar et al., 2002). The elevated sulfur that is required to precipitate As and Sb sulfur-bound phases in Baker Pond is derived from many sources including sulfide oxidation, roaster-derived atmospheric  $\text{SO}_2$  fallout, and additions of copper sulfate and ferric sulfate during water treatment. It is interesting to note that other metals, including Pb, Zn, Cu, and Ga are also associated with this grain (Fig. 5).

#### 4.4. Coincident use of bulk and $\mu\text{XANES}$

Both the mine waste and the Baker Pond sediment are silty-clay sized with many grains <5  $\mu\text{m}$  (the size of the micro-beam). Therefore, additional As and Sb phases may be present but more finely disseminated. By comparing the bulk XANES signal (using a wider beam size to get a signal representative of the whole sample), to the  $\mu\text{XANES}$  spectra we can determine whether another phase not identified in the grain-by-grain analysis is present in the sample. It can be seen in Table 1 that the relative proportions of the different As and Sb oxidation states are similar in the maghemite grains and in the bulk signal in the calcine, and in the ESP residue in the case of Sb, demonstrating that As and Sb are largely associated with the roaster oxides. Fitting of the bulk ESP residue As spectra yields a more dominant  $\text{As}^{3+}$ -O signature compared to the maghemite spectra (88% compared to 76% in maghemite) which suggests the presence of another  $\text{As}^{3+}$ -O phase. In fact, arsenolite ( $\text{As}^{3+}_2\text{O}_3$ ) has been identified by conventional XRD in the ESP residue (Walker et al., submitted manuscript).

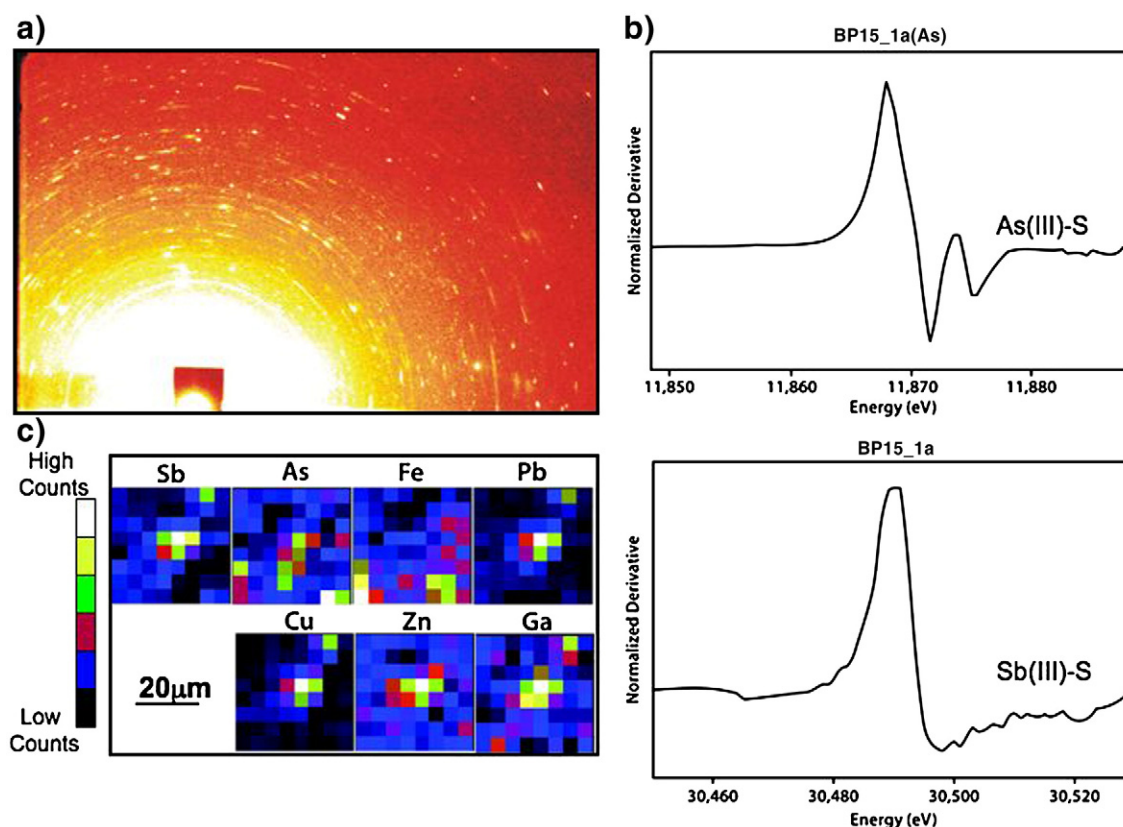


Fig. 5.  $\mu\text{XRD}$  (a)  $\mu\text{XANES}$  (b) and  $\mu\text{XRF}$  (c) results of a grain in sediment collected from –16 cm in Baker Pond (BP15\_1a). Linear combination fitting results show that both the As and Sb associated with the grain are in the 3<sup>+</sup> oxidation state and bound to S. The absence of smooth rings suggests that the phase is not nanocrystalline in nature and therefore could not be fit using the methods described in this study. The linear combination fitted spectra is shown in Fig. 7.

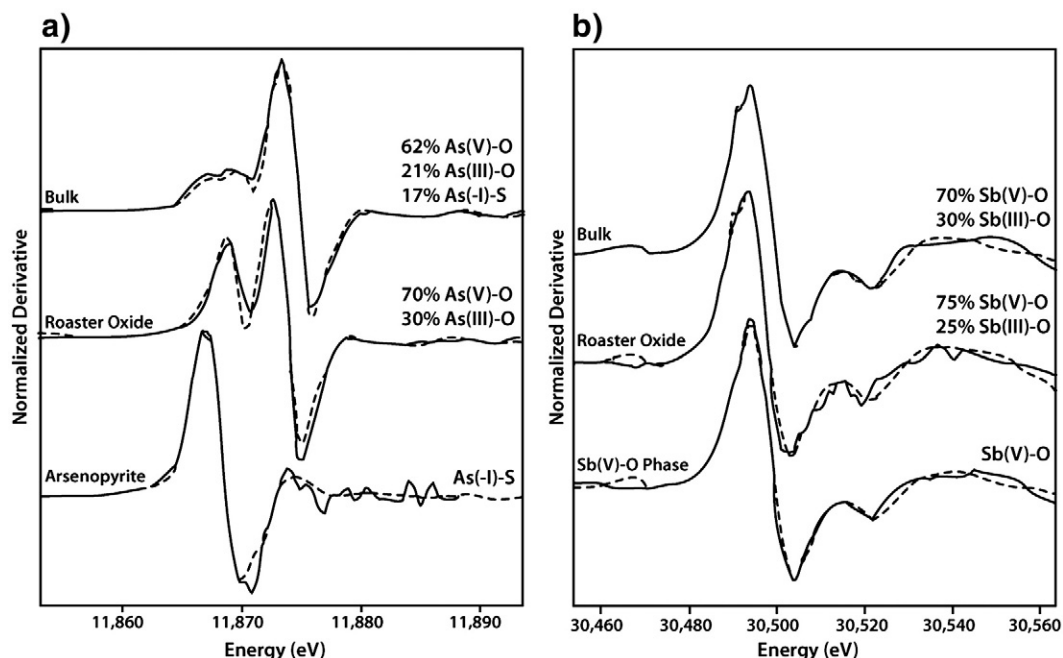


Fig. 6. As (a) and Sb (b) bulk (BP01) and  $\mu$ XANES (BP01\_2b, BP01\_6a) derivative spectra (solid), and linear combination fitting results (dashed).

The only  $\text{As}^{5+}\text{-O}$  and  $\text{As}^{3+}\text{-O}$  bearing grains identified in the surficial sediment of Baker Pond were the roaster oxides, yet the ratio of  $\text{As}^{5+}\text{-O}:\text{As}^{3+}\text{-O}$  in the bulk signal is 2.95, greater than the value of 2.33 in the roaster oxides (see Table 1 and Fig. 6). There may be variability in the As species composition in the roaster oxides (Walker et al., 2005) or, there may be an  $\text{As}^{5+}\text{-O}$  phase that was not identified in the grain-by-grain analyses. Antimony<sup>5+</sup> was found to be associated with roaster oxides and as an  $\text{Sb}^{5+}\text{-O}$  amorphous phase. The Sb compositions associated with roaster oxides were highly variable, so the bulk signal does not provide an indication whether another discrete  $\text{Sb}^{3+}\text{-O}$  phase exists.

A comparison of the bulk XANES and the  $\mu$ XANES spectra collected on the As and Sb-rich grains in the deeper sediment is shown in Fig. 7.

The ratio of  $\text{As}^{5+}\text{-O}:\text{As}^{3+}\text{-O}$  is slightly higher (0.36) in the bulk than in the roaster oxide (0.18). However, within the range of error the results of the bulk As XANES fitting are consistent with  $\text{As}^{5+}\text{-O}$  and  $\text{As}^{3+}\text{-O}$  being hosted primarily by roaster oxides. The Sb bulk XANES spectra identify a significant  $\text{Sb}^{5+}\text{-O}$  dominant phase not identified in the grain-by-grain analyses, which suggests that it is finely disseminated.

## 5. Discussion

### 5.1. Relationship between arsenic, antimony, and the roaster oxides

The exact relationship between the roaster oxides and the associated As and Sb is unclear. The majority of the literature pertaining to the

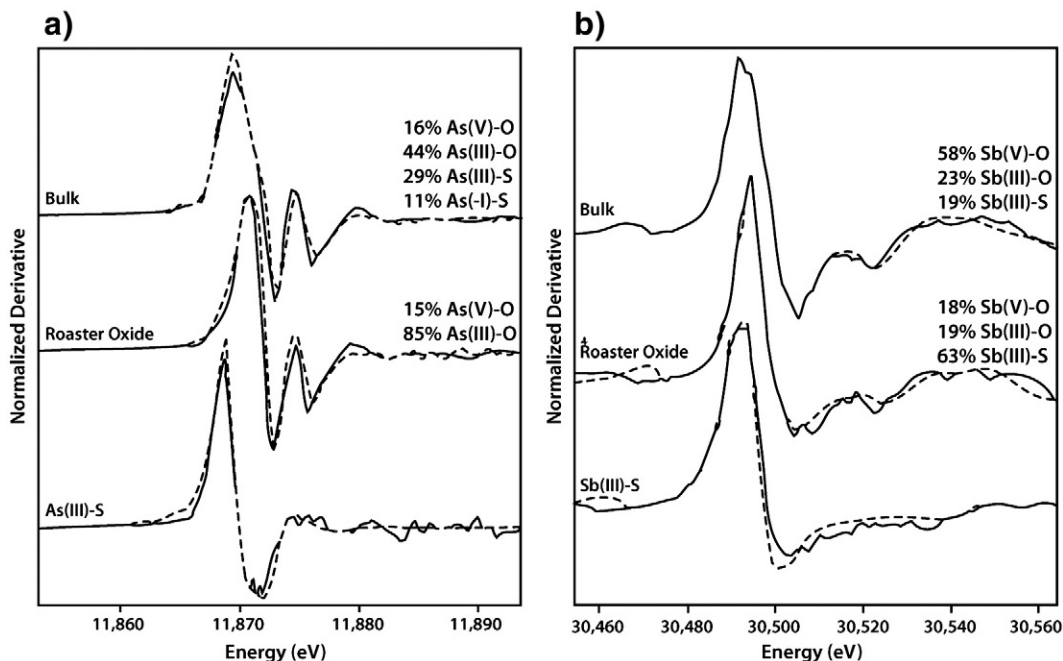


Fig. 7. As and Sb bulk (BP15) and  $\mu$ XANES derivative spectra (BP15\_1b, BP15\_1a) (solid) and linear combination fitting results (dashed).

relationship between As, Sb, and maghemite, hematite, and magnetite, describes low-temperature adsorption mechanisms and reactions occurring between As and Sb in solution and solid-phase Fe-oxides (Auffan et al., 2008; Kirsch et al., 2008; Morin et al., 2008; Wang et al., 2008). It is unclear whether As and Sb in the gaseous phase would react in a manner similar to As and Sb in solution, or whether the vapour–solid phase reactivity is different. Walker et al. (2005) describe some potential relationships between As and the roaster oxides including: structural incorporation, surface adsorption, and the formation of nanocrystalline As phases in the pores and fractures of roaster oxides. The structural incorporation of  $\text{As}^{3+}$  into the defect maghemite structure was deemed possible (Walker et al., 2005), whereas incorporation of  $\text{As}^{5+}$  and  $\text{Sb}^{5+}$  would cause a charge imbalance, and  $\text{Sb}^{3+}$  ions are probably too large (0.76 pm, 30% larger than  $\text{As}^{3+}$ , Shannon, 1976) to be accommodated in the crystal structure of the roaster oxides.

Discrete As or Sb mineral phases were not identified using  $\mu\text{XRD}$ . However, unless the crystal is perfectly oriented relative to the beam,  $\mu\text{XRD}$  used in the experimental setup described can only define nanocrystalline phases (the phases that produce rings in the 2D diffraction pattern). Given that As and Sb are present as two oxidation states, the nanocrystalline phases detected using  $\mu\text{XRD}$  would have to be a composite of an  $\text{As}^{3+}\text{-O}$  and  $\text{As}^{5+}\text{-O}$ ,  $\text{Sb}^{3+}\text{-O}$  and  $\text{Sb}^{5+}\text{-O}$ . It seems that  $\text{Sb}^{3+}\text{Sb}^{5+}\text{O}_4$  is not a significant component as evident by the non-unity ratios of  $\text{Sb}^{5+}:\text{Sb}^{3+}$  (0.69 to 1.6 in the calcine, and 0 to 0.19 in the ESP residue). However, the formation of other nanocrystalline phases cannot be discounted.

The large surface area of the roaster oxides, resulting from their nanocrystalline, porous, and fractured nature, suggests that adsorption of As and Sb to the surface of the roaster oxides is a prominent attenuation mechanism. In low-temperature experiments involving adsorption of As and Sb onto maghemite, magnetite, and hematite, strong inner-sphere complexes have been reported to form (Manning et al., 2002; Ona-Nguema et al., 2005; Coker et al., 2006; Auffan et al., 2008; Kirsch et al., 2008; Morin et al., 2008; Wang et al., 2008).

## 5.2. Roaster oxides in mine waste and the environment

The speciation of As and Sb is different in the two roaster waste streams (5+ in the calcine and 3+ in the ESP residue). Therefore, without supplementary data (i.e. aqueous analyses) it is difficult to distinguish between redox-controlled or anthropogenically-influenced speciation. For example, it is possible that the  $\text{As}^{3+}$  dominance associated with the roaster oxides in the deeper Baker Pond sediment has not undergone any transformations but originates from the ESP residue. Or, the As speciation associated with the same roaster oxide may suggest a preferential desorption or reduction of  $\text{As}^{5+}$ . The pore-water As and Sb totals and speciation (Fawcett, 2009) provide evidence that the latter is occurring. Pore-water As concentrations are as high as 62.5 mg/L, and the  $\text{As}^{5+}$  species dominates only within the first 5 cm below the sediment–water interface, suggesting post-depositional transformation of As associated with roaster oxides.

To account for the binding of Sb to sulfur in the deeper sediment, Sb must undergo desorption and subsequently re-precipitate as a sulfide, or adsorb onto a sulfide. Antimony cycling from the roaster oxide to the S-bound phase, and its low concentrations in pore-water (Fawcett, 2009), is evidence that this dynamic cycling between solid phases efficiently attenuates Sb. The presence of the  $\text{Sb}^{3+}\text{-S}$  within the area of  $\mu\text{XANES}$  analyses of the roaster oxide grains is an indication that Sb mobility is very limited.

The co-existence of multiple As and Sb-bearing phases indicates complex and dynamic cycling of these elements, and overlapping stability fields are related in part to redox processes, but also to the relationship with the host mineral. The  $\text{As}^{3+}\text{-O}$  phase has been observed to persist in maghemite in subaerially exposed tailings (Walker et al., 2005) and in roaster oxides in the suboxic environment

of the surficial sediment in Baker Pond. Wang et al. (2008) found that  $\text{As}^{3+}$  can occupy the vacant Fe-tetrahedral sites forming a tridentate hexanuclear complex on the surface of magnetite. Similarly, Auffan et al. (2008) found that  $\text{As}^{3+}$  replaced tetrahedral sites on the surface of maghemite, binding to a high number of Fe octahedra. In addition to the potential structural incorporation of  $\text{As}^{3+}$ , the formation of this adsorption complex may account for apparent stability of  $\text{As}^{3+}$  and its persistent association with maghemite under a variety of environmental conditions.

## 6. Concluding remarks

The complexity of speciation in waste streams entering the aqueous and sedimentary environments is important to understand. Roasters and smelters typically emit reduced species of metalloids but, as shown in this study, may also produce complex mixtures of species. In these types of systems it is important to understand and recognize the complex nature of the source materials, in order to predict their stability in the environment, and to accurately describe any transformations these phases may undergo, or have undergone, in the environment.

This study has also suggested that As and Sb exhibit distinctive behaviour, most notably in the deeper sediment. Both elements are hosted in multiple phases, undergo post-depositional transformations, and are subsequently attenuated by bonding to S. However, the efficiency of attenuation is different. Following desorption from the roaster oxides it appears as though Sb is mobile only at a very local scale while As is mobile over a larger scale, as evidenced by the presence of  $\text{Sb(III)-S}$  but not  $\text{As(III)-S}$  within the analytical range of the roaster oxides.

The prevalence of  $\text{Sb}^{5+}$  in the deeper sediment where most of the As has been reduced, is an indication that the redox chemistry of Sb is not fully understood, and that the  $\text{Sb}^{5+}$  oxidation state is apparently stable over a wide range of Eh conditions. This finding is consistent with that of Mitsunobu et al. (2006) who also found that  $\text{Sb}^{5+}$  bound to  $\text{Fe}^{3+}$  oxyhydroxide in soil is stable over a wide range of Eh conditions.

The combination of bulk XANES and  $\mu\text{XANES}$  was critical to understand the significance of the  $\text{Sb}^{5+}\text{-O}$  phase which otherwise would have been underestimated by a considerable margin. In these types of environments where multiple phases and associations exist, some in lower concentrations, the combination of  $\mu\text{XANES}$  and bulk XANES is capable of resolving the complexity.

The many advantages of coupling  $\mu\text{XRD}$ ,  $\mu\text{XRF}$ , and  $\mu\text{XANES}$  techniques are outlined in Walker et al. (2005) and so will not be discussed at length here. However, this study illustrates that the coincident use of these techniques also provides valuable information on Sb associations. This finding is especially significant because gaining useful information from the Sb XANES region is more challenging compared to As. The Sb spectra are much broader, the crystallographic environment around Sb can be complex, and extracting a signal can be more difficult (Fawcett et al., 2009). To confound the problem, in environmental samples Sb is generally present in much lower concentrations than As. However, if the total Sb in the bulk sample is too low to acquire a useful spectra, the combination of  $\mu\text{XRF}$ ,  $\mu\text{XRD}$ , and  $\mu\text{XANES}$  is useful in targeting and characterizing Sb-bearing phases.

Antimony is emerging as a contaminant of concern, yet broad gaps in our knowledge of the geochemical cycling of Sb in the environment persist. Reliable and useful results can be achieved in a short amount of time using this combination of techniques and may prove to be an invaluable tool in advancing our understanding of the fate of Sb in the environment.

## Acknowledgements

PNC/XOR facilities at the Advanced Photon Source, and research at these facilities, are supported by the US Department of Energy – Basic

Energy Sciences, a major facilities access grant from NSERC, the University of Washington, Simon Fraser University and the Advanced Photon Source. Use of the Advanced Photon Source is also supported by the U.S. Department of Energy, Office of Science, Office of Basic Energy Sciences, under Contract DE-AC02-06CH11357. This study was partly funded through the NSERC Northern Research Internship and by the Mineralogical Association of Canada. We thank the Giant Mine Remediation Team for site access and kind support, and Kelly Sexsmith for her comprehensive overview of the complex environmental issues associated with the Giant mine. S. R. Walker and J. Peacey (both at Queen's University) provided helpful insights into the roasting operations and products. Dave Kempson of Queen's University contributed EPMA technical assistance and Robert Gordon and Stephanie DeSisto provided beamline assistance at PNC/XOR.

## References

- Asryan, N.A., Alikhanyan, A.S., Nipan, G.D., 2004. Thermodynamic stability of antimony oxides. *Russian Journal of Physical Chemistry* 78, 5–11.
- ATHENA software, <http://cars9.uchicago.edu/ravel/software/accessed> and downloaded July 2007.
- Auffan, M., Rose, J., Proux, O., Borschneck, D., Masion, A., Chaurand, P., Hazemann, J., Chaneac, C., Jolivet, J., Wiesner, M.R., Van Geen, A., Bottero, J., 2008. Enhanced adsorption of arsenic onto maghemite nanoparticles: As(III) as a probe of the surface structure and heterogeneity. *Langmuir* 24, 3215–3222.
- Banfield, J.F., Zhang, H.Z., 2001. Nanoparticles in the environment. *Nanoparticles and the Environment* 44, 1–58.
- Beauchemin, S., Kwong, Y.T.J., 2006. Impact of redox conditions on arsenic mobilization from tailings in a wetland with neutral drainage. *Environmental Science and Technology* 40, 6297–6303.
- Berube, Y., Frenette, M., Gilbert, R., Antcl, C., 1974. Studies of Mine Waste Containment at Two Mines near Yellowknife, NWT, ALUR 1972–73. QS-3038-000-EE-A1, 1–181.
- Canam, T.W., 2006. Discover, mine production, and geology of the Giant Mine. In: Anglin, C.D., Falck, H., Wright, D.F., Ambrose, E.J. (Eds.), *Gold in the Yellowknife Greenstone Belt, Northwest Territories: results of the EXTECH III Multidisciplinary Research Project: Geological Association of Canada-Mineral Deposits Division*.
- Coker, V.S., Gault, A.G., Pearce, C.I., van der Laan, G., Telling, N.D., Charnock, J.M., Polya, D.A., Lloyd, J.R., 2006. XAS and XMCD evidence for species-dependent partitioning of arsenic during microbial reduction of ferrihydrite to magnetite. *Environmental Science and Technology* 40, 7745–7750.
- Coleman, L.C., 1957. Mineralogy of the Giant Yellowknife Gold Mine, Yellowknife, NWT. *Economic Geology* 52, 400–425.
- Cornell, R.M., Schwertmann, U., 1996. *The Iron Oxides*. Weinheim, NY.
- Farquhar, M.L., Charnock, J.M., Livens, F.R., Vaughan, D.J., 2002. Mechanisms of arsenic uptake from aqueous solution by interaction with goethite, lepidocrocite, mackinawite, and pyrite: an X-ray absorption spectroscopy study. *Environmental Science and Technology* 36, 1757–1762.
- Fawcett, S.E., Andrade, C.F., Walker, S.R., Jamieson, H.E., 2006. Understanding the environmental legacy of the Giant gold mine, Yellowknife, NWT: lessons from recent research. Proceedings of CLRA/ACRS 2006 Annual Meeting, Reclamation and Remediation: Policy to Practice, August 20–23, Ottawa, Canada.
- Fawcett, S.E. (2009) Speciation and mobility of Sb and As in mine waste and the aqueous environment in the region of the Giant mine, Yellowknife, PhD Thesis, Queen's University.
- Fawcett, S.E., Gordon, R.A., Jamieson, H.E., 2009. Optimizing experimental design, overcoming challenges, and gaining valuable information from the Sb K-edge XANES region. *American Mineralogist* 94, 1377–1387.
- Fialin, M., Remy, H., Richard, C., Wagner, C., 1999. Trace element analysis with the electron microprobe: new data and perspectives. *American Mineralogist* 84, 70–77.
- Filella, M., Belzile, N., Chen, Y., 2002a. Antimony in the environment: a review focused on natural waters: I. Occurrence. *Earth-Science Reviews* 57, 125–176.
- Filella, M., Belzile, N., Chen, Y., 2002b. Antimony in the environment: a review focused on natural waters: II. Relevant solution chemistry. *Earth-Science Reviews* 59, 265–285.
- Foster, A.L., Brown, G.E., Tingle, T.N., Parks, G.A., 1998. Quantitative arsenic speciation in mine tailings using X-ray absorption spectroscopy. *American Mineralogist* 83 (5–6), 553–568.
- Froelich, P.N., Klinkhammer, G.P., Bender, M.L., Luedtke, N.A., Heath, G.R., Cullen, D., Dauphin, P., Hammond, D., Hartman, B., Maynard, V., 1979. Early oxidation of organic-matter in pelagic sediments of the eastern equatorial Atlantic – suboxic diagenesis. *Geochimica Cosmochimica Acta* 43, 1075–1090.
- Gallegos, T.J., Hyun, S.P., Hayes, K.F., 2007. Spectroscopic investigation of the uptake of arsenite from solution by synthetic mackinawite. *Environmental Science Technology* 41, 7781–7786.
- Hammersley, A.P., 1998. FIT2D V10.3 Reference Manual V4.0, European Synchrotron Research Facility, Paper ESRF98-HA01T. program and manual available at [http://www.esrf.fr/computing/expg/subgroups/data\\_analysis/FIT2D](http://www.esrf.fr/computing/expg/subgroups/data_analysis/FIT2D).
- Heald, S.M., Cross, J.O., Brew, D.L., Gordon, R.A., 2007. The PNC/XOR X-ray microprobe station at APM sector 20. *Nuclear Instruments and Methods in Physics Research A* 582, 215–217.
- Herbel, M., Fendorf, S., 2006. Biogeochemical processes controlling the speciation and transport of arsenic within iron coated sands. *Chemical Geology* 228, 16–32.
- Kirsch, R., Scheinost, A.C., Rossberg, A., Banerjee, D., Charlet, L., 2008. Reduction of antimony by nano-particulate magnetite and mackinawite. *Mineralogical Magazine* 72, 185–189.
- Kneebone, P.E., O'Day, P.A., Jones, N., Hering, J.G., 2002. Deposition and fate of arsenic in iron-and arsenic-enriched reservoir sediments. *Environmental Science and Technology* 36, 381–386.
- Kocar, B.D., Herbel, M.J., Tufano, K.J., Fendorf, S., 2006. Contrasting effects of dissimilatory iron(III) and arsenic(V) reduction on arsenic retention and transport. *Environmental Science and Technology* 40, 6715–6721.
- La Force, M.J., Hansel, C.M., Fendorf, S., 2000. Arsenic speciation, seasonal transformations, and co-distribution with iron in a mine waste-influenced palustrine emergent wetland. *Environmental Science and Technology* 34, 3937–3943.
- Makovicky, E., 1989. Modular classification of sulfosalts – current status – definition and application of homologous series. *Neues Jahrbuch Fur Mineralogie-Abhandlungen* 160, 269–297.
- Manning, B.A., Fendorf, S.E., Bostick, B., Suarez, D.L., 2002. Arsenic(III) oxidation and arsenic(V) adsorption reactions on synthetic birnessite. *Environmental Science and Technology* 36, 976–981.
- Marsden, J.O., House, C.I., 2006. *The Chemistry of Gold Extraction*. Society for Mining, Metallurgy, and Exploration, Inc, U.S.A.
- Martin, A.J., Pedersen, T.F., 2002. Seasonal and interannual mobility of arsenic in a lake impacted by metal mining. *Environmental Science and Technology* 36, 1516–1523.
- McCreadie, H., Blowes, D.W., 2000. Influence of reduction reactions and solid phase composition on porewater concentrations of arsenic. *Environmental Science and Technology* 34, 3159–3166.
- Mitsunobu, S., Harada, T., Takahashi, Y., 2006. Comparison of antimony behavior with that of arsenic under various soil redox conditions. *Environmental Science and Technology* 4, 7270–7276.
- Moore, J.N., Ficklin, W.H., Johns, C., 1988. Partitioning of arsenic and metals in reducing sulfidic sediments. *Environmental Science and Technology* 22, 432–437.
- More, M.A., Pawson, H.E., 1978. *Giant Yellowknife Mines Limited*. In: Pickett, D.E. (Ed.), *Milling Practice in Canada*, pp. 63–65.
- Morin, G., Ostergerd, J.D., Juillot, F., Ildefonse, P., Calas, G., Brown, G.E., 1999. XAFS determination of the chemical form of lead in smelter-contaminated soils and mine tailings: importance of adsorption processes. *American Mineralogist* 84, 420–434.
- Morin, G., Ona-Nguema, G., Wang, Y., Menguy, N., Juillot, F., Proux, O., Guyot, F., Calas, G., Brown Jr., G.E., 2008. Extended X-ray absorption fine structure analysis of arsenite and arsenate adsorption on maghemite. *Environmental Science and Technology* 42, 2361–2366.
- Navrotsky, A., 2001. Thermochemistry of nanomaterials. *Nanoparticles and the Environment* 44, 73–103.
- Newman, D.K., Beveridge, T.J., Morel, F.M.M., 1997. Precipitation of arsenic trisulfide by *Desulfotomaculum auripigmentum*. *Applied Environmental Microbiology* 63, 2022–2028.
- O'Day, P.A., Carroll, S.A., Waychunas, G.A., 1998. Rock-water interactions controlling zinc, cadmium, and lead concentrations in surface waters and sediments, US Tri-State Mining District. 1. Molecular identification using X-ray absorption spectroscopy. *Environmental Science and Technology* 32, 943–955.
- Ona-Nguema, G., Morin, G., Juillot, F., Calas, G., Brown, G.E., 2005. EXAFS analysis of arsenite adsorption onto two-line ferrihydrite, hematite, goethite, and lepidocrocite. *Environmental Science Technology* 39, 9147–9155.
- Paktunc, D., Kingston, D., Pratt, A., McMullen, J., 2006. Distribution of gold in pyrite and in products of its transformation resulting from roasting of refractory gold ore. *Canadian Mineralogist* 44, 213–227.
- Pedersen, H.D., Postma, D., Jakobsen, R., 2006. Release of arsenic associated with the reduction and transformation of iron oxides. *Geochimica Cosmochimica Acta* 70, 4116–4129.
- Ravel, B., 2007. ATHENA User's Guide V1.2 for Athena Version 0.8.53. program and manual available at <http://cars9.uchicago.edu/~ravel/software/exafs>.
- Savage, K.S., Tingle, T.N., O'Day, P.A., Waychunas, G.A., Bird, D.K., 2000. Arsenic speciation in pyrite and secondary weathering phases, Mother Lode Gold District, Tuolumne County, California. *Applied Geochemistry* 15 (8), 1219–1244.
- Shannon, R.D., 1976. Revised effective ionic-radii and systematic studies of interatomic distances in halides and chalcogenides. *Acta Crystallographica Section A* 32, 751–767.
- Smedley, P.L., Kinniburgh, D.G., 2002. A review of the source, behaviour and distribution of arsenic in natural waters. *Applied Geochemistry* 17, 517–568.
- SRK Consulting and SENES Consultants Ltd., 2007. *Giant Mine Remediation Plan*. Submitted to Indian and Northern Affairs Canada, 1C1001.013.
- Tufano, K.J., Fendorf, S., 2008. Confounding impacts of iron reduction on arsenic retention. *Environmental Science and Technology* 42, 4777–4783.
- Vink, B.W., 1996. Stability relations of antimony and arsenic compounds in the light of revised and extended Eh-pH diagrams. *Chemical Geology* 130, 21–30.
- Walker, S.R., Jamieson, H.E., Lanzirotti, A., Andrade, C.F., Hall, G.E.M., 2005. The speciation of arsenic in iron oxides in mine wastes from the Giant gold mine, NWT: application of synchrotron micro-XRD and micro-XANES at the grain scale. *Canadian Mineralogist* 43, 1205–1224.
- Wang, Y., Morin, G., Ona-Nguema, G., Menguy, N., Juillot, F., Aubry, E., Guyot, F., Calas, G., Brown Jr., G.E., 2008. Arsenite sorption at the magnetite-water interface during aqueous precipitation of magnetite: EXAFS evidence for a new arsenite surface complex. *Geochimica et Cosmochimica Acta* 72, 2573–2586.
- Wedepohl, K.H., 1974. Antimony. In: Wedepohl, K.H. (Ed.), *Handbook of Geochemistry*. Springer-Verlag, Berlin, pp. 1–11.
- WHO, 1993. *Guidelines for Drinking-water Quality*. Volume 1: Recommendations, 2nd ed. World Health Organization, Geneva.
- Wolthers, M., Butler, I.B., Rickard, D., 2007. Influence of arsenic on iron sulfide transformations. *Chemical Geology* 236, 217–227.
- Zhu, F., Hua, Y., Meng, Y., 2006. Kinetics of the reaction between Pb-Sb complex sulphide concentrates and water vapour. *SAIMM* 106, 713–719.

*The Canadian Mineralogist*  
 Vol. 47, pp. 533-556 (2009)  
 DOI: 10.3749/canmin.47.3.533

## ARSENIC MINERALOGY OF NEAR-SURFACE TAILINGS AND SOILS: INFLUENCES ON ARSENIC MOBILITY AND BIOACCESSIBILITY IN THE NOVA SCOTIA GOLD MINING DISTRICTS

STEPHEN R. WALKER

*Department of Geological Sciences and Geological Engineering, Queen's University, Kingston, Ontario K7L 3N6, Canada*

MICHAEL B. PARSONS

*Natural Resources Canada, Geological Survey of Canada (Atlantic), 1 Challenger Drive,  
 Dartmouth, Nova Scotia B2Y 4A2, Canada*

HEATHER E. JAMIESON<sup>§</sup>

*Department of Geological Sciences and Geological Engineering, Queen's University, Kingston, Ontario K7L 3N6, Canada*

ANTONIO LANZIROTTI

*Consortium for Advanced Radiation Sources, University of Chicago, Chicago, Illinois 60637, USA*

### ABSTRACT

The mineral form, grain size and texture of As-bearing particles are important factors influencing the risk to human health associated with exposure to As-contaminated soils, sediments and mine wastes. Mining of arsenopyrite-bearing gold ores in Nova Scotia in the late 1800s and early 1900s has left a legacy of weathered, As-rich tailings deposits in more than 60 gold districts across the province. Fourteen samples of near-surface tailings and one of soil from several former gold mines frequented by the public were sieved to <150 µm and characterized using conventional mineralogical techniques (XRD, microscopy and EPMA) and synchrotron micro-analysis (µ-X-ray diffraction, µ-X-ray fluorescence and µ-X-ray absorption spectroscopy). Two high-As (>20% As) mill concentrates exposed at the surface within the tailings deposits are dominated by a single As mineral, fine-grained scorodite (FeAsO<sub>4</sub>•2H<sub>2</sub>O) in one case, and massive unweathered arsenopyrite in the other. In the tailings (0.7 to 7% As), scorodite and amorphous hydrous ferric arsenate (HFA) are the most common As-bearing major components, occurring as discrete grains or grain coatings on gangue minerals. Other major As phases identified in the tailings include As-bearing amorphous hydrous ferric oxyhydroxides (HFO), kañkite (FeAsO<sub>4</sub>•3.5H<sub>2</sub>O), pharmacosiderite [KFe<sub>4</sub>(AsO<sub>4</sub>)<sub>3</sub>(OH)<sub>4</sub>•6–7H<sub>2</sub>O], yukonite [Ca<sub>7</sub>Fe<sub>12</sub>(AsO<sub>4</sub>)<sub>10</sub>(OH)<sub>20</sub>•15H<sub>2</sub>O], amorphous Ca–Fe arsenates, and arsenopyrite. Minor or trace constituents include: As-bearing ferric oxyhydroxides with up to 10% As (HFO, goethite, lepidocrocite and akaganeite), As-bearing sulfates (jarosite [(K,Na,H<sub>3</sub>O)Fe<sub>3</sub>(SO<sub>4</sub>)<sub>2</sub>(OH)<sub>6</sub>], tooeleite [Fe<sub>6</sub>(AsO<sub>3</sub>)<sub>4</sub>(SO<sub>4</sub>)(OH)<sub>4</sub>•4H<sub>2</sub>O]) and realgar (As<sub>4</sub>S<sub>4</sub>). Arsenic-bearing HFO (2.5% As) and goethite (0.08% As) were identified in the single B-horizon soil sample. This study is part of a broader coordinated effort by a multi-department federal and provincial advisory committee formed to coordinate the study of ecosystem and human health risks associated with historical gold mine sites in Nova Scotia. Our study shows that (i) the mineralogy of As in weathered tailings is highly variable, with aggregates of more than one As-bearing phase common in a given sample, and (ii) major differences in As mineralogy in the tailings are mainly controlled by factors that influence the weathering history (*e.g.*, presence or absence of mill concentrates, degree of water saturation, and abundance of relict carbonate minerals). The variable solubility of these primary and secondary As-bearing minerals influences both the environmental mobility and the bioaccessibility of As in near-surface tailings and soil samples.

**Keywords:** arsenic-rich tailings, gold mining, bioaccessibility, arsenopyrite, secondary minerals, scorodite, amorphous iron arsenate, yukonite, pharmacosiderite, iron oxyhydroxides, Nova Scotia.

<sup>§</sup> E-mail address: jamieson@geol.queensu.ca

## SOMMAIRE

La forme minéralogique, la granulométrie et la texture des particules arsenifères s'avèrent des facteurs importants qui influencent le risque à la santé associé à une exposition aux sols, sédiments et déchets miniers contaminés en arsenic. L'extraction de minerais aurifères en Nouvelle-Écosse vers la fin des années 1800 et au début du siècle dernier a laissé comme succession des rejets altérés riches en As dans plus de 60 districts aurifères répandus dans la province. Nous avons pris quatorze échantillons de ces rejets exposés à la surface et un échantillon de sol au site de plusieurs mines d'or accessibles au public. Ceux-ci ont été tamisés à <150 µm et caractérisés au moyen de techniques minéralogiques conventionnelles (diffraction X, microscopie, et analyse avec une microsonde électronique) et de micro-analyses avec un synchrotron (µ-diffraction X, µ-fluorescence X et µ-spectroscopie d'absorption X). Deux concentrés à haute teneur en As (>20% As) exposés dans ces amas de rejets contiennent un seul minéral d'arsenic, la scorodite (FeAsO<sub>4</sub>•2H<sub>2</sub>O) à grains fins dans un cas, et l'arsénoxyrite massive dans un autre. Dans les rejets (entre 0.7 et 7% As), la scorodite et un arsenate ferrique amorphe (HFA) sont les porteurs les plus répandus d'arsenic; on les trouve en grains distincts ou en liserés en bordure des minéraux de la gangue. Ont aussi été identifiés dans ces rejets des oxyhydroxydes amorphes ferriques hydratés arsenifères (HFO), kaňkite (FeAsO<sub>4</sub>•3.5H<sub>2</sub>O), pharmacosiderite [KFe<sub>4</sub>(AsO<sub>4</sub>)<sub>3</sub>(OH)<sub>4</sub>•6–7H<sub>2</sub>O], yukonite [Ca<sub>7</sub>Fe<sub>12</sub>(AsO<sub>4</sub>)<sub>10</sub>(OH)<sub>20</sub>•15H<sub>2</sub>O], des arsenates amorphes à Ca–Fe, et l'arsénoxyrite. Parmi les composants mineurs ou présents en traces sont des oxyhydroxydes ferriques contenant plus de 10% d'arsenic (HFO: goéthite, lépidocrocite et akaganéite), des sulfates arsenifères (jarosite [(K,Na,H<sub>3</sub>O)Fe<sub>3</sub>(SO<sub>4</sub>)<sub>2</sub>(OH)<sub>6</sub>], tooéléite [Fe<sub>6</sub>(AsO<sub>3</sub>)<sub>4</sub>(SO<sub>4</sub>)(OH)<sub>4</sub>•4H<sub>2</sub>O]) et réalgar (As<sub>4</sub>S<sub>4</sub>). Nous avons identifié la phase HFO (2.5% As) et la goéthite (0.08% As) dans l'échantillon de la couche B du sol. Notre travail fait partie d'un effort coordonné plus large impliquant plusieurs départements aux niveaux fédéral et provincial et un comité consultatif formé pour coordonner l'étude de l'écosystème et des risques à la santé associés aux sites d'extraction historique de minerais aurifères en Nouvelle-Écosse. Nous démontrons que (i) la minéralogie de l'arsenic dans les rejets sujets à l'altération de surface est très variable, avec des agrégats répandus de plus d'une espèce arsenifère dans un seul échantillon, et (ii) les différences importantes en minéralogie de l'arsenic dans ces rejets seraient régies par l'évolution de l'altération de surface, influencée par la présence ou l'absence de concentrés du minerai, le degré de saturation en eau, et l'abondance de reliquats de minéraux carbonatés. La solubilité variable de ces minéraux primaires et secondaires porteurs d'arsenic exerce une influence à la fois sur la mobilité environnementale et la bioaccessibilité de l'arsenic dans les déchets non enfouis et les sols.

(Traduit par la Rédaction)

**Mots-clés:** déchets miniers riches en arsenic, extraction de l'or, bioaccessibilité, arsénoxyrite, minéraux secondaires, scorodite, arsenate amorphe de fer, yukonite, pharmacosidérite, oxyhydroxydes de fer, Nouvelle-Écosse.

## INTRODUCTION

Inhalation or ingestion of As-bearing soil and dust poses a risk to human health at many locations around the world. For those exposed, the health risk is manifested in terms of not only the total concentration of As, but also the bioavailability of the As inhaled or ingested (Reeder *et al.* 2006). The physical characteristics of As-bearing particles (crystallinity, mineralogy, density, size, shape or morphology, and surface charge) combined with the mode of As occurrence (surface sorbed or incorporated within a crystal structure, oxidation state, and coordination environment) determine the behavior (solubility) of As in human body fluids and thus bioavailability (Ruby *et al.* 1999, Plumlee *et al.* 2006, Reeder *et al.* 2006). Understanding the kinetic and thermodynamic controls on As release is important, given the relatively short transit-times (*i.e.*, hours or days) of ingested or inhaled particles through the human gastrointestinal system (Plumlee & Ziegler 2003).

In practice, bioaccessibility is a more useful concept than bioavailability in dealing with contaminated materials (Semple *et al.* 2004). A bioaccessible compound is one that is available to cross a physiological membrane, whereas the bioavailable component is the quantity

actually absorbed across that membrane (Ruby *et al.* 1996, 1999, Reeder *et al.* 2006). Although dissolved As forms are by definition bioaccessible, the bioaccessibility of As in solids depends on solubility and the rate of dissolution or desorption in human fluids. Solid-bound As poses a challenge in risk assessments of contaminated sites, as the form of As can be difficult to determine. In turn, the ability to predict the bioavailability or bioaccessibility of As may be hampered by a limited understanding of the complex physicochemical properties of the As-bearing solids. An assumption of 100% bioavailability may seriously overestimate the environmental risk for solid-bound As; therefore, methods capable of inferring bioaccessibility either quantitatively or qualitatively can be useful in evaluating potential risk. Understanding the solid-phase speciation of As at the particle scale has the potential to provide a fundamental basis for predicting As bioaccessibility and thus bioavailability from inhalation or ingestion.

Gold mining in Nova Scotia, mostly between 1861 and 1942, has left many As-rich tailings areas across the province owing to the widespread occurrence of arsenopyrite in Au-bearing quartz veins and surrounding host-rocks (Parsons *et al.* 2004). Today,

frequent activity in the form of dirt bike racing, all-terrain-vehicle (ATV) traffic, hiking, gold panning and other human visitation has been observed or inferred at many of these tailings areas. Residential land use also exists in close proximity to some tailings deposits (in some cases within 100 m).

The objective of this research is to examine the As mineralogy in a range of near-surface tailings and soil samples collected from several Nova Scotia Au minesites frequented by the public. To accomplish this, we have expanded on an earlier study (Corriveau 2006) by advancing previously developed micro-analytical methods (Walker *et al.* 2005) that combine petrography, electron-microprobe analysis, and synchrotron-based  $\mu$ -XRF with grain-by-grain  $\mu$ -XRD and  $\mu$ -XANES. The ultimate goal of this detailed mineralogical study is to link and interpret results of bioaccessibility tests completed on these samples and to be reported elsewhere. Results reported here also highlight specific associations of minerals among different types of tailings and the ability of these mineralogical techniques to help explain the geochemical fate and mobility of As in arsenopyrite-rich mine tailings.

The data supporting this study are extensive, and only selected and summary results are presented in this paper. We therefore also direct the reader to a full compilation of chemical, mineralogical, and sequential extraction data collected for this project (Parsons *et al.*, in press).

#### BACKGROUND INFORMATION

Arsenopyrite is unstable under surface oxidizing conditions. The most frequently observed product of its weathering is scorodite ( $\text{FeAsO}_4 \cdot 2\text{H}_2\text{O}$ ), less commonly, one encounters amorphous hydrous ferric arsenate-sulfate (*e.g.*, pitticite) and pharmacosiderite [ $\text{KFe}_4(\text{AsO}_4)_3(\text{OH})_4 \cdot 6-7\text{H}_2\text{O}$ ] and, rarely, arsenolite ( $\text{As}_2\text{O}_3$ ) (King 2002). Arseniosiderite [ $\text{Ca}_2\text{Fe}_3(\text{AsO}_4)_3\text{O}_2 \cdot 3\text{H}_2\text{O}$ ] is fairly widespread in occurrence, usually as a product of alteration of arsenopyrite or an earlier oxidized phase (*e.g.*, scorodite) under supergene processes (Anthony *et al.* 2000). Numerous site-specific studies have been completed documenting the importance of secondary minerals in attenuating As during the weathering of arsenopyrite (*e.g.*, Ashley 2002, Morin *et al.* 2002, Courtin-Nomade *et al.* 2003, Gieré *et al.* 2003, Salzsauler *et al.* 2005). It is also increasingly evident that investigations at the micrometer scale (*e.g.*, by synchrotron micro-analysis) fill an important gap between macro- (*i.e.*, bulk-) scale and nanoscale analyses, such as are made by methods of transmission electron microscopy (*e.g.*, Manceau *et al.* 2002, Sutton *et al.* 2002, Paktunc *et al.* 2004, Walker *et al.* 2005, Arai *et al.* 2006, Kirpichtchikova *et al.* 2006, Vodyanitskii 2006, Courtin-Nomade *et al.* 2008, Endo *et al.* 2008).

#### ARSENIC-BEARING GOLD MINE TAILINGS, NOVA SCOTIA

Between 1861 and 1942, approximately 1.2 million ounces of Au were produced from over three million tonnes of crushed ore in 64 mining districts in the Meguma Terrane of Nova Scotia (Nova Scotia Department of Mines 1943, Bates 1987). Only minor production has occurred since that time, although the recent resurgence in Au prices has led to increased exploration in these former mining districts. The historic volumes of Au and tailings are small by today's mining standards; the particularly high As content of the ores and resulting tailings, however, and the fact that tailings were routinely dispersed to local water-courses (as was the practice of the day), have led to numerous high-As tailings areas throughout southeastern Nova Scotia (Parsons *et al.* 2004). Many of these tailings areas are now located close to residential areas and are publicly accessible. The broader environmental impact of the As-bearing Au mine tailings has been the subject of some study (Brooks *et al.* 1982, Dale & Freedman 1982, Wong *et al.* 1999, Wong *et al.* 2002), and the downstream effects and risks from historic gold-mining activities are presently the subject of multidisciplinary study by federal, provincial and university researchers.

#### GEOLOGY, MINING AND MINERAL PROCESSING HISTORY

The Meguma Terrane makes up most of the southern mainland of Nova Scotia (Fig. 1) and consists of folded Cambro-Ordovician metagreywacke to slate and metasilstone rocks of the Goldenville and Halifax groups, of greenschist to amphibolite grade (Ryan & Smith 1998). Most of the Au production was from bedding-concordant auriferous quartz veins in the interstratified slate and metasilstone sequences (Kontak & Kerrich 1997). The most abundant accessory minerals in the veins include: chlorite, biotite, muscovite, and plagioclase (early Ca-rich and later Na-rich). Carbonates (ferroan dolomite to ankerite and calcite) and sulfides are associated with all types of auriferous veins (for both carbonate and sulfide 0.1 to 5 modal %, locally 50 to 75%) (Kontak & Jackson 1999). Arsenopyrite is the predominant sulfide, with variable amounts of pyrrhotite, pyrite, chalcopyrite, galena and rare sphalerite and molybdenite (Kontak & Jackson 1999, Morelli *et al.* 2005).

Stamp milling with Hg amalgamation was the principal method used to recover the Au in Nova Scotia ores (Malcolm 1929). Gravity-separated sulfide concentrates, usually carrying less than 15% of the Au, were routinely collected at practically all the larger plants *ca.* 1900 and later (Cole 1927, Malcolm 1929, Parsons 1935, Henderson 1935, Roach 1940). The sulfide concentrates typically comprised between two and five percent of the

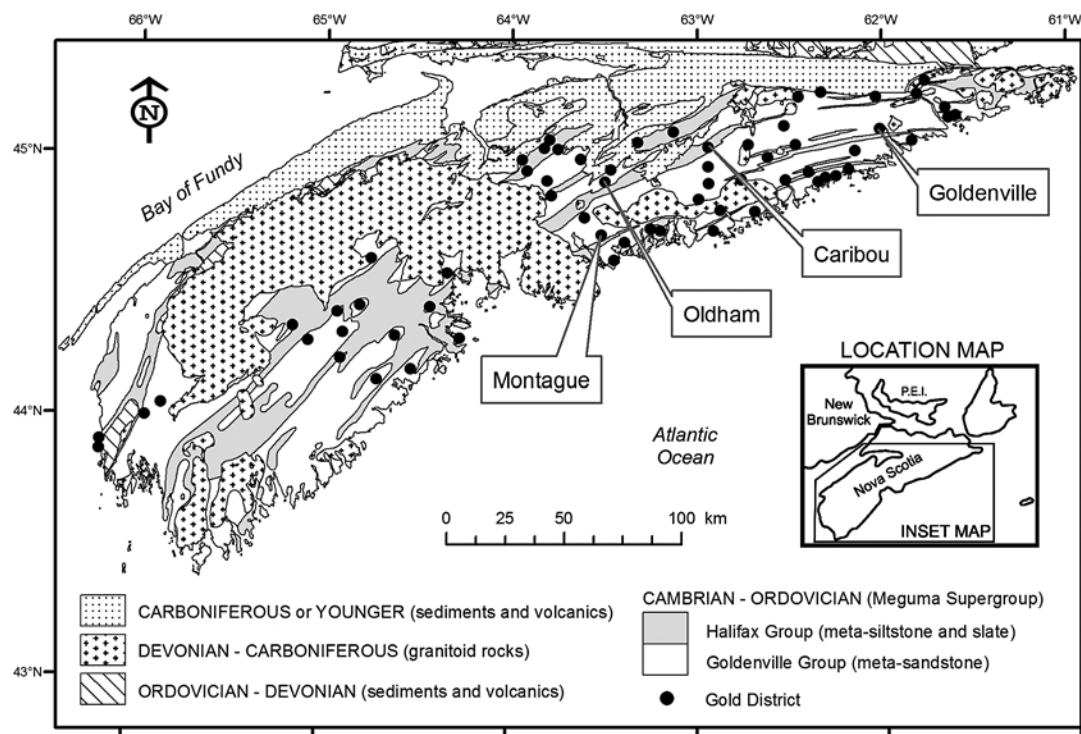


FIG. 1. Generalized geological map of southern Nova Scotia, showing the location of historical gold districts within rocks of the Meguma Supergroup, after Ryan & Smith (1998), with bedrock geology simplified from Keppie (2000).

ore and were either stored for future on-site or off-site (smelter) treatment, reground and barrel-amalgamated, or reground and cyanided (Messervy 1928, Parsons 1935, Timm 1935). Reprocessing of older tailings using improved technologies also occurred at many sites (Messervy 1928, Roach 1940).

Tailings were generally deposited close to the mills in low-lying areas and along creeks. Prolonged breaks in production, erosion and reprocessing of tailings have led to complicated patterns of weathering within tailings areas. Changes in ore character and milling processes (especially concentration) over time led to heterogeneity in the distribution of arsenopyrite and other sulfides in the tailings. At sites with high levels of recent human activity (especially the construction of racetracks for off-road vehicles), any systematic depositional and weathering patterns may have been disturbed near the surface.

For this study, tailings were collected from the Goldenville (GD), Caribou (CAR), and Montague (MG) Au districts (Fig. 1). One sample of well-oxidized tailings (OLD04) was collected at Oldham from the foundation of a former stamp mill that is now adjacent to residential properties. These districts rank as four of the top

five historical Au producers in Nova Scotia, each with >100,000 tonnes of ore crushed (approximately equal to the volume of tailings at each site; Nova Scotia Department of Mines 1943). Additional details on the mining and ore-processing history at each site, field descriptions of tailings, and maps showing the precise location of each sample can be found in Parsons *et al.* (in press).

#### SAMPLING AND ANALYTICAL METHODS

##### *Sample collection and bulk chemical analysis*

Fourteen samples were collected from near-surface tailings at the Caribou, Goldenville, Montague and Oldham sites in the fall of 2005. Sample designations were made according to the site (CAR, GD, MG and OLD, respectively). Samples from Caribou were collected along a community walking trail on the tailings (CAR01 to CAR03) and in areas disturbed by ATVs (CAR04), whereas all samples from Montague and Goldenville were collected in areas frequented by off-road vehicles. All samples of tailings except two were visibly oxidized and were selected on the basis of distinct visual characteristics considered to be indica-

tive of different mineralogy. Of the two unoxidized samples, one was distinctly arsenopyrite-rich (CAR02), and another was from saturated tailings immediately beneath a thin layer of organic matter (MG04). One sample of B-horizon soil (MG06) was collected over mineralized bedrock at Montague for comparison with the fourteen samples of tailings. At each sampling site, a test pit was excavated to examine the stratigraphy of the tailings or the soil horizons, and then 1–2 kg samples were collected at specified depth-intervals using a stainless steel hand trowel and plastic sampling containers.

Samples were air-dried and dry-sieved to <150  $\mu\text{m}$ . Both the bulk and the <150  $\mu\text{m}$  fraction were analyzed for their bulk chemical composition; however, only the <150  $\mu\text{m}$  fraction was characterized mineralogically. This finer fraction corresponds to the maximum size of particle that likely remains on the hands of children and may be incidentally ingested (Duggan *et al.* 1985).

Analyses of major and trace elements were performed at ACME Analytical Laboratories in North Vancouver, British Columbia. Samples were digested using modified *aqua regia* (0.50 g of sample digested in a solution containing 2.0 mL HCl, 2.0 mL HNO<sub>3</sub> and 2.0 mL H<sub>2</sub>O at 95°C for one hour), and analyzed for 53 elements following the ACME 1F-MS ultra-trace inductively coupled plasma – mass spectrometry (ICP-MS) protocol. Certified reference materials CANMET STSDs 1–4 (Lynch 1990) and duplicate samples were used to monitor analytical accuracy and precision, which were generally within  $\pm 5$  to 10% of the expected values for most elements. Total carbon content of the tailings and soils was measured in 0.5 g subsamples at the Geological Survey of Canada in Dartmouth, Nova Scotia, using a LECO WR-112 carbon analyzer. Concentrations of organic carbon were analyzed following removal of the inorganic carbon using 1 M HCl. Concentrations of inorganic carbon were calculated by difference. Precision and accuracy were approximately  $\pm 0.03$  wt.% on the basis of replicate analyses of calibration standards. Further details of the sampling and analytical methods are provided in Parsons *et al.* (in press).

#### *Petrographic analyses*

A split subsample of the <150  $\mu\text{m}$  fraction was prepared as a “liftable” polished thin section (Walker *et al.* 2005) using low-temperature set epoxy (Sealtronic™) and with kerosene instead of water for all grinding to avoid dissolution of soluble phases. All grinding was done by hand on diamond laps, and final polishing was completed dry in two-minute intervals separated by cool-down periods of similar duration. Each sample was examined with a petrographic microscope in transmitted and reflected light. Epoxy-impregnated thin sections (bonded to glass slides using cyanoacrylate adhesive) were “lifted” from the glass substrate by soaking in ACS (or better) grade acetone and remounted on kapton tape

to facilitate transmission-mode synchrotron  $\mu$ -XRD. Kapton mounts were reapplied to glass slides with double-sided tape prior to carbon coating and electron-probe micro-analysis (EPMA).

In each section, distinct Fe–As phases in terms of color (transmitted and reflected light), transparency, reflectivity, optical relief and texture could be determined petrographically, but in most cases (owing to fine grain-size, poor crystallinity or amorphous nature), they could not be uniquely identified by petrography alone. Synchrotron microprobe and EPMA data (see below), when combined with the petrographic observations, enable us to unambiguously identify a range of As minerals and aided in confirming that significant As-bearing phases were not missed in each section. Using all available data for each section, it was then possible to establish a scale of abundance (dominates section, major, minor to trace, or not observed) for each phase identified.

#### *Conventional XRD*

X-ray powder-diffraction analyses were carried out using a Siemens D-500 X-ray diffractometer with a Co lamp (18 mA, 20 keV). The <150  $\mu\text{m}$  fraction of each sample was finely ground using an agate mortar and pestle, then run from 2° to 70° 2 $\theta$ , in steps of 0.02°, with a 1 s count time at each step. Zincite (ZnO) was used as an internal standard. The diffraction data were analyzed using DIFFRACplus EVA software, and semiquantitative estimates of abundances of the major minerals were obtained by comparing the integrated intensities of diffraction peaks.

#### *Synchrotron micro-analysis*

Polished thin-section samples were characterized at beamline X26A, National Synchrotron Light Source, using methods similar to those described by Walker *et al.* (2005). Techniques included micro-X-ray fluorescence ( $\mu$ -XRF), transmission mode X-ray diffraction ( $\mu$ -XRD) and fluorescence-mode X-ray absorption near-edge structure ( $\mu$ -XANES). All synchrotron micro-analyses were conducted with a beam spot-size of ca. 7 to 10  $\mu\text{m}$ . Petrographically preselected targets were supplemented with additional targets from XRF maps based on element associations. Elements where distribution was routinely mapped included: K, Ca, Ti, Cr, Mn, Fe, Ni, Cu, Zn and As.

#### *Micro-X-ray-absorption near-edge structure ( $\mu$ -XANES)*

Micro-XANES spectra on selected targets were obtained by scanning through the As *K*-edge at three seconds per step in three segments (11,800 eV to 11,845 eV in 5 eV steps, 11,850 eV to 11,880 eV in 0.4 eV steps and 11,882 eV to 11,970 eV in 2 eV steps). The XANES

spectra were calibrated (using first-derivative maxima) to a scorodite standard (11,874 eV), background-corrected and edge-step-normalized at 11,950 to 11,970 eV. Edge position and spectral shape were compared to a set of As standard spectra (Walker *et al.* 2005).

#### *Micro-X-ray diffraction (μ-XRD)*

Micro-XRD was imaged in a similar manner to that previously reported (Walker *et al.* 2005). Diffraction patterns were collected at just above the As *K*-edge of 12 keV (1.0332 Å) or at *ca.* 17 keV (0.7208 or 0.7138 Å). The detector was calibrated at each diffraction energy; exposure times for unknowns ranged from 60 to 300 seconds. Each unknown pattern was background-minimized by scaled subtraction of blank XRD patterns collected on kapton tape. Corrections for detector distortions (camera-sample distance, camera tilt and rotation, and the beam center on the camera plane) were made using FIT2D™ software (Hammersley 1998). Unknown patterns were inspected for types of diffraction (rings, arcs or points), and identification was made by masking all point reflections, integrating (over the azimuthal angle) to create a simulated 1-D powder pattern and importing into X-Pert HIGH-SCORE software, Version 2.2a (PANalytical) for conventional search-match phase identification using the PDF2 database (ICDD 2003).

#### *Electron-probe micro-analysis (EPMA)*

Quantitative electron-probe micro-analysis (EPMA) was carried out on carbon-coated thin sections using a JEOL JXA-8200 in wavelength-dispersive (WDS) mode. Operating conditions were 15 keV and a beam current of 20 nA with spot analysis and background collection times of 20 and 10 seconds, respectively. Analytical standards were: arsenopyrite (As, S), magnetite (Fe), sanidine (K, Al, Si), kaersutite (Ca, Mg), jadeite (Na), apatite (P) and pyrolusite (Mn). Matrix corrections were applied using ZAF. X-ray mapping for As, Fe, S, Ca, Si and Mn was carried out in selected regions (50 nA beam current and all elements by WDS except Mn, by energy-dispersion spectroscopy).

Schneiderhöhnite ( $\text{Fe}^{2+}\text{Fe}^{3+}_3\text{As}^{3+}_5\text{O}_{13}$ ) and scorodite ( $\text{Fe}^{3+}\text{As}^{5+}\text{O}_4 \cdot 2\text{H}_2\text{O}$ ) were routinely run as secondary analytical standards for the primary elements of interest (Fe and As). A beam spot-size of 5 μm was used to minimize beam damage on the sample, but still allowing analysis of fine features such as grain coatings. Analytical data were recalculated on the basis of stoichiometric As and Fe (average result of six analyses) from the secondary scorodite standard when it was determined that uncorrected results consistently reported high totals (*ca.* 110%, allowing for H<sub>2</sub>O) and somewhat low molar Fe:As ratios (0.8 to 0.9). Scorodite (a hydrous mineral) was deemed more suitable for the hydrous target materials being analyzed than the primary

arsenopyrite standard. This correction also resulted in a distinct improvement in the Fe/As values reported from unknown grains of scorodite in thin sections that exhibited high-quality μ-XRD patterns. The WDS microprobe dataset was supplemented by additional quantitative EDS microprobe data for selected samples where necessary to further elucidate Fe, As, S and Ca relationships. The analytical set-up was kept as similar as possible to the WDS method described above, with a 5 μm beam-spot size, scorodite as the primary standard for Fe and As, and an energy of 15 keV (beam current was 40 nA). Pyrite was the standard for S. Other details concerning instrumentation are the same as those described in Walker *et al.* (2005). Repeat analyses were conducted on a number of the previous WDS targets to confirm reproducibility between the techniques. Details can be found in Parsons *et al.* (in press). The greater sensitivity of the WDS analysis (over EDS) was not required for the high concentrations of As and Fe (and S, Ca where present) in the phases of interest. In addition, WDS data for potentially interfering elements such as Mg, Sb and Pb confirmed these to be present at only trace levels in the arsenate and Fe oxyhydroxide phases of interest in these samples. The EDS instrument was therefore appropriate, offered short setup time, and was locally available for follow-up work.

## RESULTS AND DISCUSSION

### *General observations*

Historic samples of Au mine tailings from Nova Scotia can be characterized firstly in terms of total As content. Concentrations in excess of *ca.* 10 wt.% are representative of gravity concentrates that were originally rich in sulfides (Parsons 1923). The sample set in this study contains two samples of mill concentrate, one being highly oxidized, fine grained, powdery and grey green (GD01), the other being relatively unoxidized, sandy, dark grey and sulfide-rich (CAR02). Arsenic concentrations in other near-surface tailings at the study sites typically range between 0.5 and 5 wt.% (Parsons *et al.*, in press), with the As content at a given location determined by the complex interplay of ore character, mill-concentrating efforts, disposal characteristics, and post-depositional remobilization of tailings or As. Generally, the remaining tailings can be further classified on the basis of their physical state and degree of oxidation; they are (i) strongly oxidized and cemented (hard-pan tailings), (ii) oxidized with no cementation evident, or (iii) unoxidized-reduced. Cemented tailings are most commonly green to grey-green, or yellowish brown to yellow. Uncemented oxidized tailings are most commonly olive-brown to reddish brown, in contrast to the unoxidized tailings that are characteristically grey and water-saturated.

### Chemical composition

The concentrations of arsenic and other elements were determined in both the sieved and unsieved fractions of the samples. For this sample set, there is 9% to 260% more As in the sieved (<150  $\mu\text{m}$ ) fraction than in the whole sample (Parsons *et al.* in press). However, tailings sample GD03 is anomalous in this respect, exhibiting the reverse relationship, with 50% less As in the finer sample. A review of other elements analyzed for this sample indicates that the elements affiliated with mineralization (*e.g.*, Ag, Au, Cu, Fe, Pb, and S) show the same relationship as As, whereas the major elements (*e.g.*, Al, Ca and K) show the reverse (increasing in the finer fraction). Petrographically, sample GD03 was observed to contain common thick Fe–As cement coatings on silicates, with some cemented aggregates approaching the maximum grain-size in the sample. Coarsely cemented aggregates at >150  $\mu\text{m}$  are the most likely reason for the anomalous decreasing As content with decreasing grain-size in this sample.

The remainder of this paper focuses on characterization of the sieved fraction only, as this is the fraction expected to be most important for assessing risk from ingestion. The total concentrations of As, Fe, S and Ca in the soil and tailings samples (<150  $\mu\text{m}$  fraction) are provided in Table 1. The As content of the sieved tailings ranges from 0.07 to over 30 wt.% As. The Fe/As values of all tailings samples are low on a molar basis (in the range 1.3 to 5.3), and lower-As-content samples generally have higher Fe/As values (Table 1). In contrast, the Ca and S contents vary from sample to sample by two to almost three orders of magnitude,

respectively. These data are consistent with arsenopyrite-rich source material in relatively Fe-poor gangue. The S:As ratio in tailings samples is usually significantly less than 1 (Table 1), which suggests the preferential leaching of S over As during oxidative weathering of these samples. Samples MG04, CAR02 and CAR04 are the only samples containing S in excess of As on a molar basis, reflecting the abundance of sulfides in these samples (see mineralogical discussion that follows). The sample set also exhibits a distinctive excess of As over Ca, with only two tailings samples (GD05 and CAR04) determined to have greater Ca than As on a molar basis (Table 1). The generally low Ca content in many samples probably reflects the depletion of Ca carbonates due to (i) preferential concentration of sulfide over carbonate during processing (with an inference of deposition of more As-poor carbonate-rich material at other locations), or (ii) dissolution from oxidizing sulfides and surface exposure to meteoric water, or (iii) both of the above. Carbonate-deficient ore is also possible, but seems unlikely given the rather ubiquitous presence reported in geological studies of the ore-bearing veins and wallrock (*e.g.*, Kontak & Smith 1988, Kontak & Jackson 1999, Sangster & Smith 2007).

Therefore, As, Fe, S and Ca are particularly indicative of the underlying geochemical conditions in the Nova Scotia tailings because of the strong influence of arsenopyrite (with near-stoichiometric equivalents of Fe, As and S) and the importance of carbonates as the main source of Ca in the tailings (Kontak & Smith 1988, Kontak & Jackson 1999). This is also evident in XRF mapping conducted on selected samples, where the primary element associated with As is Fe, and

TABLE 1. GRAIN SIZE AND ELEMENT CONCENTRATIONS IN TAILINGS AND SOIL SAMPLES

ID	Sample Type	% <150 $\mu\text{m}$	Element concentrations (mg/kg)				Ratios (mol/mol)				Carbon (% dry wt.)		
			As	Fe	S	Ca	Fe/As	S/As	Ca/As	Ca/S	Total	Org	Inorg
CAR01	tailings	18.3	76,500	75,200	1,900	<100	1.3	0.06	0.00	0.00	0.12	0.11	0.01
CAR02	mill concentrate	13.7	313,400	364,300	168,200	200	1.6	1.3	0.00	0.00	6.47 <sup>a</sup>	6.47 <sup>a</sup>	0
CAR03	tailings	12.1	21,300	31,900	1,100	700	2.0	0.12	0.06	0.51	0.19	0.13	0.06
CAR04	tailings	12.5	15,200	40,800	10,700	11,300	3.6	1.6	1.4	0.84	0.64	0.09	0.55
GD01	mill concentrate	30.4	210,300	200,400	34,200	<100	1.3	0.38	0.00	0.00	0.17	0.17	0
GD02	tailings	28.6	19,200	36,000	700	1,200	2.5	0.09	0.12	1.4	0.23	0.22	0.01
GD03	tailings	17.7	38,900	48,800	900	900	1.7	0.05	0.04	0.80	0.23	0.23	0
GD04	tailings	7.4	48,700	77,600	2,900	900	2.1	0.14	0.03	0.25	0.25	0.17	0.08
GD05	tailings	61.4	7,209	28,500	1,400	8,400	5.3	0.45	2.18	4.8	0.30	0.09	0.21
MG01	tailings	11.0	62,100	81,800	2,900	600	1.8	0.11	0.02	0.17	0.13	0.11	0.02
MG02	tailings	9.4	24,000	54,800	1,100	1,200	3.1	0.11	0.09	0.87	0.13	0.12	0.01
MG03	tailings	21.4	23,700	58,800	2,100	4,500	3.3	0.21	0.35	1.7	0.55	0.49	0.06
MG04	tailings	18.4	21,400	52,500	16,800	1,400	3.3	1.8	0.12	0.07	0.83	0.81	0.02
MG06 <sup>b</sup>	soil	16.0	318	59,200	1,100	200	250	8.1	1.18	0.15	4.93	3.11	1.82
OLD04	tailings	18.5	33,900	80,100	5,200	600	3.2	0.4	0.03	0.09	2.23	1.89	0.34

<sup>a</sup> Analytical results for carbon for CAR05–T02 may contain interference from high sulfide content of sample.

<sup>b</sup> B-horizon soil sample collected beneath an uprooted tree over mineralized bedrock.

uncommonly Ca and Mn. On the basis of Acid Rock Drainage (ARD) fundamentals, the near-surface oxidative weathering of the arsenopyrite source will vary depending on the presence or absence of pH buffering by carbonate (e.g., Jambor & Blowes 1991, Jambor 1994, Ritchie 1994, Blowes *et al.* 1998). The presence of carbonate leads to neutral-pH drainage, whereas the lack of carbonate allows for the possibility of ARD.

The single soil sample (MG06) included in this study is chemically distinct from the tailings. Although Fe, S and Ca concentrations for this sample fall within the range of tailings samples (Table 1), the As content at 300 mg/kg is one to three orders of magnitude lower than in the tailings samples. This sample also has the highest content of organic carbon (OC) at 3.1% (Table 1), and also the highest content of inorganic carbon (IC) at 1.8%. Given the low Ca content, the elevated IC suggests the presence of Fe carbonate (siderite), as calculated molar IC to Ca ratios are greater than 300.

### Mineralogy

Categorization of the samples studied is presented in Table 2. Consistent with the mineralogy of the Au deposits, quartz is the dominant mineral observed by XRD for most samples, with subordinate muscovite, chlorite and plagioclase. Biotite is in some cases

observed petrographically, but it is usually subordinate to muscovite and chlorite. Being in low abundance, it is difficult to distinguish by XRD; however, vermiculite possibly representing weathered biotite is interpreted to be present in the XRD patterns of several samples (Table 2). Two particular exceptions to the dominant quartz mineralogy are the two mill-concentrate samples CAR02 and GD01, in which arsenopyrite and scorodite, respectively, dominate the XRD patterns (Table 2), with relatively minor peaks evident for other phases (muscovite, pyrite and chlorite for CAR02, quartz, muscovite for GD01). The XRD pattern for soil sample MG06 is dominated by both muscovite and quartz, with relatively weak peaks from plagioclase and chlorite. In addition to the mill-concentrate samples, As-bearing phases are identified by conventional XRD in CAR01 (kañkite and scorodite), GD02, GD03 and MG01 (scorodite), MG03 (pharmacosiderite) and MG04 (arsenopyrite). Jarosite detected by bulk XRD in OLD04 was confirmed to be As-bearing by subsequent micro-analysis. Bulk XRD data are available in Parsons *et al.* (in press).

Samples CAR04 and GD05 are the only samples that contain Ca carbonates (ankerite and calcite, respectively), detected by bulk XRD. The remaining samples for the most part are probably devoid of Ca carbonate or contain only minute quantities, on the basis of the contents of Ca and inorganic C (Table 1). The typical subequal quantity of carbonate and sulfide (<5 modal %) identified by other researchers (Kontak & Jackson 1999) in Nova Scotia Au-bearing veins means that where gravity concentration was employed, there would have been a preferential separation of carbonate to the tailings and a concentration of sulfide (including arsenopyrite) in the heavy fraction. In the absence of gravity concentration, the neutralization potential of the tailings is determined by the ratio of carbonate to sulfide in the processed ore.

Of the 15 samples characterized, seven (including the soil sample MG06) had no As phases confirmed by field observation or conventional XRD, even though most of these samples contain As concentrations in the wt% range (>10,000 ppm). With micro-scale characterization (petrography,  $\mu$ -XRF,  $\mu$ -XANES,  $\mu$ -XRD and EPMA), we were able to confirm As forms identified by bulk characterization, and in all cases, to identify additional As forms as well as potentially important textural distinctions and relationships among As phases. Specifically, with grain-scale mineralogical analysis, we unambiguously identified a minimum of two and typically four or more As-bearing phases in each tailings sample (Fig. 2, Table 2). Common textures of products of secondary alteration include: (i) structureless translucent or transparent grains, (ii) micrometric layering that may be evident in either transmitted or reflected light, (iii) rims (oxide replacement of sulfides or precipitate coatings), (iv) pseudomorphs, (v) aggregates, (vi) mixtures of two or more optically distinct phases at the micrometer scale, or (vii) combinations of the above.

TABLE 2. MINERALOGY OF TAILINGS AND SOIL SAMPLES

Sample	Depth interval (cm)	Major gangue <sup>1</sup>	As-bearing major <sup>2</sup>	As-bearing minor to trace <sup>2</sup>
CAR01	0 to 5	Qtz, Ms, Pl, Chl	<b>Scd, Knk</b>	HFA, HFO
CAR02	0 to 4	Qtz, Pl, Ms, Chl	<b>Apy, Py</b>	HFA, Yuk, HFO
CAR03	0 to 8	Qtz, Ms, Pl, Chl	HFA, HFO	Yuk, Gt, Lpc, Akg, Apy, Py
CAR04	0 to 4	Qtz, Ms, Pl, Chl, Ank	Apy, Py	Yuk, HFO
GD01	0 to 5	Ms, Qtz	<b>Scd</b>	Apy, Py
GD02	0 to 5	Qtz, Pl, Ms, Chl	<b>Scd, HFA</b>	HFO, Yuk, Apy, Py, Jrs
GD03	0 to 5	Qtz, Ms, Pl, Chl	<b>Scd, HFA</b>	Knk, HFO, Apy, Py
GD04	0 to 5	Qtz, Ms, Pl, Chl	HFA	HFO, Gt, Lpc, Apy, Py
GD05	0 to 5	Qtz, Ms, Chl, Pl, Cal	Apy	Py, HFO
MG01	0 to 6	Qtz, Ms, Pl, Chl	<b>Scd, HFA</b>	Gt, Lpc, HFO, Apy, Py, Toe
MG02	0 to 5	Qtz, Ms, Chl, Vrm, Pl	HFA	HFO, Apy, Scd, Py, Yuk, Pha, Akg, Hem*
MG03	0 to 15	Qtz, Vrm, Ms, Chl, Pl	<b>Pha, Yuk</b>	HFA, Ca-FA, Gt, Lpc, HFO, Apy, Py
MG04	15 to 20	Qtz, Vrm, Ms, Chl, Pl	<b>Apy</b>	HFA, HFO, Py, Rgr
MG06	0 to 5	Qtz, Ms, Pl, Chl	HFO	Gt**
OLD04	0 to 5	Qtz, Ms, Pl, Chl	HFA, <b>Jrs</b>	Gt, HFO, Sch, Toe

Bold and underlined: indicates the As-bearing phase that dominates the sample. Bold indicates a phase detected in bulk XRD. Symbols: Ank: ankerite, Cal: calcite, Chl: chlorite, Ms: muscovite, Pl: plagioclase, Qtz: quartz, Vrm: vermiculite, Akg: akaganeite, Apy: arsenopyrite, Ca-FA: amorphous Ca ferric arsenate, Gt: goethite, HFA: hydrous ferric arsenate, HFO: hydrous ferric oxyhydroxide, Hem: hematite, Jrs: jarosite, Knk: kañkite, Lpc: lepidocrocite, Pha: pharmacosiderite, Rgr: realgar, Sch: schwertmannite, Scd: scorodite, Toe: tooleite, Yuk: yukonite.  
<sup>1</sup> In decreasing order of abundance based on semiquantitative fitting of XRD patterns. <sup>2</sup> In estimated decreasing order of abundance. \* Single more reflective Fe oxyhydroxide identified appears to be mixture of nanocrystalline hematite and ferrihydrite with relatively low arsenic content (6.7% As<sub>2</sub>O<sub>3</sub>). \*\* EPMA analysis for As in a single grain was just above detection (0.08%). Arsenic was confirmed by synchrotron  $\mu$ -XRF, but not quantified. Note: Py was confirmed to contain trace As (<0.1%) in some cases, but was not systematically analyzed in each sample where present.

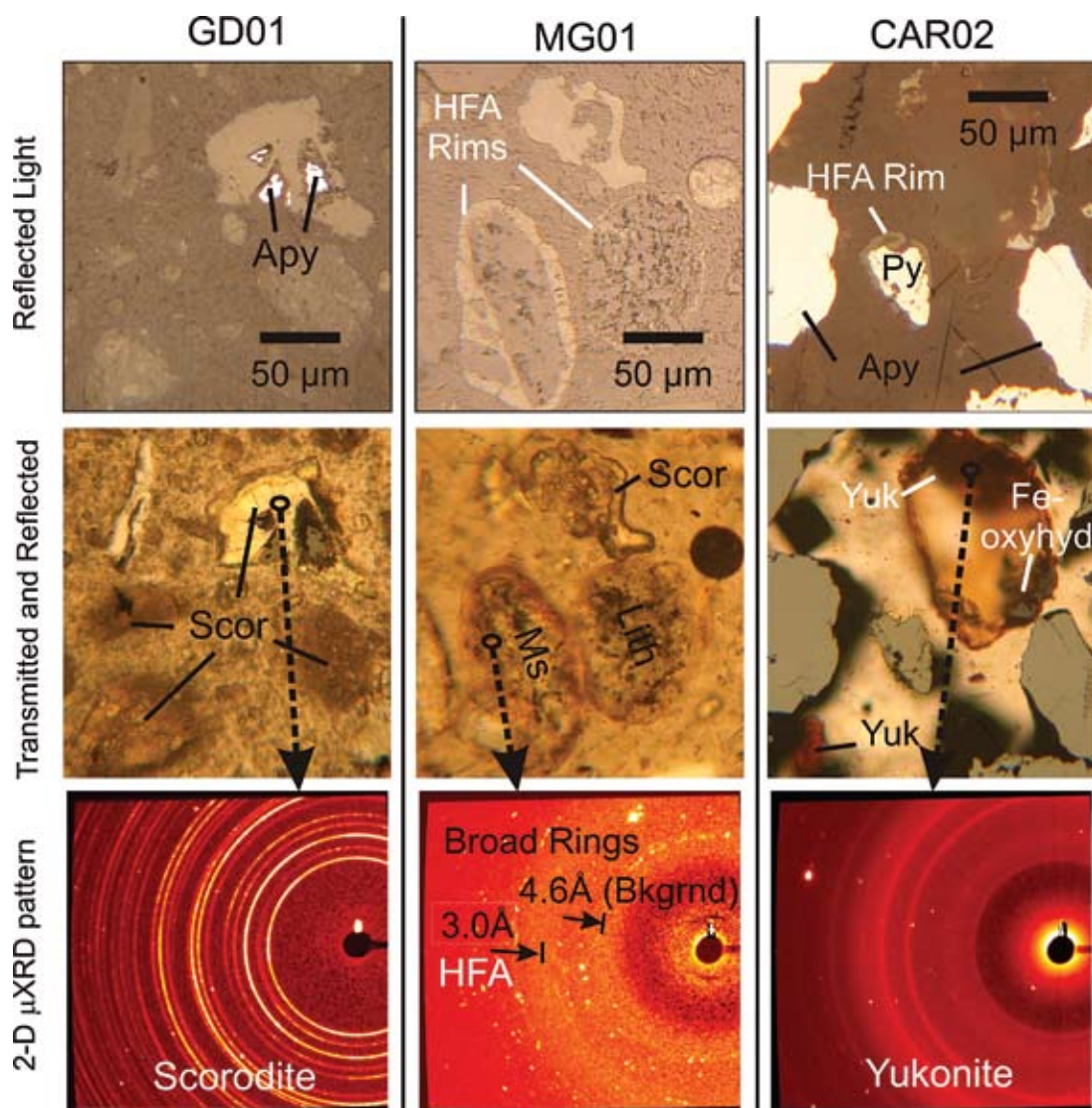


FIG. 2. A variety of As phases occur in weathered gold-mine tailings in Nova Scotia, with mixtures of different forms varying from sample to sample. A combination of optical microscopy and  $\mu$ -XRD allows definitive identification of a range of mineral forms and textures at the micrometer scale. These As-bearing mineral forms range from finely crystalline transparent to translucent aggregates of scorodite (e.g., GD01 and MG01), to amorphous forms that in some cases coat or cement other grains (e.g., MG01 and CAR02). Note the broad diffraction-ring at *ca.* 3 Å (MG01) indicative of amorphous hydrous ferric arsenate (HFA). Yukonite, a Ca-Fe arsenate, occurs most commonly in carbonate-rich samples. In CAR02, it is present in an arsenopyrite-rich mill concentrate along with other trace oxidized forms of As.

Qualitative information on the degree of crystallinity is obtained from the 2-D  $\mu$ -XRD patterns, with smooth rings suggesting very fine crystallites (nanocrystalline) and spotty rings (microcrystalline) for similar analytical volume (He *et al.* 2003, Walker *et al.* 2005). Micro-XRD confirms that secondary phases are generally aggregates

of micro- or nanoscale crystallites, or in some cases they are amorphous or short-range ordered. Arsenic-mineral associations within individual grains are commonly complex, with up to three As forms associated within an individual grain (10 to 100  $\mu$ m). The only macrocrystalline (*e.g.*, >2  $\mu$ m) As-bearing phases identified are the

primary arsenopyrite and pyrite, although the spotty nature of diffraction rings from pharmacosiderite and jarosite (see below) suggests the presence of discrete crystallites ( $>0.1 \mu\text{m}$ ) for these phases.

Relict primary sulfides remain in some samples, whereas in others, oxidation has been sufficiently extensive to completely (or nearly completely) oxidize all sulfides. Where sulfides are present, arsenopyrite is always the most commonly observed, followed by pyrite and, in some cases, pyrrhotite. The generally low abundance of pyrrhotite may be due to the low content in the original ore or greater depletion by more rapid oxidation of pyrrhotite than other sulfides in the vadose zone (*e.g.*, Jambor 1994). Galena and chalcopyrite were observed on occasion, but their presence was not systematically evaluated owing to their low abundance.

For each thin section, As-bearing phases were determined to be present as: major, minor or trace constituents (Table 2). The two samples of mill concentrate, GD01 and CAR02, contain scorodite and arsenopyrite, respectively, that dominate each section. This is consistent with conventional XRD results already discussed. In addition to scorodite and arsenopyrite, amorphous hydrous ferric arsenate (HFA) is commonly detected as a major constituent in several samples. This phase may be present as the only major phase (GD04 and MG02), with hydrous ferric oxyhydroxide (HFO) (CAR03) or scorodite as another major phase (GD02, GD03, and MG01), or with As-bearing jarosite (OLD04). Pharmacosiderite and yukonite are identified as the only major As-bearing phases in MG03, yukonite or amorphous Ca-Fe arsenates are the main phases present in GD05, and kañkite (along with scorodite) is identified as a major phase in CAR01.

In addition to the major As-bearing phases identified above, several others are present as only minor or trace constituents in specific samples. These include: As-bearing ferric oxyhydroxides (HFO, goethite, lepidocrocite and akaganeite), tooeleite, schwertmannite and realgar, with the latter two minerals each identified in only one sample.

In a few cases, extreme alteration of phyllosilicates (biotite and chlorite) was observed, resulting in precipitation of pseudomorphic As-bearing Fe oxyhydroxides, which have been characterized along with the other Fe-As phases discussed below. Orange to yellowish alteration-induced rinds were also observed in some instances on muscovite, commonly with associated As. In addition to such alteration, particles of phyllosilicate and a clay mineral may also host As in these samples as sorbed species (*e.g.*, Lin & Puls 2000, Goldberg 2002, Chakraborty *et al.* 2007). For the high-As tailings samples in this study, the relative amount of total As sorbed onto phyllosilicates and clays is expected to be relatively small. Sorption of As onto clays and phyllosilicates was not specifically investigated in the present study; however, it is important that the role of

clay minerals be considered in any interpretation of As leaching or dissolution from these samples (*e.g.*, sequential leach and bioaccessibility testing).

#### *Ferric arsenates*

For the samples selected in this study, ferric arsenates (scorodite, HFA and, less commonly, kañkite) are most commonly the dominant carriers of As in a given sample. Scorodite may be present as brown aggregates, or as transparent to translucent pale green grains, in some cases as possible pseudomorphic rims on arsenopyrite (replacement) or as grain coatings on sulfides, oxides and silicates (cementation) (Fig. 2). Micro-XRD patterns for scorodite range from spotty rings on some targets to smooth rings on others, qualitatively suggesting a variation from coarse to fine crystallites, respectively (He *et al.* 2003). Molar values of Fe/As established by EPMA of scorodite grains that show highly crystalline XRD patterns are consistently very close to 1 (range 0.94 to 1.14, but usually between 0.97 and 1.03). Less than 1 wt.% P and Al are in some cases detected in analysis of scorodite grains in the absence of Si, suggesting the possibility of minor substitution of  $\text{PO}_4$  for  $\text{AsO}_4$  and Al for Fe, but this was not systematically investigated. The sulfur content of scorodite grains is also low at  $<2$  wt.% as  $\text{SO}_4$  (typically  $<0.5$  wt.%). The only exception to this pertains to the scorodite-rich mill product (GD01), where S concentrations in scorodite analyzed range from 0.5 to 6 wt.% as  $\text{SO}_4$ .

The phase HFA is present as yellow-brown to red-brown grains, in some cases as a replacement rim on arsenopyrite and most commonly as grain coatings on sulfides, oxides and silicates (cementation). Petrographically, the HFA is readily discernable from scorodite by its color (scorodite is transparent to pale green in transmitted light), and from Fe oxyhydroxides because of their lower opacity and reflectivity. In rarer instances, where scorodite or HFA is present as dark brown to opaque aggregates, EPMA or  $\mu$ -XRD is required to differentiate them. Micro-XRD patterns for HFA in some cases indicate a completely amorphous phase; more commonly, short-range order is evident by the presence of a broad diffraction-ring centered at around 2.8 to 3.1 Å (Fig. 2) and consistent with similar natural and synthetic materials characterized by others (Rancourt *et al.* 2001, Carlson *et al.* 2002, Jia *et al.* 2006, LeBerre *et al.* 2007, Paktunc *et al.* 2008). Another broad diffraction-ring, commonly observed at around 4.5 Å, is attributed to variable background in the thin section and increases in intensity with reduced intersection of mineral targets by the beam (*i.e.*, intensity responds to beam-sampled volume of epoxy). Chemically, the HFA is distinguished from scorodite by a higher molar Fe/As value (range 1.1 to  $\sim 3$ ). Sulfur content also is usually higher (typically several wt.%) than in scorodite. However, the maximum analyzed concentration is only 4.9 wt.% as

SO<sub>4</sub>. Silica is usually less than 0.5 wt.% by EPMA, but in some cases as high as 2.5 wt.%. This increase may be accompanied by an increase in Al and other silicate-related elements, suggesting interference from adjacent silicates or physical mixing of fine crystallites of silicate in the HFA. This is generally supported by spotty rings due to a phyllosilicate in the  $\mu$ -XRD pattern. Where elevated silica is detected without the presence of other contaminating elements, it is not possible to determine whether the silica is in chemical or physical association with the HFA. However, it is reasonable that silica may be associated with these phases in a similar manner to that observed for natural ferrihydrite (Jambor & Dutrizac 1998).

Calcium is consistently absent (<0.1 wt.%) in most EPMA analyses of HFA. In two analyses in MG02, both on likely replacement-induced rims on arsenopyrite, up to 0.9 wt.% Ca is detected in HFA. In a single analysis of cementing material elsewhere in section MG02, we detected yukonite by  $\mu$ -XRD with a Ca content by EPMA of 1.4 wt.%. A red-brown rim of HFA on arsenopyrite in GD03 also contained anomalous Ca for that section at 0.3 wt.%. See below for a further discussion of yukonite and Ca-Fe arsenates. With micro-XANES of selected HFA particles, we consistently identified only the presence of As<sup>5+</sup>.

Kaňkite is invariably very finely crystalline and generally in low abundance relative to HFA and scorodite. Where present as distinct aggregate grains, it optically appears very similar to pale yellow HFA, but the Fe/As value established by EPMA is approximately 1 for kaňkite (as described above, HFA exhibits Fe/As values consistently greater than 1.1). In the sample where kaňkite is abundant (CAR01), it is almost always admixed with scorodite (Fig. 3) in brownish, nearly opaque aggregates.

#### Other arsenates

In addition to the ferric arsenates already described, yukonite (Ca-Fe arsenate) and pharmacosiderite (a ferric arsenate with exchangeable K, Na, H<sub>3</sub>O) are also present in abundance in some samples, and as trace constituents in others. In general, though, the presence of abundant Fe arsenates seems to preclude the significant presence of yukonite and pharmacosiderite (and *vice versa*) in this set of samples. There are limited data available on the solubility of pharmacosiderite and yukonite (see below); a thermodynamic basis for the relationships among the Fe arsenates and Ca-Fe arsenates remains to be established.

Yukonite occurs as reddish brown grains, and more rarely as a replacement-induced rim on arsenopyrite or as irregular deposits on Fe-rich carbonate (Fig. 4). Yukonite also occurs as a coprecipitate with HFO, HFA and pharmacosiderite, as confirmed by EPMA and  $\mu$ -XRD (Table 3). The identification of such mixtures is consistent with the findings of Garavelli

*et al.* (2009), who suggested that all yukonite (including the type material) may in fact be a nanoscale mixture of a semicrystalline phase and an amorphous phase of variable composition. Yukonite in our samples is distinctly poorly crystalline and invariably diffracts as broadened smooth rings (Fig. 4). In sample GD05, the rings become so broad and weak as to suggest a more amorphous character and, in some cases, no evidence of yukonite diffraction is observed amid a background of spotty diffraction-rings attributed to phyllosilicates even though EPMA results indicated a yukonite-like composition (Table 3). These data indicate that all yukonite-like grains consistently exhibit a deficiency in Ca in comparison to compositions reported by Ross & Post (1997) and Garavelli *et al.* (2009). The most Fe-rich grains tend to be amorphous, whereas the more As and Ca-rich (Fig. 4, Table 3) exhibit an XRD pattern of yukonite. This contrasts with an alternate situation where rims rich in Fe oxyhydroxide with lower concentrations of Ca and As still show two or more of the major diffraction lines of yukonite, indicating the dilute presence of yukonite coprecipitated with the Fe oxyhydroxide (Table 3). This directly confirms an earlier supposition by Jambor & Blowes (1991) and the findings of Paktunc *et al.* (2004) that Ca associated with such phases is related to a Ca-Fe arsenate coprecipitate (probably yukonite) rather than adsorbed As. Coprecipitated yukonite, among other Fe-As phases, could be a relatively common solid form of As, especially in As-rich neutral drainage conditions. The solid products of pH neutral sulfide oxidation in As-rich materials are less well studied than those under acid conditions. In addition, as we have shown here, yukonite may occur as nonstoichiometric Fe-As-Ca mixtures of poorly crystalline to crystalline phases that would require specialized techniques (*e.g.*, microdiffraction, X-ray absorption spectroscopy or TEM) for definitive identification.

Pharmacosiderite is one of the most elusive phases detected in thin section, as it is almost always admixed with yukonite. The exception is one  $\mu$ -XRD target with a unique pharmacosiderite XRD pattern and little to no evidence of yukonite. Interestingly, its abundance as a major phase in MG03 is confirmed by its very clear detection by conventional XRD in the <150  $\mu$ m fraction of this sample. The unique position of the major diffraction-peak for this phase at  $\sim$ 8 Å makes this phase stand out in both bulk and  $\mu$ -XRD, whereas the associated yukonite (which may be subequal in abundance) is only detected by  $\mu$ -XRD. This difference is due to weaker diffraction by yukonite than pharmacosiderite and key major peak-overlaps (especially with chlorite, which obscures or interferes with the main diffraction peak of yukonite at  $\sim$ 14 Å). It is important to note that major diffraction-lines for yukonite (except for the peak at the lowest angle, at 14 Å, which is not observed in every case) overlap with two of the strongest four characteristic lines of pharmacosiderite (3.2 Å and 2.8 Å). Some patterns of pharmacosiderite also contain a

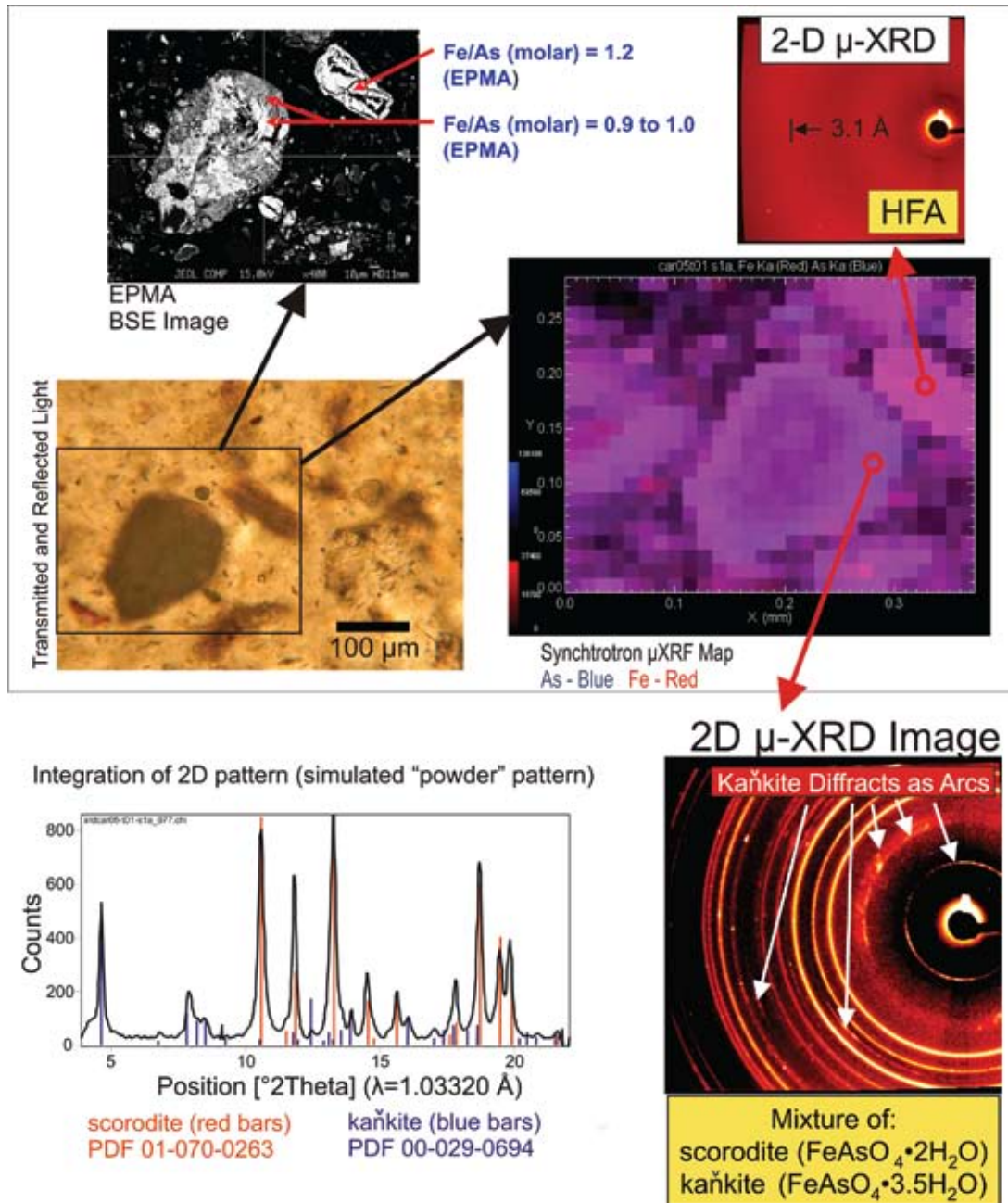


FIG. 3. (Top) Analysis of two Fe-arsenate grains in CAR01. The more As-rich grain is a mixture of kaňkite and scorodite, whereas the more Fe-rich grain consists of HFA. Micro-XRF map is a false-color image with high-As areas shown in blue and high-Fe areas shown in red. (Bottom) Micro-XRD results for mixed kaňkite and scorodite grain. Spots masked in 2D pattern and pattern integrated to 2D simulated powder pattern (Hammersley 1998). Bars indicate fit from search-match analysis. Some deviation from fit (especially for kaňkite) is a result of grain texture (preferred orientation that results in diffraction as arcs rather than rings).

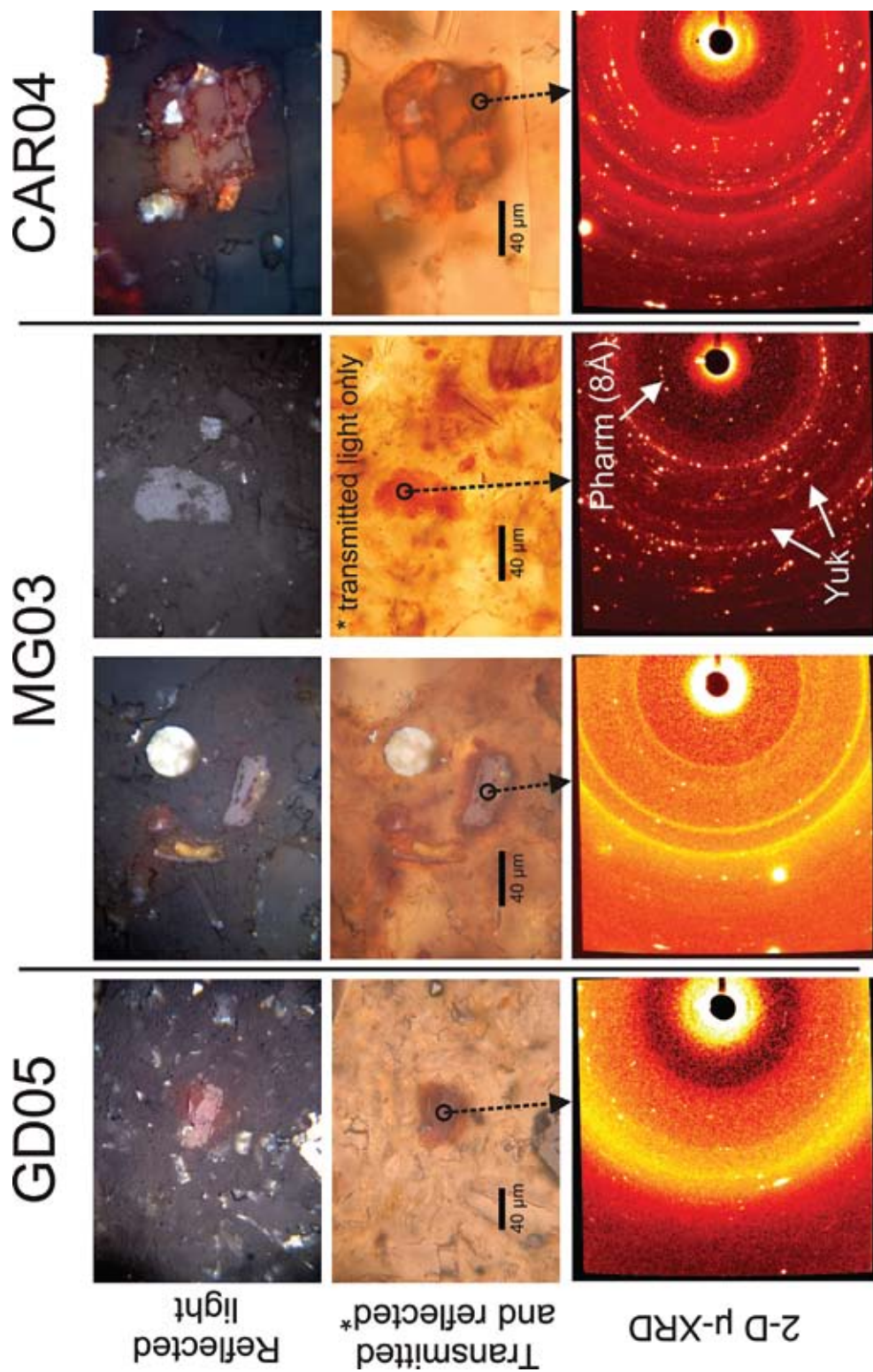


Fig. 4. Ca-Fe arsenates. (Left to right) Nearly amorphous yukonite-like grain (GD05), Mn-bearing yukonite (MG03, left), mixed pharmacosiderite-yukonite grain (MG03, right). Note: spots and spotty rings pertain to muscovite and pharmacosiderite, whereas faint broad rings pertain to yukonite. Yukonite rim on ankerite (CAR04).

TABLE 3. COMBINED MICRO-XRD AND EPMA ANALYSES AT COINCIDENT TARGETS OF YUKONITE-LIKE GRAINS

Sample	As phases	Fe <sub>2</sub> O <sub>3</sub>	As <sub>2</sub> O <sub>5</sub>	SO <sub>4</sub>	CaO	SiO <sub>2</sub>	MnO	K <sub>2</sub> O	Na <sub>2</sub> O	Al <sub>2</sub> O <sub>3</sub>	MgO	Total <sup>1</sup>
GD05	Yuk-HFA	38.93	34.03	0.30	6.83	0.91	0.00	0.23	0.53	0.19	0.63	82.52
	Yuk-HFA	40.57	31.64	0.13	6.30	0.43	0.00	0.20	0.07	0.01	0.73	80.07
	Yuk	38.61	31.37	1.50	8.45	1.38	0.00	0.14	0.27	0.20	0.49	82.16
	None observed	44.55	26.19	0.10	7.02	2.14	0.00	0.11	0.34	0.07	0.39	80.89
	None observed	43.38	29.19	2.80	5.64	3.92	0.00	0.09	0.23	0.06	0.27	85.11
	HFA or Yuk <sup>†</sup>	42.98	25.70	0.30	6.96	3.52	0.00	0.13	0.19	0.05	0.44	80.22
	Yuk <sup>‡</sup>	52.27	6.21	3.13	2.49	3.86	0.00	0.12	0.58	0.47	0.20	68.81
MG03	Yuk	32.03	33.91	0.50	7.60	0.95	2.09	0.23	0.30	0.83	0.49	78.85
	Yuk	31.24	37.24	0.41	7.12	1.48	1.73	0.29	0.00	1.46	0.82	81.72
	Yuk-Pha	46.01	33.02	0.30	3.79	0.99	1.02	0.20	0.16	1.46	0.77	87.67
	Yuk-Pha	38.56	24.86	0.84	3.67	2.41	0.81	0.25	0.00	4.63	0.25	76.14
	Yuk-Pha	39.92	30.92	1.08	5.37	3.54	1.32	0.12	0.00	4.00	0.54	86.63
	Pha-Yuk	43.07	30.77	0.69	4.59	1.67	2.22	0.43	0.99	2.34	0.50	87.16
	Pha-Yuk	42.01	26.77	0.80	3.50	3.06	1.30	0.25	0.24	1.90	0.86	80.55
	Pha-Yuk	42.18	31.06	0.85	4.54	2.07	1.79	0.34	0.41	2.52	0.66	86.29
	HFA-Yuk-Pha	40.91	33.39	0.40	0.82	0.46	0.21	0.15	0.00	0.94	0.25	77.46
	HFA-Yuk-Pha	43.18	32.45	0.31	1.24	0.57	0.74	0.21	0.28	0.91	0.33	80.16
HFO-Yuk	40.63	20.31	3.34	2.65	2.90	0.69	0.59	0.54	1.77	0.31	73.18	
MG02	HFA	37.58	38.05	0.85	1.99	2.20	0.75	0.43	0.44	1.68	0.00	83.84
Type-locality yukonite*		36.6	36.3	-	10.6	-	-	-	-	-	-	83.5

Arsenic-bearing phases were identified by  $\mu$ XRD. All patterns include spots and arcs from included or background crystallites, most commonly muscovite, chlorite or other phyllosilicates. Yukonite (Yuk) is identified by two or more broadened rings (e.g., at 2.8, 3.2, 5.6 Å), except as indicated. Pharmacosiderite (Pha) is identified by spotty rings to distinct spots at unique diffraction-angles (e.g., 8 and 4.6 Å). HFA (amorphous hydrous ferric arsenate) is identified by the presence of a very broad ring centered at 3.0 to 2.8 Å. HFO (amorphous hydrous ferric oxyhydroxide) is identified by a broad ring at 2.55 Å.

<sup>1</sup> Totals are less than 100%, as all phases are hydrous. Some variability may also be expected owing to the aggregate and poorly consolidated nature of the grains.

\* For reference, Tagish Lake, Yukon, Canada. Analytical data by J.L. Jambor reported by Dunn (1982). Water (not included in total presented) was 17.9% by DTA-TGA.

<sup>†</sup> Weak asymmetrical broad ring at 2.8 Å doesn't distinctly resolve as either Yukonite or HFA.

<sup>‡</sup> Yukonite pattern is very weak (very faint broad rings at 3.2 and 2.8 Å just above background). Few nebulous spots may be Py or marcasite. EPMA analysis was made on a 1- $\mu$ m spot (instead of standard 5- $\mu$ m spot) on a 3  $\mu$ m-wide target. Interpreted as yukonite in HFO that exhibits no evidence of ferrihydrite-like short-range order.

line at  $\sim$ 5.6 Å, the position of another major peak for yukonite. In most cases, the smooth and broad nature of the yukonite diffraction-rings in comparison to the fine-spotty rings of pharmacosiderite enables confirmation of both yukonite and pharmacosiderite together (Fig. 4). In a few cases, faint smooth diffraction-rings are evident that match the 8 Å and 4.6 Å lines of pharmacosiderite (e.g., trace phase identified in MG02); however, in these cases, there is no evidence of coincident diffraction by yukonite.

Grains in MG03 that show both pharmacosiderite and yukonite characteristically exhibit lower Ca/As values, slightly higher Fe/As values and elevated (few wt.%) Al in varying amounts (Table 3). In pharmacosiderite-group minerals described in the literature, the tunnel structure incorporates exchangeable charge-balancing mono- or divalent cations such as K, Na, H<sub>3</sub>O and Ba (e.g., Peacor & Dunn 1985, Buerger *et al.* 1967). Substitution of Al for Fe<sup>3+</sup> to form alumopharmacosiderite is also known. The lack of evidence of a

clear compensating ion (Na or K) in EPMA analyses of the pharmacosiderite-bearing grains (Table 3) suggests either the presence of Ca or H<sub>3</sub>O to balance charge, or the pharmacosiderite may be present as only minute inclusions that are detected by XRD, but have little influence on EPMA. The latter possibility is supported by the very fine and weak diffraction-spots observed for the pharmacosiderite (Fig. 4).

#### Arsenic-bearing ferric oxyhydroxides

Iron oxyhydroxides are present as translucent yellow brown, red brown or, most commonly, opaque grains. Rarely, they are present as grain coatings or inclusions. Excluding sulfides, Ti oxides and Fe-Ti oxides, they are the most reflective phases present in thin section and are invariably more reflective than the arsenate phases. As a group, these grains can thus be readily distinguished petrographically. With the EPMA results, we consistently find molar Fe/As values for these

grains in excess of 3 or 4. Grains exhibiting complex textures and mixtures of two ferric oxyhydroxides or other As-bearing phases (especially HFA) occur widely among this group (Fig. 5). Goethite or goethite–lepidocrocite mixtures are observed most commonly, but lepidocrocite, akaganeite-like phases and HFO (ferrihydrite) have also been identified. Excluding the soil sample (MG06), all of these ferric oxyhydroxides contain elevated concentrations of As. Arsenic concentrations generally range from *ca.* 4 to 20% as As<sub>2</sub>O<sub>5</sub>, with Fe/As values of 3 to 30, and sulfur from 1.1 to 6% as SO<sub>4</sub>. The limited number of grains and the wide range of forms and combinations of Fe oxyhydroxide minerals prevent a systematic analysis of composition *versus* mineralogy at this time.

In two samples, a reflective opaque Fe oxyhydroxide is observed that has an XRD pattern similar to a mixture of akaganeite and ferrihydrite. The akaganeite is suggested by the presence of a sharp, but smooth diffraction ring at 7.39 Å; however, the strong diffraction-line at 3.33 Å is unusually broad and diffuse, which is inconsistent with published ICDD XRD patterns for akaganeite.

Two different Fe oxyhydroxides with As associations were identified in the single soil sample analyzed for this study. Arsenic-bearing HFO (2.5% As) and goethite (0.08% As) were identified in the single B-horizon soil sample investigated. Although the As concentration measured in the goethite grain by EPMA is very low and near the limit of quantification, the much greater sensitivity of synchrotron  $\mu$ -XRF independently confirmed the presence of As associated with goethite.

#### *Arsenic-bearing ferric sulfates and realgar*

In general, there are relatively few sulfate minerals in these samples, which is consistent with the bulk composition (Table 1) and mineralogy (Table 2); arsenopyrite readily explains the elevated S contents where present. Sample OLD04 (discussed below) is an exception; the elevated S content is due to the presence of jarosite and other Fe–As sulfates. Gypsum can be a common constituent in weathered sulfide-mine tailings. The high As content of these materials and the geochemical conditions generally seem to have favored the stabilization of arsenate phases rather than sulfates or sulfate–arsenates. The low carbonate content in discharged tailings may have provided little dissolved Ca to precipitate with sulfate, even in the presence of acidic conditions in pore waters in the tailings. However, sulfates or sulfate–arsenates may be more common in deeper geochemical environments not represented by the surface-focused sampling here.

The presence of jarosite and several other minor sulfate minerals in OLD04 (schwertmannite and tooeleite) confirms the local presence of sulfate or arsenic–sulfate phases. However, this sample taken from the top of a stamp-mill foundation, due to its

unique appearance and proximity to a local residence, appears to be anomalous in a number of respects. The sample contains fairly typical concentrations of Fe and As for the study samples (Table 1), but contains the highest concentrations of Ba, Sn, Tl and Au in this set of samples (Parsons *et al.*, in press). Though not cemented itself, it is proximal to a scorodite hard-pan material and contains very low Ca, consistent with the expectation of relatively acidic conditions necessary to stabilize jarosite. Jarosite in this sample is present as transparent to translucent yellow reflective grains that exhibit complex smooth-ring to coarse spotty diffraction-patterns suggestive of a wide range of crystallite sizes. Arsenic is present in this jarosite phase, as confirmed by synchrotron  $\mu$ -XRF, but it has not yet been quantified.

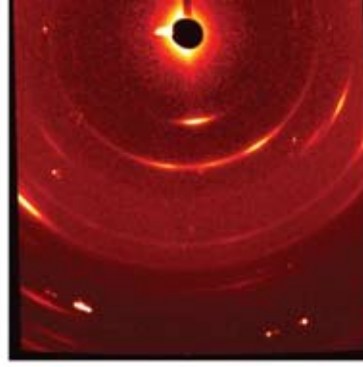
In addition to OLD04, As-bearing sulfate minerals have been identified in trace amounts in some of the other samples. Nanocrystalline tooeleite (ferric arsenite sulfate) was identified in MG01. It appears that this grain is partially transformed to HFA on the basis of EPMA,  $\mu$ -XRD and  $\mu$ -XANES data (Fig. 6). A single grain of translucent orange jarosite was identified in GD02 by a spotty ring  $\mu$ -XRD pattern suggestive of fairly coarse crystallinity.

Two small grains of realgar were identified in sample MG04 by XRF mapping (Fig. 7). This sample was collected from saturated arsenopyrite-bearing tailings beneath a thin layer of organic matter in a marshy area of the Montague tailings. Given its very fine grain-size (<10  $\mu$ m diameter) and the absence of quantitative data establishing realgar as a primary phase in the Meguma ores (P.K. Smith, pers. commun., 2009), the realgar is probably a secondary sulfide precipitate forming under reducing conditions in the Montague tailings (O'Day *et al.* 2004).

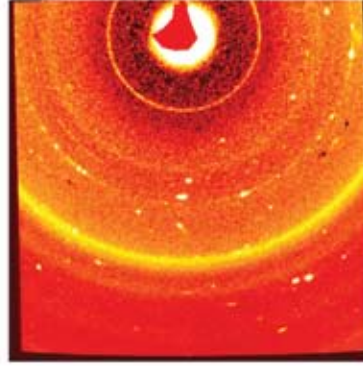
#### *Mineralogical control on arsenic stability and mobility*

The predominance of ferric arsenate and Ca–Fe arsenate phases in the tailings samples examined implies the strong attenuation of As during weathering of these arsenopyrite-rich materials. Understanding the long-term stability and solubility of these arsenate phases is critical for predicting the mobility of As in weathered Au mine tailings. The solubility and stability of scorodite in comparison to HFA have been the subject of much research in recent years, driven by the importance of scorodite as a disposal product in metallurgical processes (*e.g.*, Harvey *et al.* 2006, Langmuir *et al.* 2006, Bluteau & Demopoulos 2007) and the significantly higher solubility of HFA (*e.g.*, Krause & Ettl 1989, Langmuir *et al.* 2006). Scorodite is stable under oxidizing conditions at low pH (Vink 1996), exhibiting low solubility (typically <0.5 mg/L) between pH 2.8 and 5 (Krause & Ettl 1989, Bluteau & Demopoulos 2007). With increasing pH, scorodite dissolves incongruently

MG01



CAR03



GD04

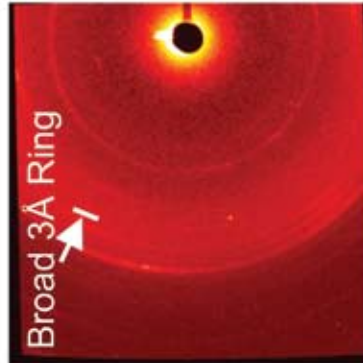
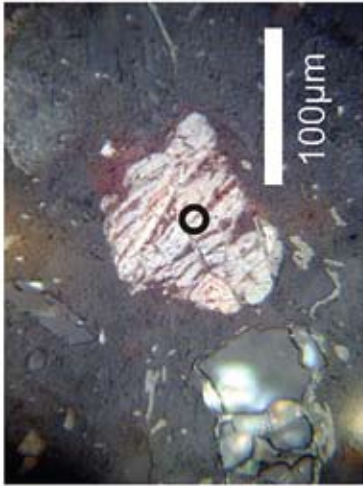


FIG. 5. Reflected light photos and  $\mu$ -XRD of selected Fe oxyhydroxides. (GD04, left) Banded grain. Smooth, thin rings in XRD image are lepidocrocite and goethite. Broad ring at 3 Å (approximate center is marked) confirms the presence of HFA. Variable and lower reflectivity than other Fe oxyhydroxides is observed, consistent with admixed HFA. (CAR03, middle) Irregular Fe oxyhydroxide with silicate inclusions. Grain is a mixture of akaganeite, ferrhydrite and goethite. (MG01, right) HFA rimming Fe oxyhydroxide, which is a mixture of goethite and lepidocrocite. Arcs rather than rings in this pattern indicate preferred orientation of the crystallites, especially for lepidocrocite (short arcs). Broad ring in this case is probably due to the surrounding rim of HFA that is partly intersected by the beam.

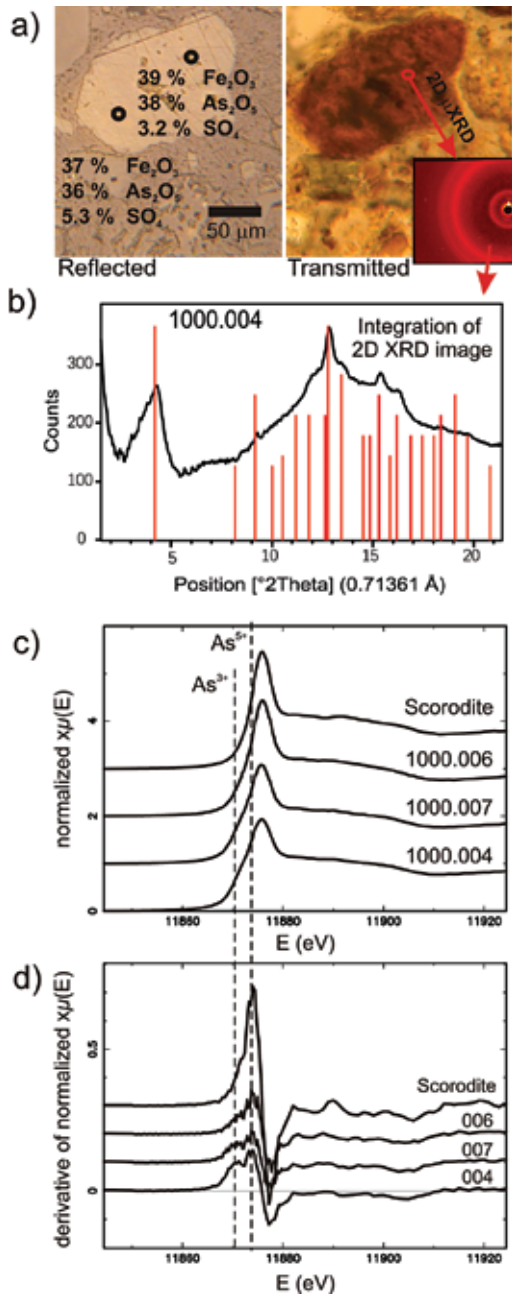


FIG. 6. Grain of tooeelite from MG01 (mixture of tooeelite and HFA). a) Transmitted-light and reflected-light photos, with As, Fe and S contents determined by EPMA; we show the location and image of the  $\mu$ -XRD analysis. b) Integrated and matched simulated powder-pattern confirming the presence of tooeelite. c) and d)  $\mu$ -XANES data and derivative data for scorodite standard and three different locations on the target grain. Spectra confirm the presence of both As<sup>3+</sup> and As<sup>5+</sup> (arranged in order of increasing As<sup>5+</sup> from bottom to top).

to Fe oxyhydroxide, and the arsenic released is partly sorbed onto the newly formed Fe oxyhydroxide. On the basis of recent laboratory studies, the dissolution kinetics of scorodite are relatively slow (Bluteau & Demopoulos 2007, Harvey *et al.* 2006). Insight into the distinct nature of HFA and its relationship to As-bearing HFO has only recently been provided in detailed

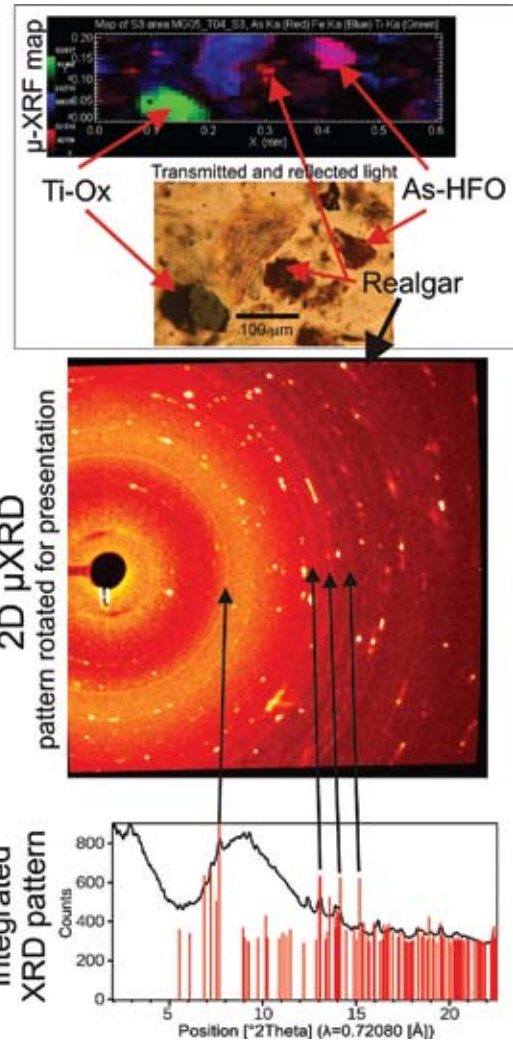


FIG. 7. Realgar in MG04. (Top)  $\mu$ -XRF map (Ti: green, As: red, Fe: blue). Arsenic-Fe grain at upper right is As-bearing HFO on phyllosilicate. As-rich grain in middle is realgar in opaque mass. (Middle) 2-D  $\mu$ -XRD image of finely crystalline realgar identified by smooth diffraction-rings. Brighter spots are diffraction from unidentified discrete crystallites. (Bottom) Integrated pattern after masking discrete spots from crystallites. Match with realgar (PDF 01-071-2434) is shown.

laboratory studies (LeBerre *et al.* 2007, Paktunc *et al.* 2008), although earlier studies pointed to differences, particularly in the greater solubility of these largely X-ray-amorphous precipitates where the Fe:As ratio is less than 3 or 4 (*e.g.*, Krause & Ettel 1989). In the present study, we clearly demonstrate that transmission  $\mu$ -XRD and petrographic methods are suitable for the difficult task of distinguishing these phases both from each other and more crystalline phases rich in As. The identification of HFA and HFO in these materials has clear implications regarding As mobility. Further work is under way to investigate the role of these and other As-bearing phases (DeSisto *et al.* 2008).

In contrast to scorodite and HFA, there is little information on the stability and solubility of other arsenate phases (*e.g.*, pharmacosiderite, kaňkite, yukonite). Pharmacosiderite has a quite widespread distribution. Some have suggested a hydrothermal origin (Morin *et al.* 2002), and have questioned its low-temperature formation, although it is a hydrous phase. Others identify it in well-crystallized form along with scorodite in weathering (supergene) environments (*e.g.*, Sejkora *et al.* 2006). This finding suggests that pharmacosiderite may be a stable phase, perhaps (like scorodite) under low-pH conditions and in the presence of abundant exchangeable cations ( $H_3O$ , Na, K, and Ba) necessary to stabilize this mineral (Buerger *et al.* 1967, Mutter *et al.* 1984, Peacor & Dunn 1985). However, there is apparently no thermodynamic information presently available for this phase (Welham *et al.* 2000). Morin *et al.* (2002) similarly identified a lack of solubility data for this mineral. In this study, pharmacosiderite is identified in a sample that also contains yukonite, but no scorodite. The coexistence of pharmacosiderite with Ca-Fe arsenates (arsenosiderite and yukonite) had previously been reported (*e.g.*, Anthony *et al.* 2000, Filippi *et al.* 2004). However, the conspicuous lack of a Ca-rich end-member in the pharmacosiderite group in nature could be indicative of the greater stability of Ca-Fe arsenates over pharmacosiderite in contact with Ca-rich waters.

Kaňkite has been described from relatively few locations and is known only as finely crystalline aggregate material existing under wet conditions (Čech *et al.* 1976, Kato *et al.* 1984). Though chemically similar to scorodite, no solubility studies of this phase have been reported. At the type locality (Čech *et al.* 1976), kaňkite is intimately associated with scorodite and, in some cases, the rarer polymorph of scorodite, parascorodite (Ondruš *et al.* 1999, Perchiazzi *et al.* 2004); scorodite is routinely considered by investigators as the most stable phase. Where present in abundance in this study, kaňkite is similarly in close association with scorodite. Therefore, the relationship between these two minerals and how they affect the mobility of arsenic warrants additional study.

Yukonite is similarly a rare secondary mineral described at relatively few localities (Tyrrell & Graham

1913, Dunn 1982, Ross & Post 1997, Pieczka *et al.* 1998, Nishikawa *et al.* 2006, Garavelli *et al.* 2009), and is invariably present as poorly crystalline material (Anthony *et al.* 2000). A few solubility experiments have been reported for yukonite. Krause & Ettel (1989) observed a minimum As concentration in stirred solution of 6.3 mg/L at a pH of 6.15 after 241 days; however, as yukonite is poorly crystalline with variable proportions of Ca, Fe and As, it is difficult to assess the purity of such a phase. The possible presence of a small amount of admixed HFA or other As-phase also exists. A recent laboratory study (Jia & Demopoulos 2008) has shown a significant reduction in As solubility over a pH range of 4 to 8 in the presence of dissolved Ca if compared with Na. The authors attributed the reduced solubility to the presence of a Ca-Fe-As coprecipitate; this appears to be confirmed by the presence of yukonite in XRD patterns after aging the material at 75°C for 7 weeks at pH 7.5 to 8.

Calcium is an essential constituent in yukonite, and is supplied mainly through carbonate dissolution in the tailings investigated in the present study. The composition of yukonite reported in the literature varies, but invariably contains an excess of Fe to As on a molar basis. Values of Fe/As of 1:1 in arsenopyrite and a low mobility of Fe at neutral pH suggest that weathering of arsenopyrite under these conditions results in a net release of As to porewaters. This inference is consistent with results of this study that show the presence of As associated with oxidation products (Fe oxyhydroxides) of non-As-bearing sulfides. Such mobility of As is also confirmed where yukonite apparently forms by the incongruent dissolution of ankerite in the presence of dissolved As (Fig. 4).

In the Nova Scotia tailings, As-bearing oxyhydroxides of Fe have scavenged As from fluids during weathering of As-poor Fe sulfides (pyrite and probably pyrrhotite). This is the case for yukonite-bearing carbonate-buffered tailings, as previously discussed, but also for carbonate-poor tailings containing more acid-stable ferric arsenate phases (scorodite, kaňkite, HFA). Data from this study confirm the importance of not only Fe sulfides and Fe carbonates, but other sources of Fe (*e.g.*, Fe in phyllosilicates) as potentially important scavengers of As in these systems. Thus far, all As associations identified are with ferric iron phases; ferrous iron sources must thus undergo oxidation as part of the attenuation process.

At both Caribou and Montague, relatively unoxidized sulfide grains are observed in near-surface arsenopyrite-rich material. At both sites, there are apparent barriers to oxidation, including water-saturated conditions (in some cases with organic cover material), or overlying hardpan material that may provide a barrier to penetration by water and oxygen. Subsequent exposure of such concentrates to moisture and air will result in the eventual onset of sulfide oxidation, leading to precipitation of secondary As-Fe minerals, and

possibly, at least local mobilization of As (DeSisto *et al.* 2008). Sample MG04, from a low-lying, saturated and marshy area, predominantly contains arsenopyrite with lesser amounts of HFA and HFO. Whereas these oxidized forms could originate from the erosion of tailings, it seems more likely that they are a result of localized oxidation in the rhizosphere at plant roots (Jacob & Otte 2003).

#### *Mineralogical control on As bioaccessibility*

Mineralogy, grain size, and inclusions or rinds of grains are expected to be significant controls on arsenic bioaccessibility and bioavailability (Ruby *et al.* 1999), because they influence solid–fluid interaction, and particularly rates of dissolution. Ruby *et al.* (1999) stated that, for a given grain-size, arsenopyrite will have low bioaccessibility, soluble phases such as  $\text{As}_2\text{O}_3$  will have high bioaccessibility, and other phases such as Fe–As oxides will be somewhere in between. However, the relationship between mineralogy and bioaccessibility or bioavailability for arsenic has rarely been studied directly. Makris *et al.* (2008) included bioaccessibility testing of arsenopyrite and scorodite, two minerals common in some of our samples. However, the reported total As content of both the arsenopyrite and scorodite were only 41 and 34%, respectively, of the As concentration expected for the pure minerals. This may reflect incomplete dissolution during the characterization of their study materials, or the presence of impurities in the mineral samples. These issues aside, their results show that the percent bioaccessibility of As from the arsenopyrite is extremely low (<1 %) under pH conditions ranging from 0.2 to 4.3. The bioaccessibility of scorodite was found to be only slightly higher, with a maximum of 7% at a pH of 0.2 and even less at a pH of 2, which is more typical of the gastric environment (Ruby *et al.* 1999).

In a study of the bioavailable fraction of As in soil ingested by the cynomolgus monkeys, Roberts *et al.* (2007) concluded that the link to mineralogy may be more complicated than originally conceived. The link to mineralogy in the context of the Roberts *et al.* (2007) study was actually defined as the form of As determined by EPMA, with phases being grouped according to chemical similarity only. This approach was also used in another study of mineralogical controls on bioavailability from smelter-contaminated soils (Davis *et al.* 1996). Such an approach to mineralogy may be an oversimplification, particularly in comparing samples from such diverse origins (*e.g.*, smelter soils, chemical-plant or pesticide-contaminated soils and mine tailings). Roberts *et al.* (2007) did correlate As in undifferentiated Fe sulfates to the bioavailable fraction in monkeys, but could find no link with other chemical fractions differentiated, including Fe oxides and Fe–As oxides. The study included a single sample of mine tailings

originating in California, with no other details on source provided. The apparent lack of Fe–As oxides in that sample suggests only partial similarity to the samples in our study. The percent bioavailable As from that sample was 19%. Assuming that little As was available from the arsenopyrite that constituted 70% of the sample on a mass basis, a significant portion of the oxidized As [identified as Fe oxides (27%) and Fe sulfates (2.3%)] was bioavailable. Interestingly, a similar bioavailability was reported for a Colorado residential soil (percent bioavailability of 17%) identified as containing over 87% As as  $\text{As}_2\text{O}_3$ .

The amorphous, nanocrystalline or finely crystalline nature of the As weathering products identified in the present study points to particle porosity, permeability, surface area and degree of crystallinity as potentially more important factors to dissolution than particle size measured in the traditional sense. Clearly, a better understanding of the link between mineral solubility (and particle texture) and bioaccessibility is required, not only to assess whether mineralogy can be used as a predictor of bioavailability, but also to add rigor to the fundamental understanding of the dissolution mechanisms that lead to the bioavailability of As. A particular challenge for As continues to be the multitude of different sources and processes (anthropogenic and natural), which result in diverse and mixed solid forms of As in soils.

#### SUMMARY AND CONCLUSIONS

Detailed mineralogical characterization of a visually distinct set of near-surface weathered tailings samples and one soil sample from four As-rich Au mine sites in Nova Scotia has revealed a diversity and complexity in both the mineral species within a given sample and the mineral form and texture at the grain and subgrain scale. Samples range from arsenopyrite-rich mill concentrates (one of which has almost completely weathered to very fine grey-green aggregates of scorodite) to As-rich tailings containing from four to nine different amorphous to crystalline host-phases of As. Gravity concentration of arsenopyrite during milling seems to have been a major factor in determining the geochemical fate of As in the Nova Scotia tailings, by concentrating As and altering the ratio of carbonate to sulfide in As-rich tailings. Locally, acidic pore-waters related to oxidation of these mill concentrates (DeSisto *et al.* 2008) are believed to be the cause of the As-rich tailings hardpans cemented by ferric arsenate, as observed at the Montague, Goldenville and Caribou sites.

Secondary forms of As are all micro- to nanoparticulate or crystalline aggregate grains or grain coatings. In addition to mineral solubility and grain size, therefore, the grain texture (massive *versus* grain coatings) and subgrain porosity and permeability may control dissolution processes and rates, especially for

kinetically limited situations (*e.g.*, the release of As in gastrointestinal fluids following accidental ingestion of tailings).

In summary, we have determined that there are at least six distinct types of tailings that exhibit unique mineralogical and geochemical signatures:

1) Mill concentrates comprised largely of arsenopyrite, with As contents approaching those of the original arsenopyrite (>10% w/w).

2) Mill concentrates that have been fully oxidized to fine-grained, grey-green scorodite.

3) Acid-influenced tailings samples dominated by ferric arsenates and commonly associated with cemented tailings. Scorodite-rich, scorodite-kañkite-rich and HFA-rich (one with jarosite) have all been identified.

4) Carbonate-buffered samples exhibiting neutral weathering characteristics with Ca-Fe arsenates (yukonite or amorphous) as the dominant mineral form. Ferric oxyhydroxides may contain coprecipitated Ca-Fe arsenate rather than sorbed As-Fe<sup>3+</sup> oxyhydroxides or coprecipitated HFA. These samples may contain significant relict primary sulfide owing to the coarse grain-size (fine sand and silt) or slow kinetic reactions (*e.g.*, CAR04). For GD-T05, the one finer-grained sample (silt and clay) that contains little relict sulfide, the Ca-Fe arsenates exhibit a very broad diffraction pattern of yukonite suggesting an almost amorphous form.

5) Transitional samples of tailings in which the original buffering capacity by carbonate has given way to an acid weathering environment. Though requiring further study, it seems plausible to us that yukonite-rich carbonate-buffered tailings may gradually alter to pharmacosiderite-bearing tailings (MG03) in response to increasingly acidic conditions upon depletion of the carbonate phase.

6) Samples of saturated tailings in low-lying areas where reducing conditions prevail. These samples contain largely unoxidized arsenopyrite with some oxidized HFA and HFO that may be the result of localized oxidation in the rhizosphere at plant roots. The presence of realgar (detected by  $\mu$ -XRD) in these reduced tailings suggests that precipitation of authigenic sulfides may limit the mobility of As. The realgar is suspected to be secondary in origin, as there are no confirmed reports of primary realgar in the Nova Scotia Au districts (P.K. Smith, pers. commun., 2009).

This detailed mineralogical work has confirmed synchrotron  $\mu$ -XRD to be a powerful tool for the characterization of samples with a complex mineralogy. The Nova Scotia sites of mine tailings contain As in a wide range of mineralogical forms that are not yet understood in terms of their relationship to human bioaccessibility. Comparison of this diverse mineralogy with bioaccessibility tests completed on these samples is presently under way and will be reported separately. Once the most bioaccessible forms of As are determined, the

mineralogical links to spatial and geochemically distinct tailings at these sites offer the possibility of improved management and prioritization of tailings for remediation on the basis of human health and environmental stability criteria rather than total As content.

#### ACKNOWLEDGEMENTS

We thank Kaye Savage and two anonymous referees for their thoughtful reviews that substantially improved the paper, and the careful editorial oversight of guest editor Karen Hudson-Edwards. This paper has also benefitted from early constructive comments by Peter Chapman, Alexandre Desbarats, Bob Garrett and Jeanne Percival. We are grateful to Paul Smith and Terry Goodwin from the Nova Scotia Department of Natural Resources for their capable assistance during fieldwork for this project. Bob Fitzgerald and Bill LeBlanc of the Geological Survey of Canada (Atlantic) are acknowledged for their help with sample processing and conventional XRD analyses, respectively. We also thank Karina Lange and Lori Wrye for their assistance in conducting analysis at the synchrotron facility. Patricia Stoffyn at Dalhousie University is thanked for her assistance with the electron-microprobe analyses. The authors gratefully acknowledge the support of the NSERC MITHE Strategic Network. A full list of sponsors is available at: [www.mithe-sn.org](http://www.mithe-sn.org). S. Walker thanks the Davies Charitable Foundation for supplemental Post-Doctoral financial support. This study was also funded in part through the Environment and Health Program, Earth Sciences Sector, Natural Resources Canada. Portions of this work were performed at Beamline X26A, National Synchrotron Light Source (NSLS), Brookhaven National Laboratory. X26A is supported by the Department of Energy (DOE) – Geosciences (DE-FG02-92ER14244 to The University of Chicago – CARS) and DOE – Office of Biological and Environmental Research, Environmental Remediation Sciences Division (DE-FC09-96-SR18546 to the University of Georgia). Use of the NSLS was supported by DOE under Contract No. DE-AC02-98CH10886. This is contribution number 20080489 of the Earth Sciences Sector, Natural Resources Canada.

#### REFERENCES

- ANTHONY, J., BIDEAUX, R., BLADH, K. & NICHOLS, M.C. (2000): *Handbook of Mineralogy. IV. Arsenates, Phosphates, Vanadates*. Mineral Data Publishing, Tuscon, Arizona.
- ARAI, Y., LANZIROTTI, A., SUTTON, S.R., NEWVILLE, M., DYER, J. & SPARKS, D.L. (2006): Spatial and temporal variability of arsenic solid-state speciation in historically lead arsenate contaminated soils. *Environ. Sci. Technol.* **40**, 673-679.
- ASHLEY, R.P. (2002): Geoenvironmental model for low-sulfide gold-quartz vein deposits. *In Progress on Geoenvironmen-*

- tal Models of Selected Mineral Deposit Types (R.R. Seal II & N.K. Foley, eds.). *U.S. Geol. Surv., Open-File Rep.* **02-195**, 176-195.
- BATES, J.L.E. (1987): Gold in Nova Scotia. *Nova Scotia Department of Mines and Energy, Halifax, Nova Scotia, Information Ser.* **13**.
- BLOWES, D.W., JAMBOR, J.L., HANTON-FONG, C.J., LORTIE, L. & GOULD, W.D. (1998): Geochemical, mineralogical, and microbiological characterization of a sulphide-bearing carbonate-rich gold-mine tailings impoundment, Joutel, Québec. *Appl. Geochem.* **13**, 687-705.
- BLUTEAU, M.-C. & DEMOPOULOS, G.P. (2007): The incongruent dissolution of scorodite – solubility, kinetics and mechanism. *Hydrometallurgy* **87**, 163-177.
- BROOKS, R.R., FERGUSSON, J.E., HOLZBECHER, J., RYAN, D.E., ZHANG, H.F., DALE, J.M. & FREEDMAN, B. (1982): Pollution by arsenic in a gold-mining district in Nova Scotia. *Env. Pollut. (Ser. B)* **4**, 109-117.
- BUERGER, M.J., DOLLASE, W.A. & GARAYCOCHEA-WITKE, I. (1967): The structure and composition of the mineral pharmacosiderite. *Z. Kristallogr.* **125**, 92-108.
- CARLSON, L., BIGHAM, J.M., SCHWERTMANN, U., KYEK, A. & WAGNER, F. (2002): Scavenging of As from acid mine drainage by schwertmannite and ferrihydrite: a comparison with synthetic analogues. *Environ. Sci. Technol.* **36**, 1712-1719.
- ČECH, F., JANSÁ, J.J. & NOVÁK, F. (1976): Kaňkite,  $\text{FeAsO}_4 \cdot 3.5\text{H}_2\text{O}$ , a new mineral. *Neues Jahrb. Mineral., Monatsh.*, 426-436.
- CHAKRABORTY, S., WOLTERS, M., CHATTERJEE, D. & CHARLET, L. (2007): Adsorption of arsenite and arsenate onto muscovite and biotite mica. *J. Coll. Inter. Sci.* **309**, 392-401.
- COLE, G.E. (1927): The development of gold mining in Canada. *Can. Inst. Mining Trans.* **30**, 10-150.
- CORRIVEAU, M.C. (2006): *Characterization of Arsenic-Bearing Near-Surface and Airborne Particulates from Gold Mine Tailings in Nova Scotia, Canada*. M.Sc. thesis, Queen's University, Kingston, Ontario, Canada.
- COURTIN-NOMADE, A., BRIL, H., NÉEL, C. & LENAIN, J.-F. (2003): Arsenic in iron cements developed within tailings of a former metalliferous mine – Enguialès, Aveyron, France. *Appl. Geochem.* **18**, 395-408.
- COURTIN-NOMADE, A., SOUBRAND-COLIN, M., MARCUS, M.A. & FAKRA, S.C. (2008): Evidence for the incorporation of lead into barite from waste rock pile materials. *Environ. Sci. Technol.* **42**, 2867-2872.
- DALE, J.M. & FREEDMAN, B. (1982): Arsenic pollution associated with tailings at an abandoned gold mine in Halifax County, Nova Scotia. *Proc. N.S. Inst. Sci.* **32**, 337-349.
- DAVIS, A., RUBY, M.V., BLOOM, M., SCHOOF, R., FREEMAN, G. & BERGSTROM, P.D. (1996): Mineralogic constraints on the bioavailability of arsenic in smelter-impacted soils. *Environ. Sci. Technol.* **30**, 392-399.
- DESISTO, S.L., JAMIESON, H.E. & PARSONS, M.B. (2008): Geochemistry of scorodite-bearing hardpan and its significance to arsenic cycling at a former gold mine. *Geol. Soc. Am., Abstr. Programs* **40**(6), 112.
- DUGGAN, M.J., INSKIP, M.J., RUNDLE, S.A. & MOORCROFT, J.S. (1985): Lead in playground dust and on the hands of schoolchildren. *Sci. Tot. Environ.* **44**, 65-79.
- DUNN, P.J. (1982): New data for pitticite and a second occurrence of yukonite at Sterling Hill, New Jersey. *Mineral. Mag.* **46**, 261-264.
- ENDO, S., TERADA, Y., KATO, Y. & NAKAI, I. (2008): Chemical speciation of arsenic-accumulating mineral in a sedimentary iron deposit by synchrotron radiation multiple X-ray analytical techniques. *Environ. Sci. Technol.* **42**, 7152-7158.
- FILIPPI, M., GOLÍÁŠ, V. & PERTOLD, Z. (2004): Arsenic contaminated soils and anthropogenic deposits at the Mokrsko, Roudný, and Kašperské Hory gold deposits, Bohemian Massif (CZ). *Environ. Geol.* **45**, 716-730.
- GARAVELLI, A., PINTO, D., VURRO, F., MELLINI, M., VITI, C., BALIĆ-ŽUNIĆ, T. & DELLA VENTURA, G. (2009): Yukonite from the Grotta della Monaca cave, Sant'Agata di Esaro, Italy: characterization and comparison with cotype material from the Daulton mine, Yukon, Canada. *Can. Mineral.* **47**, 39-51.
- GIERÉ, R., SIDENKO, N.V. & LAZAREVA, E.V. (2003): The role of secondary minerals in controlling the migration of arsenic and metals from high-sulfide wastes (Berikul gold mine, Siberia). *Appl. Geochem.* **18**, 1347-1359.
- GOLDBERG, S. (2002): Competitive adsorption of arsenate and arsenite on oxides and clay minerals. *Soil Sci. Soc. Am. J.* **66**, 413-421.
- HAMMERSLEY, A.P. (1998): FIT2D V 10.3, Reference Manual V 4.0. European Synchrotron Research Facility, Paper **ESRF98-HA01T** (program and manual available at <http://www.esrf.eu/computing/scientific/FIT2D/>).
- HARVEY, M.C., SCHREIBER, M.E., RIMSTIDT, J.D. & GRIFFITH, M.M. (2006): Scorodite dissolution kinetics: implications for arsenic release. *Environ. Sci. Technol.* **40**, 6709-6714.
- HE, B.B., PRECKWINKEL, U. & SMITH, K.L. (2003): Comparison between conventional and two-dimensional XRD. *Adv. X-ray Anal.* **46**, 37-42.
- HENDERSON, E.H. (1935): Stamp milling and amalgamation practice at Goldenville, N.S. *Can. Inst. Mining Trans.* **35**, 222-242.

- ICDD (2003): Powder Diffraction File (PDF 2), Release 2003. International Centre for Diffraction Data, Newtown Square, Pennsylvania.
- JACOB, D.L. & OTTE, M.L. (2003): Conflicting processes in the wetland plant rhizosphere: metal retention or mobilization? *Water Air Soil Pollut.* **3**, 91-104.
- JAMBOR, J.L. (1994): Mineralogy of sulfide-rich tailings and their oxidation products. In *The Environmental Geochemistry of Sulfide Mine-Wastes* (D.W. Blowes & J.L. Jambor, eds.). *Mineral. Assoc. Can., Short Course Handbook* **22**, 59-102.
- JAMBOR, J.L. & BLOWES, D.W. (1991): Mineralogical study of low-sulfide, high carbonate, arsenic-bearing tailings from the Delnite minesite, Timmins, Ontario. In *Proc. 2<sup>nd</sup> Int. Conf. on the Abatement of Acid Drainage* (Montreal) **4**, 173-197. CANMET, Ottawa, Ontario, Canada.
- JAMBOR, J.L. & DUTRIZAC, J.E. (1998): Occurrence and constitution of natural and synthetic ferrihydrite, a widespread iron oxyhydroxide. *Chem. Rev.* **98**, 2549-2586.
- JIA YONGFENG & DEMOPOULOS, G.P. (2008): Coprecipitation of arsenate with iron(III) in aqueous sulfate media: effect of time, lime as base and co-ions on arsenic retention. *Water Res.* **42**, 661-668.
- JIA YONGFENG, XU LIYING, FANG ZHEN & DEMOPOULOS, G.P. (2006): Observation of surface precipitation of arsenate on ferrihydrite. *Environ. Sci. Technol.* **40**, 3248-3253.
- KATO, A., MATSUBARA, S., NAGASHIMA, K., NAKAI, I. & SHIMIZU, M. (1984): Kaňkite from the Suzukura mine, Enzan city, Yamanashi prefecture, Japan. *Mineral. J.* **12**, 6-14.
- KEPPIE, J.D., compiler (2000): *Geological Map of the Province of Nova Scotia*. Nova Scotia Department of Natural Resources, Map **ME 2000-1** (scale: 1:500 000).
- KING, R.J. (2002): Minerals explained. 35. Arsenopyrite. *Geol. Today* **18**, 72-75.
- KIRPICHCHIKOVA, T.A., MANCEAU, A., SPADINI, L., PANFILI, F., MARCUS, M.A. & JACQUET, T. (2006): Speciation and solubility of heavy metals in contaminated soil using X-ray microfluorescence, EXAFS spectroscopy, chemical extraction, and thermodynamic modeling. *Geochim. Cosmochim. Acta* **70**, 2163-2190.
- KONTAK, D.J. & JACKSON, S.J. (1999): Documentation of variable trace- and rare-earth-element abundances in carbonates from auriferous quartz veins in Meguma lode-gold deposits, Nova Scotia. *Can. Mineral.* **37**, 469-488.
- KONTAK, D.J. & KERRICH, R. (1997): An isotopic (C, O, Sr) study of vein gold deposits in the Meguma Terrane, Nova Scotia: implications for source reservoirs. *Econ. Geol.* **92**, 161-180.
- KONTAK, D.J. & SMITH, P.K. (1988): Meguma gold studies. IV. Chemistry of vein mineralogy. In *Mines and Minerals Branch Report of Activities 1987 B. Nova Scotia Dep. Mines Energy, Rep.* **88-1**, 85-100.
- KRAUSE, E. & ETTTEL, V.A. (1989): Solubilities and stabilities of ferric arsenate compounds. *Hydrometallurgy* **20**, 311-337.
- LIN, Z. & PULS, R.W. (2000): Adsorption, desorption and oxidation of arsenic affected by clay minerals and aging process. *Environ. Geol.* **39**, 753-759.
- LANGMUIR, D., MAHONEY, J. & ROWSON, J. (2006): Solubility products of amorphous ferric arsenate and crystalline scorodite (FeAsO<sub>4</sub>•2H<sub>2</sub>O) and their application to arsenic behavior in buried mine tailings. *Geochim. Cosmochim. Acta* **70**, 2942-2956.
- LEBERRE, J.F., GAUVIN, R. & DEMOPOULOS, G.P. (2007): Characterization of poorly-crystalline ferric arsenate precipitated from equimolar Fe(III)-As(V) solutions in the pH range 2 to 8. *Metall. Mat. Trans.* **35B**, 751-762.
- LYNCH, J. (1990): Provisional elemental values for eight new geochemical lake sediment and stream sediment reference materials: LKSD-1, LKSD-2, LKSD-3, LKSD-4, STSD-1, STSD-2, STSD-3 and STSD-4. *Geostandards Newsletter* **14**, 153-167.
- MAKRIS, K.C., QUAZI, S., NAGAR, R., SARKAR, D., DATTA, R. & SYLVIA, V.L. (2008): In vitro model improves the prediction of soil arsenic bioavailability: worst-case scenario. *Environ. Sci. Technol.* **42**, 6278-6284.
- MALCOLM, W. (1929): Gold Fields of Nova Scotia. *Geol. Surv. Can., Mem.* **156** (reprinted in 1976 as Memoir 385).
- MANCEAU, A., MARCUS, M.A. & TAMURA, N. (2002): Quantitative speciation of heavy metals in soils and sediments by synchrotron X-ray techniques. In *Applications of Synchrotron Radiation in Low-Temperature Geochemistry and Environmental Science* (P. Fenter, M. Rivers, N. Sturchio & S.R. Sutton, eds.). *Rev. Mineral. Geochem.* **49**, 341-428.
- MESSERVEY, J.P. (1928): *A Review of Gold Mining in Nova Scotia*. Nova Scotia Department of Public Works and Mines, Halifax, Nova Scotia.
- MORELLI, R.M., CREASER, R.A., SELBY, D., KONTAK, D.J. & HORNE, R.J. (2005): Rhenium-osmium geochronology of arsenopyrite in Meguma Group gold deposits, Meguma Terrane, Nova Scotia, Canada: evidence for multiple gold-mineralizing events. *Econ. Geol.* **100**, 1229-1242.
- MORIN, G., LECOCQ, D., JUILLOT, F., CALAS, G., ILDEFONSE, P., BELIN, S., BRIOIS, V., DILLMANN, P., CHEVALLIER, P., GAUTHIER, C., SOLE, A., PETIT, P.-E. & BORENSZTAJN, S. (2002): EXAFS evidence of sorbed arsenic(V) and pharmacosiderite in a soil overlying the Echassières geochemical anomaly, Allier, France. *Bull. Soc. Géol. Fr.* **173**, 281-291.

- MUTTER, G., EYSEL, W., GREIS, O. & SCHMETZER, K. (1984): Crystal chemistry of natural and ion-exchanged pharmacosiderites. *Neues Jahrb. Mineral., Monatsh.*, 183-192.
- NISHIKAWA, O., OKRUGIN, V., BELKOVA, N., SAJI, I., SHIRAKI, K. & TAZAKI, K. (2006): Crystal symmetry and chemical composition of yukonite: TEM study of specimens collected from Nalychevskie hot springs, Kamchatka, Russia and from Venus mine, Yukon Territory, Canada. *Mineral. Mag.* **70**, 73-81.
- NOVA SCOTIA DEPARTMENT OF MINES (1943): Annual report of mines, 1942. King's printer, Halifax, N.S.
- O'DAY, P.A., VLASSOPOULOS, D., ROOT, R. & RIVERA, N. (2004): The influence of sulfur and iron on dissolved arsenic concentrations in the shallow subsurface under changing redox conditions. *Proc. Nat. Acad. Sci.* **101**, 13703-13708.
- ONDRUŠ, P., SKÁLA, R., VITĚ, C., VESELOVSKÝ, F., NOVÁK, F. & JANSÁ, J. (1999): Parascorodite,  $\text{FeAsO}_4 \cdot 2\text{H}_2\text{O}$  – a new mineral from Kaňk near Kutná Hora, Czech Republic. *Am. Mineral.* **84**, 1439-1444.
- PAKTUNC, D., DUTRIZAC, J. & GERTSMAN, V. (2008): Synthesis and phase transformations involving scorodite, ferric arsenate and arsenical ferrihydrite: implications for arsenic mobility. *Geochim. Cosmochim. Acta* **72**, 2649-2672.
- PAKTUNC, D., FOSTER, A., HEALD, S. & LAFLAMME, G. (2004): Speciation and characterization of arsenic in gold ores and cyanidation tailings using X-ray absorption spectroscopy. *Geochim. Cosmochim. Acta* **68**, 969-983.
- PARSONS, C.S. (1923): An investigation of the tailings and rock dumps at the gold mines of Nova Scotia. In Annual Report of the Mines. Department of Public Works and Mines, Halifax, Nova Scotia (189-201).
- PARSONS, C.S. (1935): Milling practice for small gold mines. *Can. Inst. Mining Trans.* **35**, 437-464.
- PARSONS, M.B., SMITH, P.K., GOODWIN, T.A., HALL, G.E.M., SANGSTER, A.L. & PERCIVAL, J.B. (2004): Distribution, cycling, and fate of mercury and associated elements at historical lode gold mines in Nova Scotia, Canada. *RMZ – Materials and the Geoenvironment* **51**, 185-189.
- PARSONS, M.B., WALKER, S.R., JAMIESON, H.E., HALL, G.E.M., VAIVE, J.E., & LEBLANC, K.W.G. (in press): Chemical and mineralogical characterization of arsenic and associated elements in tailings and soils from five historical gold mining districts in Nova Scotia. *Geol. Surv. Can., Open File*.
- PEACOR, D.R. & DUNN, P.J. (1985): Sodium-pharmacosiderite, a new analog of pharmacosiderite from Australia, and new occurrences of barium-pharmacosiderite. *Mineral. Rec.* **16**, 121-124.
- PERCIAZZI, N., ONDRUŠ, P. & SKÁLA, R. (2004): Ab initio X-ray powder structure determination of parascorodite,  $\text{Fe}(\text{H}_2\text{O})_2\text{AsO}_4$ . *Eur. J. Mineral.* **16**, 1003-1007.
- PIECZKA, A., GOLEBIOWSKA, B. & FRANUS, W. (1998): Yukonite, a rare Ca-Fe arsenate, from Rędziny (Sudetes, Poland). *Eur. J. Mineral.* **10**, 1367-1370.
- PLUMLEE, G.S., MORMAN, S.A. & ZIEGLER, T.L. (2006): The toxicological geochemistry of earth materials: an overview of processes and the interdisciplinary methods used to understand them. In Medical Mineralogy and Geochemistry (N. Sahai & M.A.A. Schoonen, eds.). *Rev. Mineral. Geochem.* **64**, 5-57.
- PLUMLEE, G.S. & ZIEGLER, T.L. (2003): The medical geochemistry of dusts, soils and other earth materials. In Treatise on Geochemistry **9** (B.S. Lollar, ed.). Elsevier, Amsterdam, The Netherlands (263-310).
- RANCOURT, D.G., FORTIN, D., PICHLER, T., THIBAUT, P.-J., LAMARCHE, G., MORRIS, R.V. & MERCIER, P.H.J. (2001): Mineralogy of a natural As-rich hydrous ferric oxide coprecipitate formed by mixing of hydrothermal fluid and seawater: implications regarding surface complexation and color banding in ferrihydrite deposits. *Am. Mineral.* **86**, 834-851.
- REEDER, R.J., SCHOONEN, M.A.A. & LANZIROTTI, A. (2006): Metal speciation and its role in bioaccessibility and bioavailability. In Medical Mineralogy and Geochemistry (N. Sahai & M.A.A. Schoonen, eds.). *Rev. Mineral. Geochem.* **64**, 59-113.
- RITCHIE, A.I.M. (1994): Sulfide oxidation mechanisms: controls and rates of oxygen transport. In The Environmental Geochemistry of Sulfide Mine-Wastes (D.W. Blowes & J.L. Jambor, eds.). *Mineral. Assoc. Can., Short Course Handbook* **22**, 201-246.
- ROACH, A.G. (1940): Cyanide treatment of auriferous concentrate from Nova Scotian ores. *Can. Inst. Mining Metall. Trans.* **43**, 709-731.
- ROBERTS, S.M., MUNSON, J.W., LONEY, Y.W. & RUBY, M.V. (2007): Relative oral bioavailability of arsenic from contaminated soils measured in the cynomolgus monkey. *Toxicol. Sci.* **95**, 281-288.
- ROSS, D.R. & POST, J.E. (1997): New data on yukonite. *Powder Diffraction* **12**, 113-116.
- RUBY, M.V., DAVIS, A., SCHOOF, R., EBERLE, S. & SELLSTONE, C.M. (1996): Estimation of lead and arsenic bioavailability using a physiologically based extraction test. *Environ. Sci. Technol.* **30**, 422-430.
- RUBY, M.V., SCHOOF, R., BRATTIN, W., GOLDADE, M., POST, G., HARNOIS, M., MOSBY, D.E., CASTEEL, S.W., BERTI, W., CARPENTER, M., EDWARDS, D., CRAGIN, D. & CHAPPELL, W. (1999): Advances in evaluating the oral bioavailability of inorganics in soil for use in human health risk assessment. *Environ. Sci. Technol.* **33**, 3697-3705.
- RYAN, R.J. & SMITH, P.K. (1998): A review of the mesothermal gold deposits of the Meguma Group, Nova Scotia, Canada. *Ore Geol. Rev.* **13**, 153-183.

- SALZSAULER, K.A., SIDENKO, N.V. & SHERRIFF, B.L. (2005): Arsenic mobility in alteration products of sulfide-rich, arsenopyrite-bearing mine wastes, Snow Lake, Manitoba, Canada. *Appl. Geochem.* **20**, 2303-2314.
- SANGSTER, A.L. & SMITH, P.K. (2007): Metallogenic summary of the Meguma gold deposits, Nova Scotia. In *Mineral Deposits of Canada: a Synthesis of Major Deposit-Types, District Metallogeny, the Evolution of Geological Provinces, and Exploration Methods* (W. D. Goodfellow, ed.). *Geol. Assoc. Can., Mineral Deposits Div., Spec. Publ.* **5**, 723-732.
- SEJKORA, J., ONDRUŠ, P., FIKAR, M., VESELOVSKÝ, F., MACH, Z., GABAŠOVÁ, A., SKODA, R. & BERAN, P. (2006): Supergene minerals at the Huber stock and Schnöd stock deposits, Krásno ore district, the Slavkovský les area, Czech Republic. *J. Czech Geol. Soc.* **51**, 57-101.
- SEMPLE, K.T., DOICK, K.J., JONES, K.C., BURAUER, P., CRAVEN, A. & HARMS, H. (2004): Defining bioavailability and bioaccessibility of contaminated soil and sediment is complicated. *Environ. Sci. Technol.* **38**, 228A-231A.
- SUTTON, S.R., BERTSCH, P.M., NEWVILLE, M., RIVERS, M., LANZIOTTI, A. & ENG, P. (2002): Microfluorescence and microtomography analyses of heterogeneous earth and environmental materials. In *Applications of Synchrotron Radiation in Low-Temperature Geochemistry and Environmental Science* (P. Fenter, M. Rivers, N. Sturchio & S.R. Sutton, eds.). *Rev. Mineral. Geochem.* **49**, 429-483.
- TIMM, W.B. (1935): Recent developments in gold milling practice. *Can. Inst. Mining, Trans.* **35**, 330-340.
- TYRRELL, J.B. & GRAHAM, R.P.D. (1913): Yukonite, a new hydrous arsenate of iron and calcium, from Tagish Lake, Yukon Territory; with a note on the associated symplectite. *Trans. R. Soc. Can., Third Ser.*, **VII** 13-18.
- VINK, B.W. (1996): Stability relations of antimony and arsenic compounds in the light of revised and extended Eh – pH diagrams. *Chem. Geol.* **130**, 21-30.
- VODYANITSKII, Y.N. (2006): Arsenic, lead, and zinc compounds in contaminated soils according to EXAFS spectroscopic data: a review. *EurAsian Soil Sci.* **39**, 611-621.
- WALKER, S.R., JAMIESON, H.E., LANZIOTTI, A., ANDRADE, C.F. & HALL, G.E.M. (2005): The speciation of arsenic in iron oxides in mine wastes from the Giant gold mine, N.W.T.: application of synchrotron micro-XRD and micro-XANES at the grain scale. *Can. Mineral.* **43**, 1205-1224.
- WELHAM, N.J., MALATT, K.A. & VUKCEVIC, S. (2000): The stability of iron phases presently used for disposal from metallurgical systems – a review. *Minerals Eng.* **13**, 911-931.
- WONG, H.K.T., GAUTHIER, A., BEAUCHAMP, S. & TORDON, R. (2002): Impact of toxic metals and metalloids from the Caribou gold-mining areas in Nova Scotia, Canada. *Geochem. Explor. Environ. Anal.* **2**, 235-241.
- WONG, H.K.T., GAUTHIER, A. & NRIAGU, J.O. (1999): Dispersion and toxicity of metals from abandoned gold mine tailings at Goldenville, Nova Scotia, Canada. *Sci. Tot. Environ.* **228**, 35-47.

Received November 28, 2008, revised manuscript accepted May 12, 2009.